Self-sufficient microfluidic systems using highly porous elastomeric sponges

A thesis submitted in fulfilment of the requirements for the degree of Doctor of Philosophy

Peter Thurgood

B.Eng

School of Engineering

College of Science Engineering and Health

RMIT University

December 2017

Declaration

I certify that except where due acknowledgement has been made, the work is that of the author alone; the work has not been submitted previously, in whole or in part, to qualify for any other academic award; the content of the thesis/project is the result of work which has been carried out since the official commencement date of the approved research program; any editorial work, paid or unpaid, carried out by a third party is acknowledged; and, ethics procedures and guidelines have been followed.

Peter Thurgood

12th of December 2017

For Tony.

Acknowledgements

I would like to express my sincere gratitude to my supervisors; Dr. Khashayar Khoshmanesh, Dr. Sara Baratchi and Dist. Prof. Arnan Mitchell for their encouragement and support throughout my candidature. I would also like to thank Mr. Crispin Szydzik and Mr. Jiu Yang Zhu for their invaluable contributions to my research. I acknowledge the support I have received for my research through the provision of an Australian Government Research Training Program Scholarship.

I would like to thank the following researchers and students for providing an excellent research environment: Dr. Gorgi Kostovski, Dr. Shiva Balendhran, Dr. Andreas Boes, Dr. Kiplimo Yego, Dr. Guanghui Ren, Dr. Berrak Gol, Mr. Michael Kurdzinski, Dr. Kyle Berean, Dr. Emily Nguyen, Dr. Rhiannon Clarke, Mr. Naresh Pillai, Mr. Ali Zavabeti. Mr. Steffen Schoenhardt and Mr. Markus Knoerzer. I would also like to thank the technical staff at the MNRF for facilitating my research: Mr. Yuxun Cao, Mr. Paul Jones, Ms. Chiping Wu and Dr. Zeyad Nasa. I would also like to thank my family and friends for their endless support and encouragement. A special thanks to my father and my extremely supportive brother and sister.

And finally, I would like to thank my mother, who inspired me to study engineering.

Abstract

Conventional microfluidic systems enable the manipulation of liquids in micro-scale structures. However, the majority of microfluidic systems rely on external off-chip equipment, such as pumps, tubes and valves for driving and control of flow. This in turn increases the overall costs, and dimensions of the system while decreases their utility for point-of-care purposes, and importantly their widespread application in biological laboratories.

Chapter 1 presents a brief overview of self-sufficient microfluidic devices, and explores self-sufficient microfluidic components made of polydimethylsiloxane (PDMS) capable of storage and release of aqueous solutions into fluidic environments, which can be operated without the need for external off-chip equipment, and specialised training in microfluidics. This review identified a clear gap in the current body of knowledge and motivated me to develop PDMS sponges as a building block of self-sufficient lab-on-a-chip structures.

Chapter 2 presents my first research contribution. Here, I fabricated a highly porous sponge by templating microscale droplets of water in PDMS using a microfluidic T-junction system. Scanning electron microscopy revealed the unique structure of the sponge, consisting of large pores which were only interconnected by small holes. This unique structure allowed for storage of aqueous solutions and their slow release into fluidic environments. Experiments indicated that the release characteristics of the sponge can be tuned by varying the size of the pores and interconnecting holes.

I further demonstrated the capability of the highly porous PDMS sponge for the chemical stimulation of cultured cells. As a proof-of-concept, the sponge was

loaded with ionomycin and placed into a well pre-coated with human umbilical vein endothelial cells. This enabled me to monitor the intracellular calcium signaling of cells in response to releasing ionomycin using a simple setup.

I also demonstrated the ability of the PDMS sponge for the active release of stored chemicals into a microfluidic system. A PDMS sponge was loaded with an aqueous solution, and squeezed using a simple screw mechanism. This enabled me to release the stored solution in a controlled manner over consequent cycles into the surrounding flow.

Chapter 3 presents my second research contribution. Here I demonstrated the capability of the highly porous PDMS sponge for the generation of micro-droplets of aqueous solutions in oil by simply squeezing the sponge. The small interconnecting holes located at the interface of the sponge and the surrounding oil acted as microscale orifices, enabling the generation of hundreds of droplets, with the majority of them ranging from 10 to 200 µm.

I demonstrated the ability of sponge-based droplet generation for the encapsulation of cells. As a proof-of-concept, monocytic leukaemia cells were encapsulated in droplets containing cell culture medium. The density of encapsulated cells was proportional to the volume of droplets as well as the concentration of cells, enabling me to produce hundreds of isolated droplets with various cell populations.

I further investigated the ability of produced droplets for studying the response of cells to chemical stimulation. As a proof-of-concept, the leukaemia cells were stimulated with hydrogen peroxide prior to encapsulation. The quick settling of encapsulated cells facilitated monitoring their responses using fluorescent

microscopy. Investigation of cell viability yielded similar results compared to off-chip experiments in the absence and presence of hydrogen peroxide. Experiments indicated the ability for conducting parallel experiments using multiple isolated cell clusters simultaneously.

Chapter 4 presents a summary of the key findings of this thesis. overall, the highly porous PDMS sponges developed during this research creates unprecedented opportunities for generation of self-sufficient microfluidic systems for various cellular assays.

Table of Contents

List of Abbreviations

PDMS	Polydimethylsiloxane
PMMA	Poly-methyl methacrylate
OH	Hydroxy
HIPE	High internal phase emulsions
H_2O_2	Hydrogen Peroxide
CO_2	Carbon dioxide
PI	Propidium iodide
HUVECs	Human umbilical vein endothelial cells
THP-1	Human monocytic leukaemia cell line
$[Ca^{2+}]_i$	intracellular calcium signalling
Pe	Péclet number
Ca	Capillary number
ROI	Region of interest
SEM	Scanning Electron Microscopy

List of Figures

List of Tables

CHAPTER 1: Introduction

1.1 Self-sufficient microfluidic devices

Microfluidic technologies enable the manipulation of small volumes of liquid in micro-scale structures [1]. These devices facilitate the precise prediction and control of flow variables including velocity, sheer stress, temperature, temperature gradients, and concentration of chemicals in miniaturised environments, which is difficult to achieve using traditional macro-scale devices [2]. Other benefits include reduced cost, enhanced sensitivity, portability, and the ability to integrate with other technologies such as photonics [3].

Despite these advantages, conventional microfluidic devices rely on bulky and rather expensive off-chip support equipment such as pumps, centrifuges, mixers, shakers, vortex generators, and power supplies. This increases the overall cost and footprint of microfluidic systems, and more importantly limits their application to specialist laboratories. Self-sufficient microfluidic devices aim to address these shortcomings by integrating all necessary components into one single platform, such that it can be operated with minimum reliance on off-chip equipment or specialised training, as schematically presented in **Figure 1.1**.

Storage and release of liquids are among the essential requirements for the operation of microfluidic systems. While conventional microfluidic systems rely on bulky pumps and liquid interfaces, stand-alone self-sufficient microfluidic devices require the miniaturisation and integration of such components into one single platform, which can be operated using passive, manual, or active mechanisms, as summarised in **Table 1.1**.

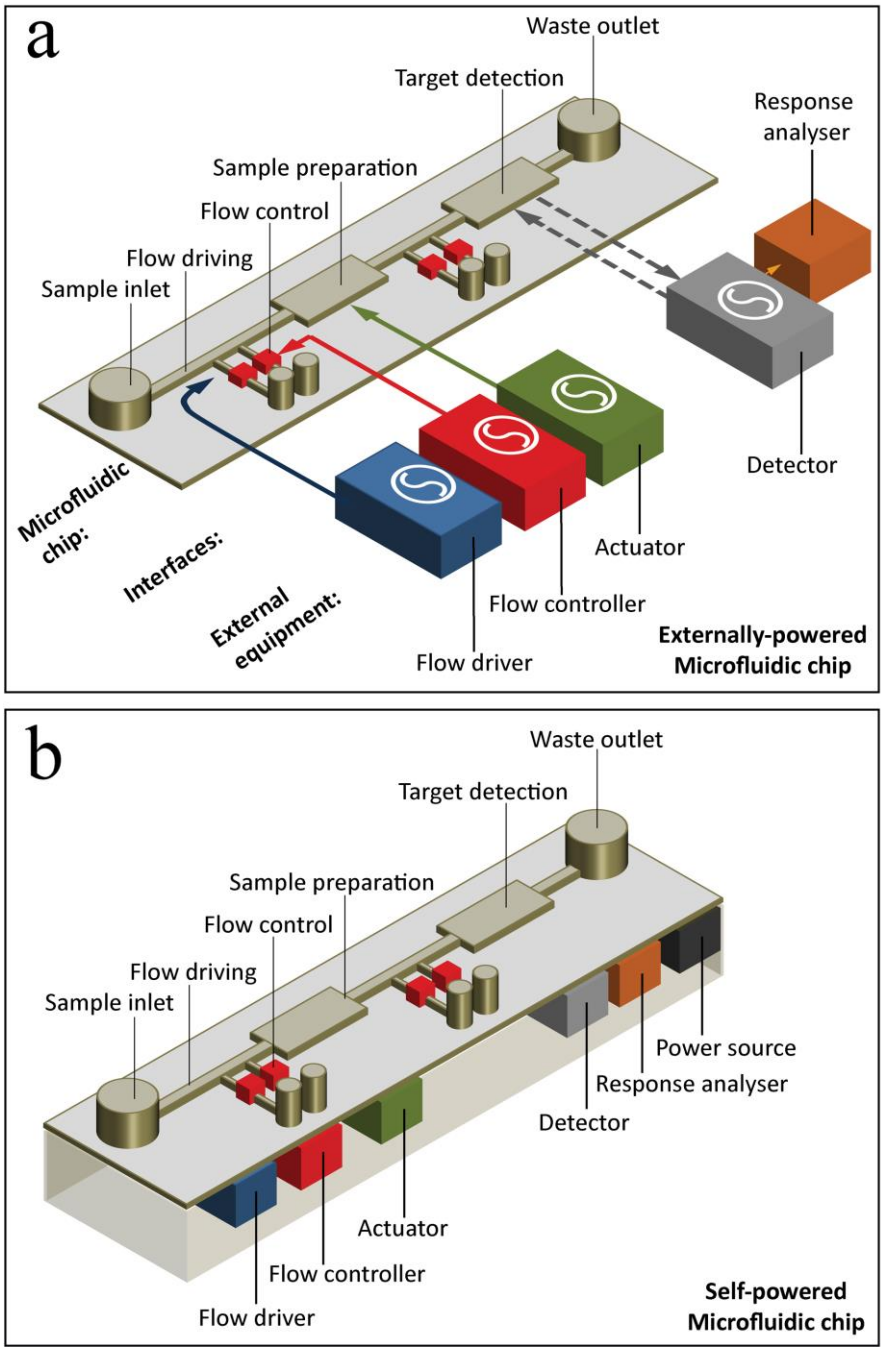

Figure 1.1: Typical microfluidic devices using various external, off-chip equipment *vs*. self-sufficient microfluidic devices. **a)** A Typical microfluidic device. **b)** A self-sufficient microfluidic device. Figure adapted from reference [4].

Table 1.1: Self-sufficient mechanisms for the storage and release of liquids in microfluidic devices.

Principle	**Mechanism**
Passive	Capillary driven flows [5, 6]
Manual	Syringe withdrawal [7-9]
	Blister pouches for manual release of liquids [6]
Manual/Passive	Blister pouches for liquid storage and on demand release along with capillary driven flows through a microfluidic chip [6]
	Manual compression of a microfluidic chip triggering a capillary based pumping [10]
Active	Centrifugally driven liquids [11, 12]
	Integrated solenoid valves with a microcontroller [13]
	Miniaturised peristaltic pumps [14]
	Braille module using peristaltic actuation [15]
	Piezoelectric micro-diaphragm pumps [16]
	Electrokinetic transport [17, 18]
	DC diaphragm pumps [19]
	Smartphone controlled devices [19]
	Surface acoustic waves [20]

1.2 Storage and release of liquids in self-sufficient microfluidic systems

Passive driving mechanisms rely on the tendency of liquids to pass though micro-scale structures. The capillary pumping is the most common passive driving mechanism, which relies on the adhesion forces between the microfluidic structures and the liquid resulting in pumping though the device [4, 21]. Capillary pumping has been extensively used in point-of-care devices for driving biological samples though micro-fabricated structures over short periods (in the order of minutes).

A good example of a self-sufficient microfluidic system using passive mechanisms is a microfluidic blood analysis system, developed by Dimov *et al*., [5], as shown in **Figure 1.2**. This microfluidic chip consists of a PDMS slab sandwiched between two glass slides and stored in a degassed state in vacuum packages. Removal of the seal triggers a degas-driven flow due to air absorption into the PDMS structures. Next, 5 µl of whole blood is placed at the inlet and drawn into the chip via suction. Whole blood passes over a filter trench, separating blood cells from the plasma. Plasma based proteins are detected using a fluorescent scanner as the plasma passes over the trench and flows across a biomarker detection zone patterned on the top glass slide using micro-contact printing. This system allows for the detection of biomarkers from whole blood using a passive degas-driven flow.

Despite the simplicity, the main disadvantages of capillary driven devices are: low flow rate, short operation periods, strong dependency on the properties of the sample as well as environmental parameters, including temperature and relative humidity [4].

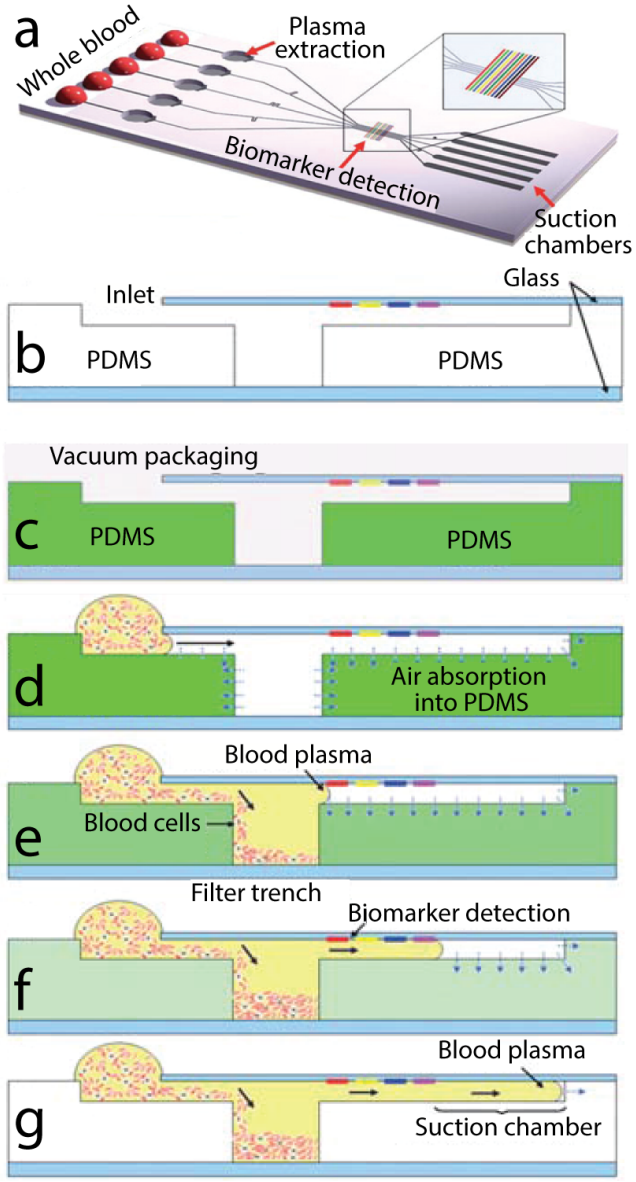

Figure 1.2: Self-sufficient integrated blood analysis system on a microfluidic chip using passive mechanisms. **a)** Schematic of the PDMS microfluidic chip. **b-g)** Schematic showing the operating principles of the chip. Absorption of air into degassed PDMS device draws whole blood into the chip where the blood cells are filtered and the plasma is drawn across biomarker detectors. Figure adapted from reference [5].

Another method for driving fluids though self-sufficient devices is the use of manual mechanisms, in which an end-user triggers the device. The main advantage of manual driving mechanisms is to eliminate the dependency on environmental parameters as well as driving larger volumes of liquid. Infusion or withdrawal of liquids using a manually operated syringe is the most common manual driving mechanism [7].

Liquid flow can also be controlled in self-sufficient microfluidic devices by manual means. For example, Garstecki *et al*., [7] presents a device for the mixing two laminar streams in a microfluidic channel by the introduction of air bubbles into the main channel using a set T-junctions shown in **Figure 1.3**. Flow of the liquids through the chip as well as the generation of the air bubbles into the main channel is via negative pressure applied manually at the outlet of the chip with a hand operated syringe. Mixing of the liquids is completed in micro-mixer structures consisting of branched channels in which the air bubbles travelling though the branched channels cause the two liquids to mix. This approach allows for the efficient mixing of liquids in a microfluidic device using a manual hand pump.

Despite such advantages, such devices are limited by the ability of the end-user to precisely apply a targeted flow rate as well as producing similar flow rates over repeated experiments [4].

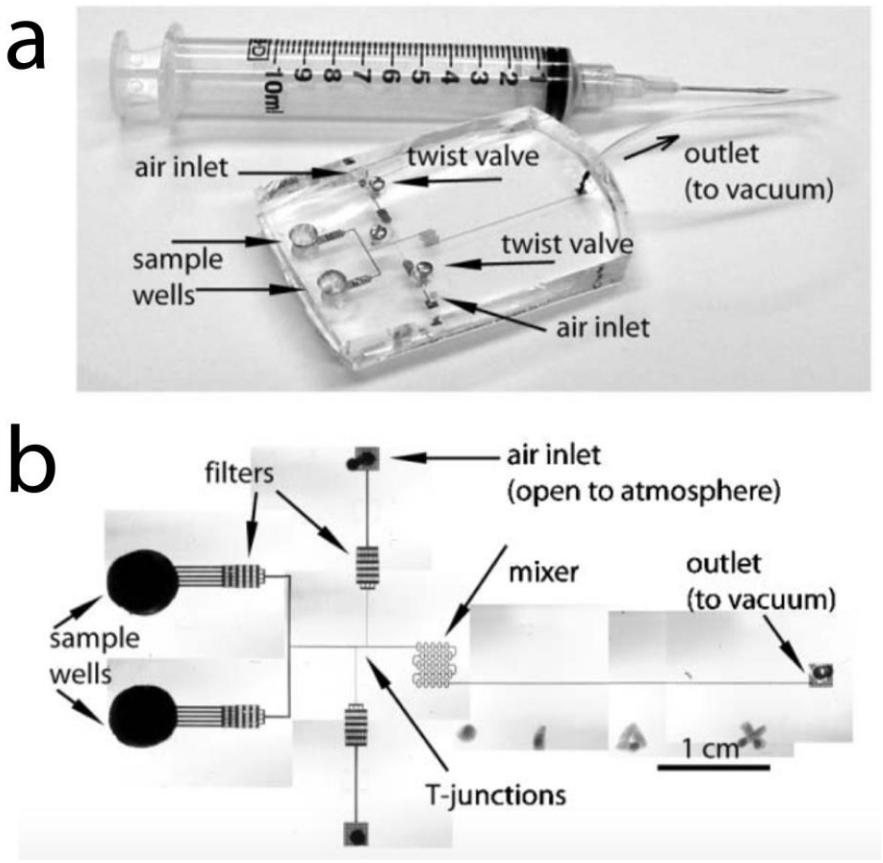

Figure 1.3: A microfluidic setup used for mixing liquids using droplets of gas drawn into the microfluidic chip manually withdrawing a syringe. **a)** Experimental setup showing the microfluidic chip and syringe. **b)** Stitched microscope images showing the microfluidic chips components. Figure adapted from reference [7].

The combination of passive and manual mechanisms has been used in conjunction to facilitate the manual release and passive driving of liquids [6, 10].

An example is a self-sufficient point-of-care device by Smith *et al.*, [6], in which reagents are stored in blister pouches that can be released by manually squeezing the pouch, after release from the pouch, the liquid can then flow though the microfluidic chip using passive capillary mechanisms, as shown in **Figure 1.4**. This device allows for the on demand, manual release of stored liquids into a microfluidic environment coupled with the passive pumping of the released liquids though the chip.

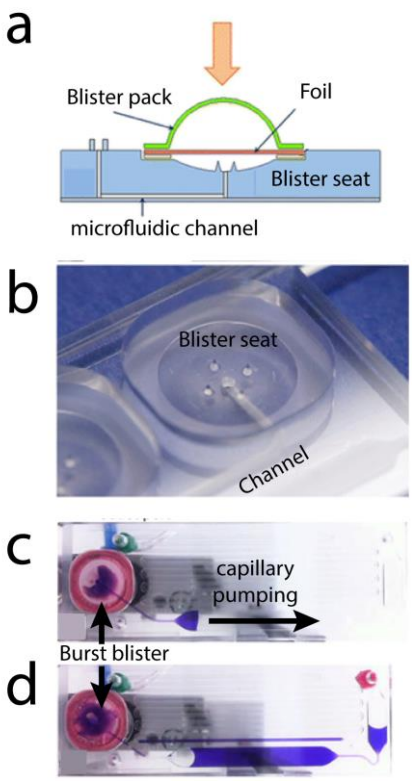

Figure 1.4: A microfluidic chip utilising both manual and passive mechanisms for the release and pumping of stored liquids. **a)** Schematic of the blister reservoir and seat. **b)** photo of the blister seat. **c-d)** Liquids are released from an integrated blister pack upon squeezing, the released liquid is then passively. Figure adapted from reference [6].

The integration of miniaturised components such as diaphragm, peristaltic, and piezoelectric pumps in combination with on-chip valves such as solenoids [13] allow for the active control of liquids in a self-sufficient manner.

For example, Addae-Mensah *et al.*, [13] present a microfluidic with an integrated, battery, diaphragm pump, and solenoids to actuate membrane valves to control the flow of liquid in the device without the need for external equipment shown in **Figure 1.5**. This device was used for the detection of horseradish peroxidase enzyme. Buffers, reagents, horseradish peroxidase enzyme same along with a fluorescent dye are drawn into the microfluidic device using the integrated diaphragm pump and mixed using a serpentine mixer. Solenoids are used to actuate the membrane valves to confine the mixed samples required for the incubation and detection at the fluorescent detection zones.

These devices allow for increasingly complex multi-step assays to be carried out in which multiple samples/reagents/buffers can be driven to facilitate target bio-reactions. The ongoing advancement of smartphones has enabled these devices to be truly mobile as they enable the control and programming of experiments as well as image acquisition and processing of results [19].

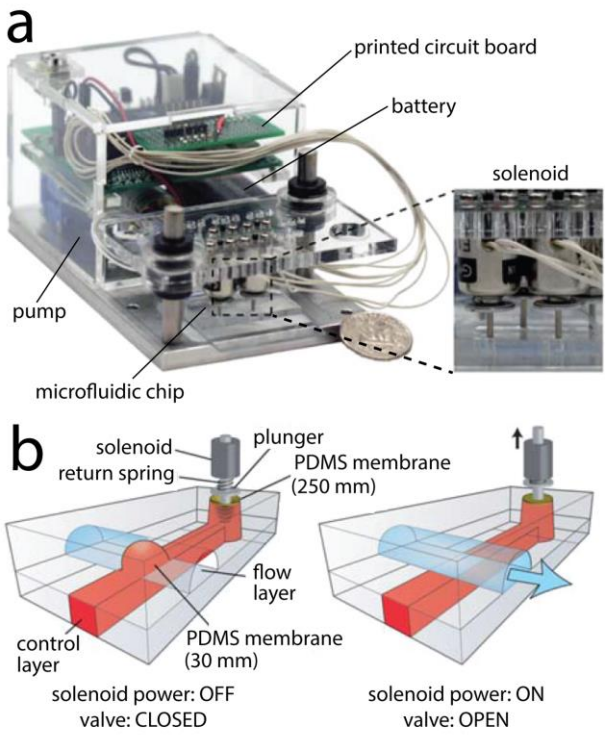

Figure 1.5: A self-contained microfluidic system integrating a PDMS microfluidic chip with a microcontroller and solenoids and integrated battery for the control of on chip valves for the detection of horseradish peroxidase enzymes. **a)** Photo of the integrated device. **b)** operating principle of the on-chip valves. Figure adapted from reference [13].

Alternative flow driving mechanisms such as centrifugally driven flows induced by the rotation of the microfluidic device have also been used for the realisation of complex multistep assays.

An elegant example is the "LabDisk" presented by Stumpf *et al*., [11], as shown in **Figure 1.6**. In this device, reagents are centrifugally driven though the microfluidic system by simply adjusting the rotational speed of the disk. Reagents are pre-stored in miniature stick-packs, which burst at specific rotational frequencies. Using this approach, real-time reverse transcription polymerase chain reaction is conducted on an influenza A H3N2 sample through the sequential application lysing agents, RNA extraction buffers, as well as various washing steps. Finally, a real-time fluorescent signal readout allows for the detection of the target pathogens.

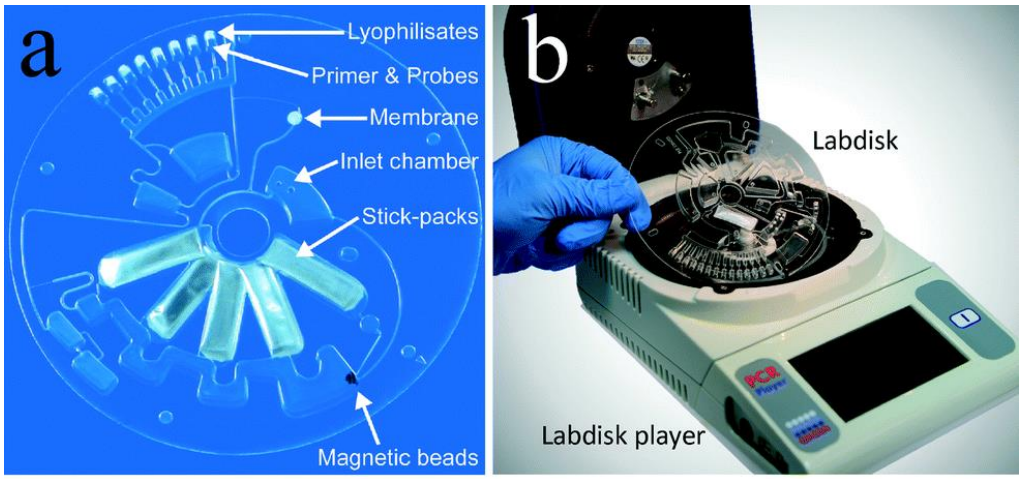

Figure 1.6: A transparent "LabDisk" for the nucleic acid based detection of influenza A H3N2 virus related pathogens. **a)** Photo of the "LabDisk" microfluidic system, which utilises multiple inlet, reagent, and reaction cavities. **b)** The "LabDisk player" centrifugally drives liquids through the chip by varying the rotational speed of the chip. Figure adapted from reference [11].

1.3 Droplet based microfluidics systems

While the majority of applications in microfluidics involve water based miscible liquids such as blood and cell culture media, some applications involve the application of immiscible liquids such as water and oil or air and water. The injection of water droplets into oil using a pipette leads to the generation of several droplets in the range of hundreds of microns to millimetres in diameter. These droplets can be further broken into smaller droplets by sonication. Despite this simplicity, this does not allow for the continuous production of micro-scale droplets in a controlled manner in such a way that the size, gap, and frequency of the droplets can be precisely controlled. Microfluidics has enabled the production of uniformly sized droplets.

There are various ways to generate droplets in microfluidics. this can be achieved by the configuration of the microfluidic system as well as the flow rations between continuous and dispersed phases [22]. The most common geometries are coaxial, flow focusing, and T-junctions, as shown in **Figure 1.7**. More complex droplet generation systems can be realised by combining the above geometries or the incorporation of additional injection channels [23]. Different regimes can regimes can be produced by simply varying the ratio between the continuous and dispersed flows. In general, operating at high ratios of continuous/dispersed flow leads to the dripping regime, where droplets are formed at the injection site due to strong shear forces induced by the continuous phase. In comparison, operating at lower ratios of continuous/dispersed flow leads the formation of parallel streams of the dispersed phase in the continuous phase moving along the channel before the capillary pressure destabilised the interface and breaks the jet into individual droplets. Among the three commonly

used microfluidic droplet generation configurations, flow focusing systems are popular as they enable a higher degree of control over the flow ratios.

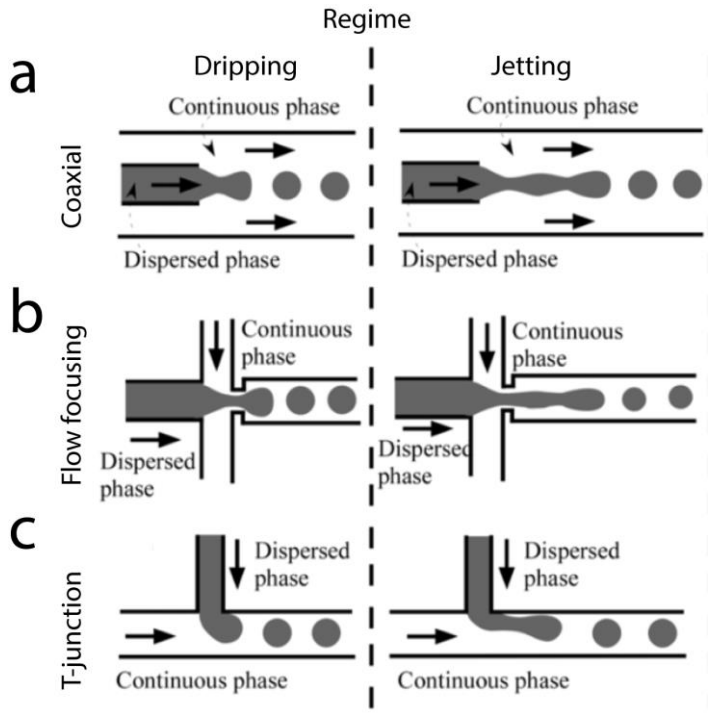

Figure 1.7: Typical on-chip micro droplet generation principles. **a)** Co-axial droplet generation. **b)** Flow-focusing droplet generation. **c)** T-Junction droplet generation. Figure adapted from reference [22].

Microfluidic droplet generation systems enable the precise control over the size, inter-droplet gap, and frequency of droplets using various configurations, as presented in **Figure 1.7**.

The generated droplets can be precisely manipulated within microfluidic structures this involves driving the droplets through channels with variable cross-sections to decelerate or accelerate them, transferring droplets across neighbouring liquid interfaces, merging neighbouring droplets, sorting droplets based on their size or composition, changing the composition of droplets by injecting small volumes of liquid, controlling the size of the droplets by changing the interfacial properties, and capturing the target droplets for analysis. Each of these manipulations can be achieved using various mechanisms, as summarised in **Table 1.2**.

The droplets, which have been manipulated, as described above, present ideal platforms for studying various physical, chemical, biochemical, and biological reactions. The very small volume of each droplet enhances the reaction efficiently, which can be further boosted by recirculation flows inside moving droplets. Depending on the rate of reactions occurring inside the droplets, the droplets can be analysed in real time or stored either on-chip or off-chip to be analysed following the completion of reactions, as presented in **Table 1.2**.

Figure 1.8 to **1.10** present some examples of microfluidic droplet generation systems for physical and biological applications.

Table 1.2: Droplet based microfluidic applications:

Purpose	Description

Generation:	• Two phase emulsions (eg: w/o) [24]
	• Multiphase emulsions (eg: w/o/w/o…) [25]
	• Encapsulation of microscale objects:
	  o Micro/nano particles [26]
	  o Cells [26, 27]
	  o Multicellular organisms [28]

Manipulation:	• Controlling the size of droplets using electrocapillary forces [29]
	• Lateral transfer of droplets across liquid phases:
	  o One liquid phase using rails [30]
	  o One liquid phase using acoustic forces [31]
	  o Two liquid interfaces using surface tension driven forces [24, 32]
	• Droplet merging using:
	  o Pillars [33]
	  o Channel widening [34]
	  o Electrocoalescence [35]
	• Capturing droplets using:
	  o Pillars [36]
	  o Hydrodynamic arrays [37]

	• Sorting of droplets based on their properties:
	  o Electrical forces (dielectrophoresis) [27]
	  o Mechanical traps (pillars) [34].
	• Reagent mixing [7, 38]

Reactions:	• Mixing of reagents using recirculation of flow inside moving droplets [7, 38]
	• Injection of solutions into moving droplets [39]
	• Synthesis of micro-particles:
	  o Janus particles [40, 41]
	  o Hybrid particles (non-symmetric Janus particles) [42, 43]
	  o Shape controlled particles [44-46]
	  o Micro-structured particles [47-49]
	• Cell based assays:
	  o Chemical stimulation [26, 27, 50, 51]
	  o Sorting [27, 50, 52-55]
	  o Culturing [27, 50, 55-57]
	  o Cell electroporation [58-60]
	  o UV stimulation [26]
	  o Lysis [26, 54, 61-63]
	  o Encapsulation of functionalised beads [26]
	  o Capture of nucleic acids [54, 55, 59-63]
	  o Capturing of proteins [64]

Gol *et al*., [24] presents the generation of galinstan liquid metal droplets using a microfluidic flow focusing chip, as shown in **Figure 1.8**. Galinstan is injected though the central channel and is pinched off by glycerol flow injected through the side channels, the high viscosity of glycerol produces enough shear force to overcome the high surface tension of the liquid metal droplets and pinch them into micro-scale droplets. The droplets are later transferred into a low viscosity sodium hydroxide solution using surface tension driven forces, to supress the oxidation of the liquid metal droplets. This approach was extended to selectively transfer the liquid metal droplets into parallel streams under hydrodynamic forces [32].

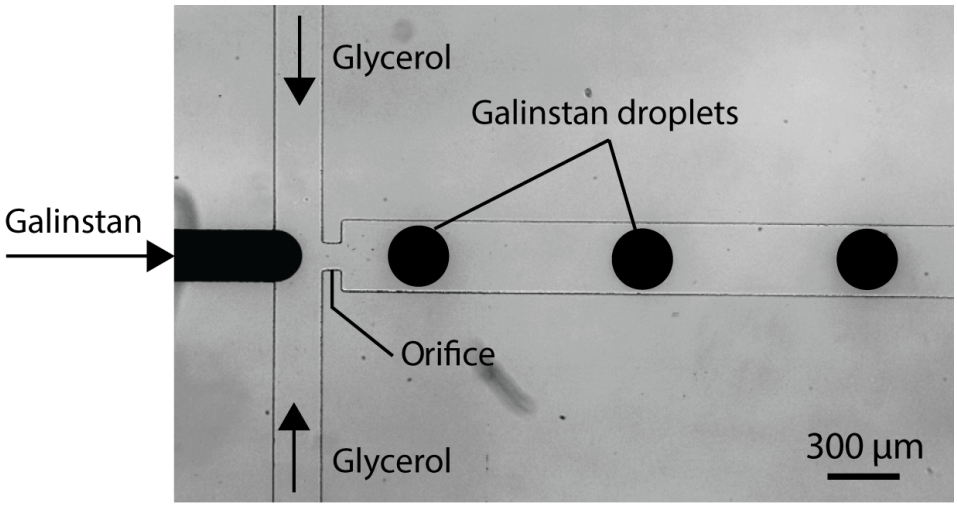

Figure 1.8: The continuous generation of galinstan liquid metal droplets in glycerol using a PDMS flow focusing microfluidic chip. Figure adapted from reference [24].

Baret *et al*., demonstrate a microfluidic system for culturing E. coli cells, as shown in **Figure 1.9**. Cells with fluorogenic substrate are encapsulated in fluorinated oil using a flow focusing chip. The droplets are then collected in a pipette off-chip and incubated at 20 °C for 14 hours to allow for cell growth and production of an enzyme that causes the hydrolysis of the fluorogenic substrate. This process causes the droplets containing cells to become highly fluorescent. The droplets are then reinjected into a secondary microfluidic device in which each droplet is illuminated by a 488 nm laser, and the fluorescent response of each droplet is detected using a photomultiplier tube. Fluorescent droplets containing cells are then sorted using dielectrophoresis by deflecting the fluorescent droplets into a secondary channel. This method allows for collection of droplets containing the E. coli cells.

Zilionis *et al*., [63] present a microfluidic droplet generation system for barcoding and genetic sequencing of cell, as shown in **Figure 1.10**. Droplets are generated using a flow focusing microfluidic chip in which the reagents, and hydrogel beads and the cell suspension are injected the central channel upstream of the orifice. Injection of oil from the side channels leads to the formation of droplets, which contain cells, reagents, and beads. The encapsulated cells are lysed due to the presence of the lysis buffers. The mRNA released from the cells is dispersed though the droplet. The droplets are then exposed to UV light, which in turn releases barcoding cDNA components from the hydrogel to capture mRNA of the lysed cell. This facilitates the reverse transcription of the genetic materials.

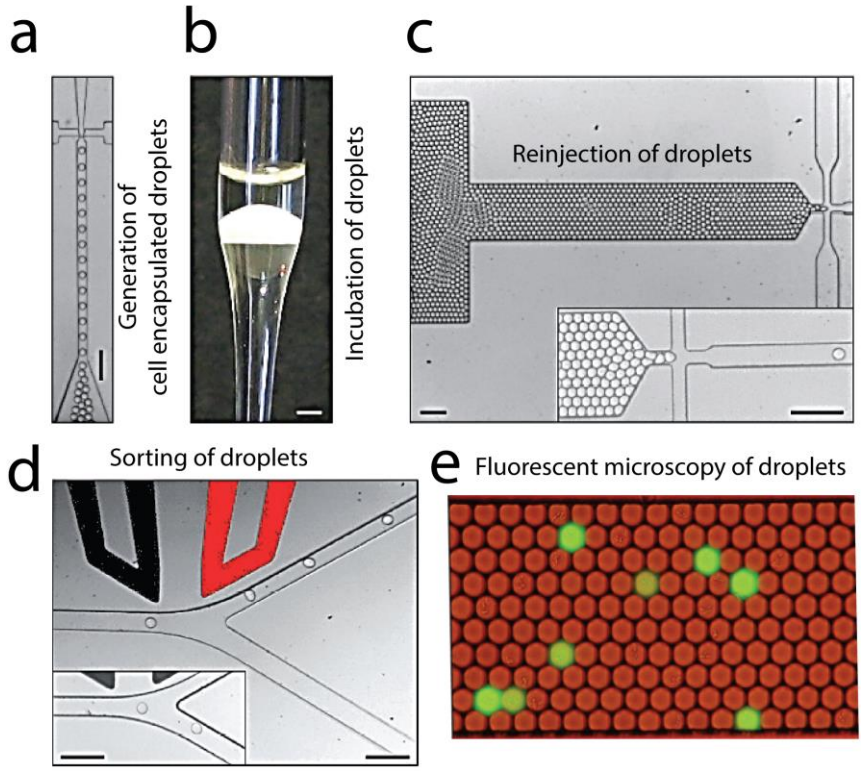

Figure 1.9: A microfluidic droplet generation and cell sorting system. **a)** Microfluidic droplet generation utilising a flow focusing chip. **b)** Subsequent off chip collection and incubation in a Pasteur pipette. **c)** Re-injection of the droplets into a microfluidic chip prior to droplet sorting based on the droplet contents. **d)** Droplet sorting using dielectrophoresis. Figure adapted from reference [27].

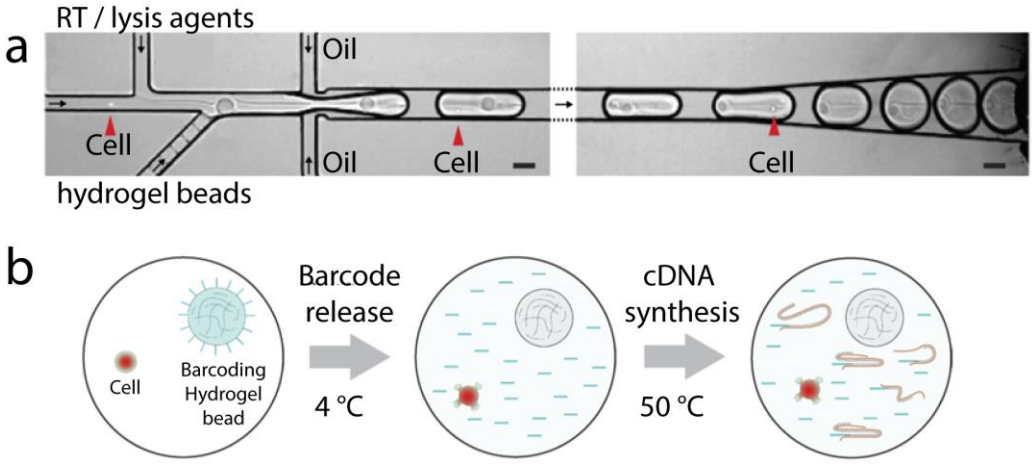

Figure 1.10: Genetic sequencing of droplet encapsulated cells. **a)** Microfluidic droplet generation system including side channels for the injection of cell culture medium, reagents, and hydrogel barcoding beads followed by a flow focusing droplet generation system. **b)** Lysis of the encapsulated cells for subsequent genetic analysis. Figure adapted from reference [63].

1.4 Porous sponges

Porous structures have been traditionally used for cleaning due to their ability to absorb liquids. A common example is sponges made from cellulose, which are routinely used in kitchens. The porosity of sponges enables them to store liquids. The flexibility of sponges enables the active release of stored liquids upon squeezing. Also, the surface of a sponge can be readily functionalised with various nano-materials or chemicals to enhance their selectivity and sensitivity to specific solutions and materials. In addition, the high surface to volume ratio of porous sponges enhances the efficiency of surface mediated reactions [65]. Due to their unique features, sponges have been used for various applications such as the selective absorption of liquids, the selective filtering of ions, chemical catalysers, flexible electric components such as: sensors and capacitors, and scaffolds for tissue engineering and drug delivery using different materials, as summarised in **Table 1.3**.

Table 1.3: Highly porous sponges

Material	Application
Cellulose sponges	• Scaffold for supporting nanoparticles serving as a catalyser [66] • Piezoresistive sensors with the integration of carbon nanotubes [67]
Other polymers	• Piezoresistive sensors with the integration of sputtered gold on polyurethane sponges [68] • Selective absorption of emulsified droplets using a chitosan and linear polyacrylamide composite sponges [69] • Surface-mediated drug delivery using micro-porous films of polyethylenimine and polyacrylic acid [70]
Hydrogels	• Scaffold for *in vivo* tissue generation in mice [71] • Scaffold for soft tissue engineering and culturing of human skin fibroblast cells [72] • Scaffold for the *in vivo* repair of cranial bone defects in rats [73]

PolyHIPEs	• Selective absorption of oils and organic solvents [74] • Selective capture of carbon dioxide gas from air [75] • Selective nitrite ion exchange using a functionalised polyHIPE [76] • Removal of silver, lead and cadmium ions from aqueous solutions [77] • Photocatalytic water purification a titanium dioxide surface modified polyHIPE [78] • Chemical sensing using polyHIPE membranes, modified with conductive particles, enzymes and electron mediators [79] • Energy storage (capacitors) by incorporating cobalt hydroxide nanorods [80] • A scaffold for culturing bacteria [81] • Slow release of bone growth factors *in vivo* using polyHIPE microspheres [82] • Droplet templated PolyHIPEs with controllable porous structures [83]

Polydimethylsiloxane (PDMS) is among the polymers used to fabricate porous sponges. PDMS is commonly used the fabrication of microfluidic systems due to its ability to be easily patterned, chemical stability, elasticity, transparency and biocompatibility [84].

PDMS sponges are fabricated using various techniques for a wide range of applications such as: selective absorption of oil from water, filtering of ions, flexible electronics, and acoustic metamaterials, and manually actually pumps for microfluidic applications, as presented in **Table 1.4**.

Sacrificial crystal templating is the most widely used method for fabricating PDMS sponges due to its simplicity, as further discussed in **Figure 1.11**. The elasticity of the PDMS sponges has made them suitable for manual release of stored liquids, as presented in **Figure 1.12** as well as well as the selective absorption of oil from water, as shown in **Figure 1.13**.

Table 1.4: Porous PDMS sponges

Fabrication method	Applications
Crystal templated structures using sugar, salt, citric acid monohydrate, or ice:	• Pressure pump for the active release of stored liquids for microfluidic systems [85, 86] • Selective absorption of oils in water [87-90] • Enhanced selective absorption of oils in water by the incorporation of carbon nanotubes [91] • Filtering heavy metal ions [92] • Making flexible electronics with the incorporation of carbon nanotubes [93], metals [94, 95], or liquid metals [96]
Gas foaming	• Transport of fluorescent molecules across a thin film [97]
Emulsion templating	• Acoustic metamaterials by adjusting the porosity [98]
Sacrificial polymer microparticle templating	• PDMS films with tuneable micro/nano pores [99]

Cha *et al*., [86] present a simple method for fabricating porous PDMS sponges using a sugar cube as a sacrificial scaffold, as shown in **Figure 1.11**. First, sugar cubes are placed into a Petri dish filled with uncured PDMS. The uncured PDMS is drawn into the sugar cubes by applying a vacuum. Following the curing of the PDMS, the sugar cubes are placed in warm water to dissolve the sacrificial sugar cube resulting in a porous PDMS sponge. Other sacrificial crystal templating materials such as salt [97], and citric acid monohydrate [100] have been used to template porous PDMS sponges.

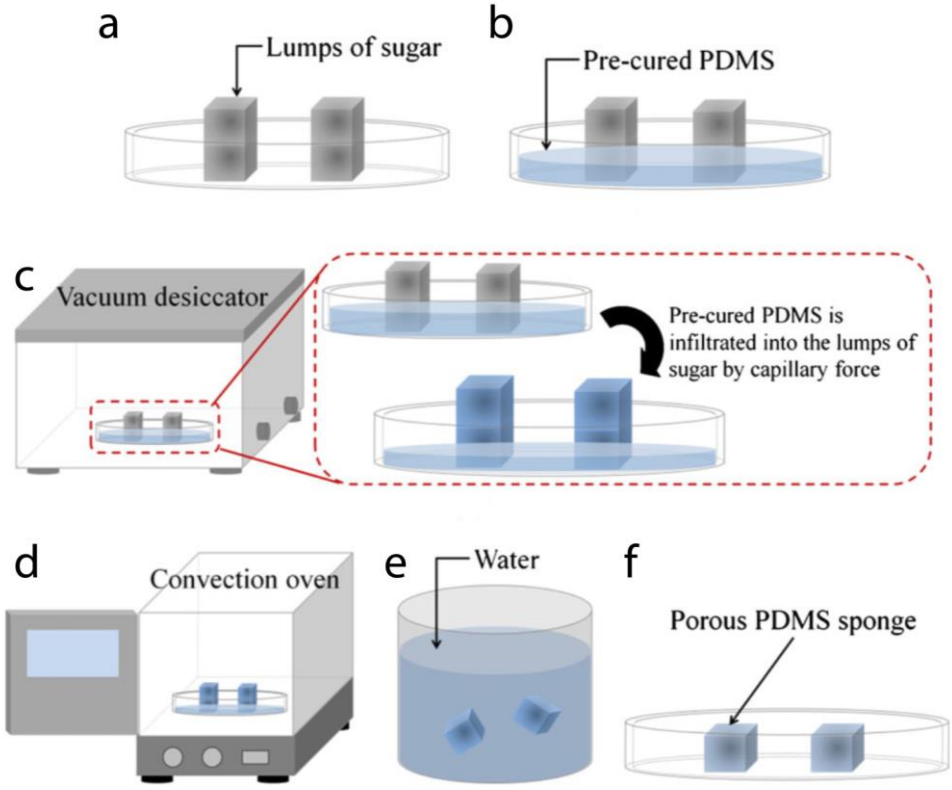

Figure 1.11: Fabrication of porous PDMS sponges via the sugar leaching technique. **a)** Sugar cubes in a petri dish. **b)** Uncured PDMS (10:1 w/w base to curing agent) is then poured into the petri dish. **c)** Absorption of the PDMS into the sugar cube due to capillary forces under vacuum. **d)** Curing of the PDMS in an oven. **e)** Dissolving the sacrificial sugar cubes in water. **f)** Porous PDMS sponges after drying. Figure adapted from reference [86].

The porous and elastically of these sugar templated PDMS sponges allows for the loading and unloading of aqueous solutions by simply squeezing the sponge manually. Yang *et al*., [85] has used this concept for the manual pumping of aqueous solutions into a microfluidic chip, as shown in **Figure 1.12**. This idea has been extended by Hong *et al*., [101] by incorporating micro scale iron powder into the PDMS matrix to make the sponge magneto-responsive. This allows for the sponge to be actively squeezed using a magnetic field to produce pulsatile flows in microfluidic channels to study the response of cultured cells.

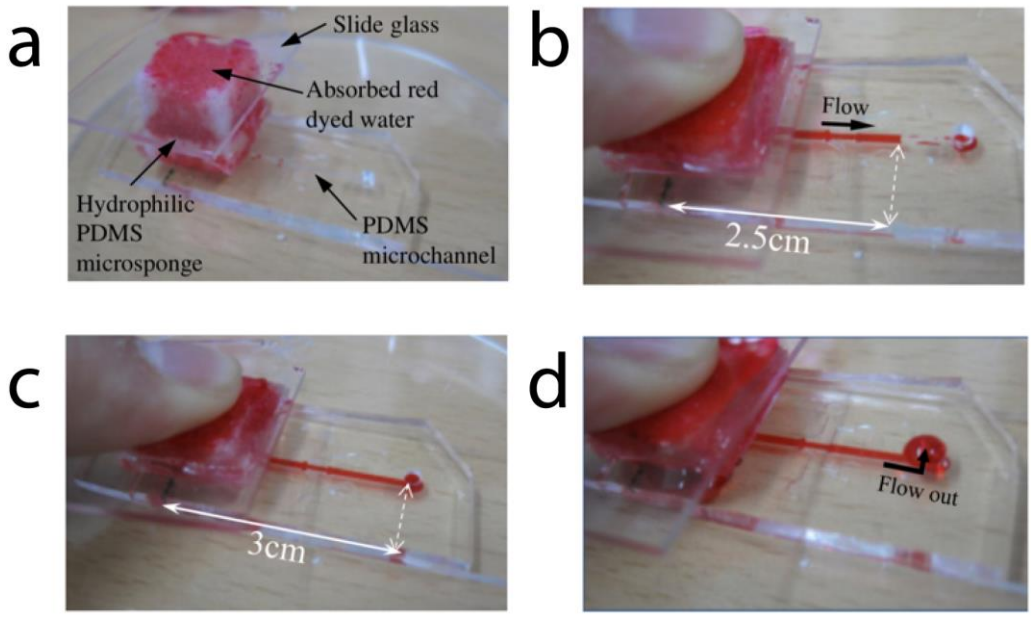

Figure 1.12: A portable, integrated pressure pump utilising a porous PDMS sponge and manual compression. **a)** A porous PDMS sponge is loaded with red stained water and interfaced with a PDMS. **b-d)** Show the stored liquid being pumped though the PDMS channel via manual compression of the sponge. Figure adapted from reference [85].

Sugar templated sponges have also been used for the selective absorption of various oils from water. Choi *et al*., [87] showed that a drop of water will remain on the surface of a sugar templated PDMS sponge due to its hydrophobicity whereas a droplet of oil will be immediately absorbed into the sponge due to its oleophilicity as shown in **Figure 1.13**. This selectivity has been used for the absorption of a layer of oil floating on water. The oil filled sponge can then be removed and squeezed to eject the stored oil enabling the reuse of the sponge. This concept has been used by Zhao *et al*., [88] to absorb oil within a tube to block oil leakage. This is facilitated by the absorption of oil into the sponge causing it to swell and seal the pipe.

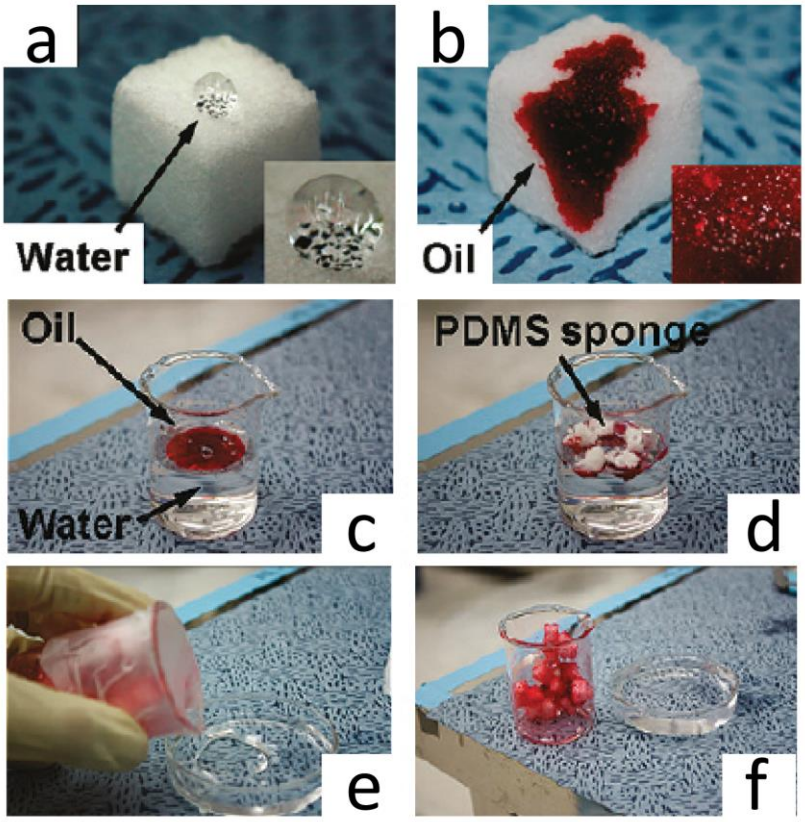

Figure 1.13: Porous PDMS sponges used as a filter to selectively absorb oil. **a)** Hydrophobic properties of the sponge. **b)** Oleophilic properties of the sponge. **c-f)** The selective absorption of oil from water. Figure adapted from reference [87].

Despite the simplicity of this fabrication method, this method does not provide control over the size and distribution of the pores.

A closer look at **Table 1.3** reveals the possibility for fabricating porous polymer structures though the injection of sacrificial micro droplets into an uncured polymer matrix, forming a high internal phase emulsion (HIPE). Once the polymer is cured and the sacrificial droplets are removed, revealing a highly ordered porous polymer network (polyHIPE).

Costantini *et al*., [83] presents a highly porous polymer structure by injecting micro droplets of cyclohexane into uncured dextran-methacrylate (DEX-MA) using a flow focusing microfluidic chip, as shown in **Figure 1.14**. The resulting cyclohexane/DEX-MA emulsion is collected in glass tubes. The DEX-MA was then crosslinked and the cyclohexane was washed out resulting in a highly ordered polymer network. By changing the flow rates of the two phases, the size of the pores can be easy adjusted. Despite these advantages such polyHIPEs have not been used for the storage and release of aqueous solutions, enabling self-sufficient microfluidic systems.

The ability for highly porous PDMS sponges for the storage and release of solutions makes them highly suitable for fabricating versatile, self-sufficient microfluidic systems, with the ability to control the porous structure of the sponge, which has been the motivation of this thesis, as further discussed in **Section 1.3**.

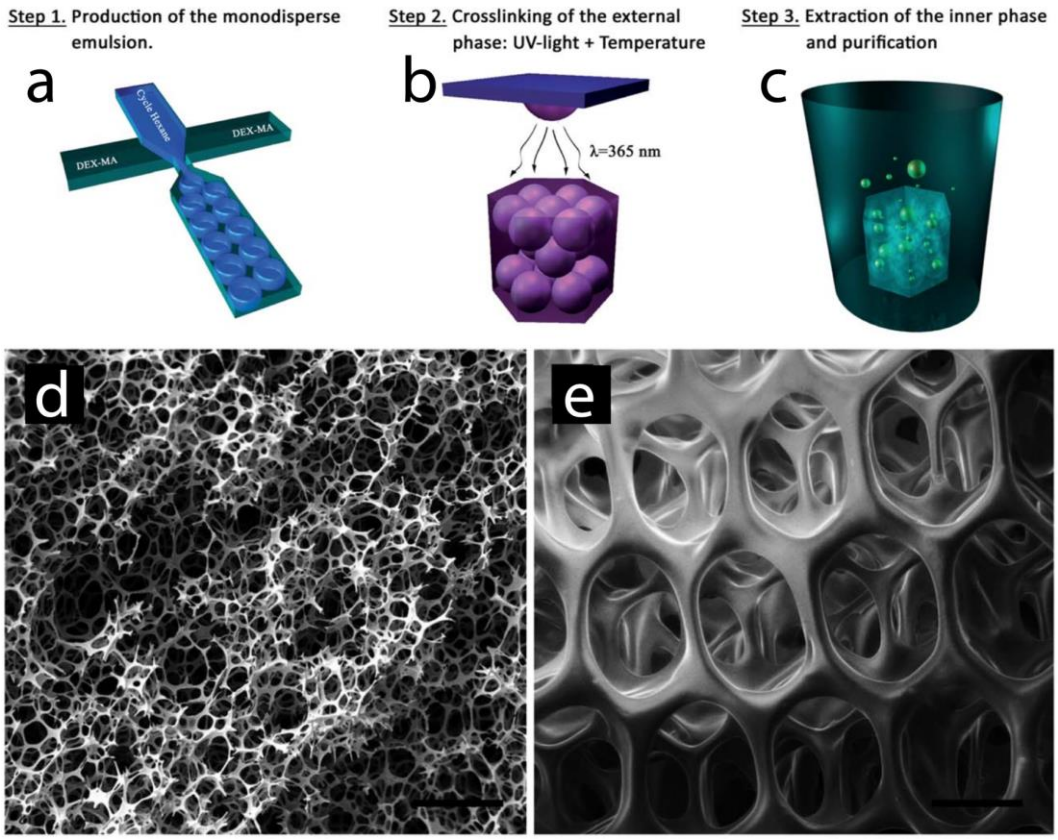

Figure 1.14: Tunable polyHIPEs using microfluidics. **a)** A microfluidic flow focusing chip is used to generate droplets of cyclohexane in an external phase of dextran-methacrylate (DEX-MA) to form a HIPE. **b)** The DEX-MA is crosslinked using UV light and temperature. **c)** The internal phase is removed using a polar solvent. **d-e)** SEM images of the resulting porous hydrogel polyHIPE. Scale bar is 30 µm. Figure adapted from reference [83].

1.5 Motivation:

Motivation 1: Self-sufficient standalone microfluidic systems for the storage and release of solutions:

Typical microfluidic systems enable the storage, driving and control of liquids in micro-scale structures. However, the operation of such systems is heavily reliant on external off-chip supporting equipment, such as pumps, tubes, and valves, which limits their utility for end-users who are not necessarily specialised in microfluidics or do not have access to such facilities. This is particularly important for the development of more complex point-of-care diagnostic devices. This motivated me to create a self-sufficient, stand-alone microfluidic device enabling the passive and manually operated storage and release of biological agents to facilitate cellular assays.

Motivation 2: Self-sufficient micro-droplet generation systems for cellular assays:

Microfluidic droplet generation systems facilitate the generation of micro-scale droplets, which have been extensively used for the encapsulation of cells. However, such systems rely on microfluidic structures, bulky and rather expensive supporting equipment such as pumps. More importantly the operation of such systems relies on specialised training and time-consuming processes. These drawbacks limit their widespread usage in biological laboratories. This motivated me to develop a self-sufficient micro-droplet generation systems, which can be used for encapsulation, chemical stimulation, and monitoring of cells.

1.6 Research Questions

Motivation 1 described in **Section 1.2** led to the following three research questions that are addressed in **Chapter 2**.

Research Question 1: Can a highly porous PDMS sponge be fabricated and utilised for the release of stored aqueous solutions?

This can be divided into the following three sub-questions:

- Can a porous PDMS sponge be manually loaded with aqueous solutions due to its elasticity and porosity?
- Can the stored solutions be released passively released into a surrounding liquid environment?
- Can the passive release characteristics of the sponge be modulated by varying the porous structure of the sponge?

Research Question 2: Can this highly porous PDMS sponge be utilised for conducting cellular assays?

This can be divided into the following two sub-questions:

- Can the PDMS sponge be used for the passive release of stored solutions into biologically relevant structures such as Petri dishes or multi-well plates or is it just limited to for microfluidic channels?
- Does the sponge enable the chemical stimulation of cells passively?

Research Question 3: Can this highly porous PDMS sponge be used for the active release of stored chemicals?

This can be divided into the following two sub-questions:

- Can the sponge me integrated into a microfluidic structure serving as active reservoir/valve at the same time?
- Is the active release characteristics of the PDMS sponge controllable and repeatable?

Motivation 2 described in **Section 1.2** led to the following three research questions that are addressed in **Chapter 3**.

Research Question 4: Can this highly porous PDMS sponge be utilised for the generation of micro-scale droplets of aqueous solutions without the need for traditional microfluidic support equipment such as syringe pumps?

This can be divided into the following three sub-questions:

- What carrier liquid provides suitable conditions for pinching off droplets?
- Are the droplets mechanically stable (do not coalesce following release)?
- Do the generated droplets have a predictable size and volume distribution?

Research Question 5: Can this highly porous PDMS sponge be utilised for the encapsulation of cells inside droplets?

This can be divided into the following five sub-questions:

- Can the droplets be filled with cell suspension to enable the generation of droplets carrying encapsulated cells?
- Do encapsulated cells remain stable and viable?
- Is there a relation between number of encapsulated cells and the parameters such as the size of the droplets, concentration of cells?
- What parameters determine the number of cells inside each droplet?
- Does the sponge enable the generation of customized cell clusters ranging from single, to multiple cells?

Research Question 6: Can the droplets be containing cells be used as "micro-Petri dishes" facilitating the chemical stimulation and microscope imaging of encapsulated cells?

This can be divided into the following four sub-questions:

- Can the droplets be loaded with chemicals, agents, and fluorescent probes to enable cellular assays?
- Are the settled cells stable enough to be easily monitored using inverted microscopy without software based tracking techniques?
- Does this encapsulation method enable the settling and monitoring of highly motile cells?
- Does this enable highly parallel cellular assays to be conducted?

1.7 Thesis Layout

This research aimed to investigate the self-sufficient microfluidic systems capable of the storage and release of solutions to facilitate cellular assays. The contents of my thesis are outlined below:

Chapter 1 presents a brief literature review of current microfluidic systems and their limitations in terms of operation, which motivated me to conduct this research.

Chapter 2 presents a porous sponge made of PDMS, which was fabricated by templating micro-scale water droplets using a T-junction microfluidic structure. The sponge contains a network of pores, interconnected by small holes. This unique structure enables the sponge to passively release stored solutions very slowly. Proof-of-concept experiments demonstrated that the sponge can be used for the passive release of stored solutions into narrow channels and circular well plates, with the latter used for inducing intracellular calcium signaling of immobilised endothelial cells. The sponge can also actively release stored solutions into microfluidic channels though the controlled compression of the sponge.

Chapter 3 presents a new droplet generation system using porous PDMS sponges, which enables the creation of hundreds of isolated micro-scale droplets containing cells and desired chemicals inside a well. These droplets can be considered isolated ‘micro-Petri dishes’, as they are chemically isolated, mechanically stable, and do not evaporate, due to the presence of oil in the well. These ‘micro-Petri dishes’ are generated manually in a quick and simple manner, and therefore can be easily used in biological laboratories to investigate various

cellular and molecular studies in a parallel manner, with minimum supportive equipment and microfluidic skills.

Chapter 4 presents concluding remarks and recommendations for future work.

1.8 References

[1] G. M. Whitesides, "The origins and the future of microfluidics," *Nature*, 10.1038/nature05058 vol. 442, no. 7101, pp. 368-373, 07/27/print 2006.

[2] T. M. Squires and S. R. Quake, "Microfluidics: Fluid physics at the nanoliter scale," *Reviews of Modern Physics*, vol. 77, no. 3, pp. 977-1026, 10/06/2005 2005.

[3] C. Szydzik *et al.*, "An automated optofluidic biosensor platform combining interferometric sensors and injection moulded microfluidics," *Lab on a Chip*, 10.1039/C7LC00524E vol. 17, no. 16, pp. 2793-2804, 2017.

[4] M. Boyd-Moss, S. Baratchi, M. Di Venere, and K. Khoshmanesh, "Self-contained microfluidic systems: a review," *Lab on a Chip*, 10.1039/C6LC00712K vol. 16, no. 17, pp. 3177-3192, 2016.

[5] I. K. Dimov, L. Basabe-Desmonts, J. L. Garcia-Cordero, B. M. Ross, A. J. Ricco, and L. P. Lee, "Stand-alone self-powered integrated microfluidic blood analysis system (SIMBAS)," *Lab on a Chip*, 10.1039/C0LC00403K vol. 11, no. 5, pp. 845-850, 2011.

[6] S. Smith, R. Sewart, H. Becker, P. Roux, and K. Land, "Blister pouches for effective reagent storage on microfluidic chips for blood cell counting," *Microfluidics and Nanofluidics*, journal article vol. 20, no. 12, p. 163, November 23 2016.

[7] P. Garstecki, M. J. Fuerstman, M. A. Fischbach, S. K. Sia, and G. M. Whitesides, "Mixing with bubbles: a practical technology for use with portable microfluidic devices," *Lab on a Chip*, 10.1039/B510843H vol. 6, no. 2, pp. 207-212, 2006.

[8] A. R. Abate and D. A. Weitz, "Syringe-vacuum microfluidics: A portable technique to create monodisperse emulsions," *Biomicrofluidics*, vol. 5, no. 1, p. 014107, 2011.

[9] K. Han, Y.-J. Yoon, Y. Shin, and M. K. Park, "Self-powered switch-controlled nucleic acid extraction system," *Lab on a Chip*, 10.1039/C5LC00891C vol. 16, no. 1, pp. 132-141, 2016.

[10] T. Kokalj, Y. Park, M. Vencelj, M. Jenko, and L. P. Lee, "Self-powered Imbibing Microfluidic Pump by Liquid Encapsulation: SIMPLE," *Lab on a Chip,* 10.1039/C4LC00920G vol. 14, no. 22, pp. 4329-4333, 2014.

[11] F. Stumpf *et al.*, "LabDisk with complete reagent prestorage for sample-to-answer nucleic acid based detection of respiratory pathogens verified with influenza A H3N2 virus," *Lab on a Chip,* 10.1039/C5LC00871A vol. 16, no. 1, pp. 199-207, 2016.

[12] M. Focke, F. Stumpf, G. Roth, R. Zengerle, and F. von Stetten, "Centrifugal microfluidic system for primary amplification and secondary real-time PCR," *Lab on a Chip,* 10.1039/C0LC00161A vol. 10, no. 23, pp. 3210-3212, 2010.

[13] K. A. Addae-Mensah, Y. K. Cheung, V. Fekete, M. S. Rendely, and S. K. Sia, "Actuation of elastomeric microvalves in point-of-care settings using handheld, battery-powered instrumentation," *Lab on a Chip,* 10.1039/C002349C vol. 10, no. 12, pp. 1618-1622, 2010.

[14] F. Truffer *et al.*, "Compact portable biosensor for arsenic detection in aqueous samples with Escherichia coli bioreporter cells," *Review of Scientific Instruments,* vol. 85, no. 1, p. 015120, 2014.

[15] N. Futai, W. Gu, J. W. Song, and S. Takayama, "Handheld recirculation system and customized media for microfluidic cell culture," *Lab on a Chip,* 10.1039/B510901A vol. 6, no. 1, pp. 149-154, 2006.

[16] J. Akagi *et al.*, "Fish on chips: Microfluidic living embryo array for accelerated in vivo angiogenesis assays," *Sensors and Actuators B: Chemical,* vol. 189, no. Supplement C, pp. 11-20, 2013/12/01/ 2013.

[17] D. Erickson, D. Sinton, and D. Li, "A miniaturized high-voltage integrated power supply for portable microfluidic applications," *Lab on a Chip,* 10.1039/B316916B vol. 4, no. 2, pp. 87-90, 2004.

[18] Y. Oyama *et al.*, "A glass fiber sheet-based electroosmotic lateral flow immunoassay for point-of-care testing," *Lab on a Chip,* 10.1039/C2LC40994A vol. 12, no. 24, pp. 5155-5159, 2012.

[19] B. Li *et al.*, "A smartphone controlled handheld microfluidic liquid handling system," *Lab on a Chip,* 10.1039/C4LC00227J vol. 14, no. 20, pp. 4085-4092, 2014.

[20] M. K. Tan, L. Y. Yeo, and J. R. Friend, "Rapid fluid flow and mixing induced in microchannels using surface acoustic waves," *EPL (Europhysics Letters),* vol. 87, no. 4, p. 47003, 2009.

[21] M. Zimmermann, H. Schmid, P. Hunziker, and E. Delamarche, "Capillary pumps for autonomous capillary systems," *Lab on a Chip,* 10.1039/B609813D vol. 7, no. 1, pp. 119-125, 2007.

[22] J. Nunes, S. Tsai, J. Wan, and H. Stone, "Dripping and jetting in microfluidic multiphase flows applied to particle and fibre synthesis," *Journal of physics D: Applied physics,* vol. 46, no. 11, p. 114002, 2013.

[23] L. Li and R. F. Ismagilov, "Protein Crystallization Using Microfluidic Technologies Based on Valves, Droplets, and SlipChip," *Annual Review of Biophysics,* vol. 39, no. 1, pp. 139-158, 2010.

[24] B. Gol *et al.*, "Continuous transfer of liquid metal droplets across a fluid-fluid interface within an integrated microfluidic chip," *Lab on a Chip,* 10.1039/C5LC00415B vol. 15, no. 11, pp. 2476-2485, 2015.

[25] W. Wang *et al.*, "Controllable microfluidic production of multicomponent multiple emulsions," *Lab on a Chip,* 10.1039/C1LC20065H vol. 11, no. 9, pp. 1587-1592, 2011.

[26] R. Zilionis *et al.*, "Single-cell barcoding and sequencing using droplet microfluidics," *Nat. Protocols,* Protocol vol. 12, no. 1, pp. 44-73, 01//print 2017.

[27] J.-C. Baret *et al.*, "Fluorescence-activated droplet sorting (FADS): efficient microfluidic cell sorting based on enzymatic activity," *Lab on a Chip,* 10.1039/B902504A vol. 9, no. 13, pp. 1850-1858, 2009.

[28] W. Shi, J. Qin, N. Ye, and B. Lin, "Droplet-based microfluidic system for individual Caenorhabditis elegans assay," *Lab on a Chip,* 10.1039/B808753A vol. 8, no. 9, pp. 1432-1435, 2008.

[29] S.-Y. Tang *et al.*, "Liquid-Metal Microdroplets Formed Dynamically with Electrical Control of Size and Rate," *Advanced Materials,* vol. 28, no. 4, pp. 604-609, 2016.

[30] P. Abbyad, R. Dangla, A. Alexandrou, and C. N. Baroud, "Rails and anchors: guiding and trapping droplet microreactors in two dimensions," *Lab on a Chip,* 10.1039/C0LC00104J vol. 11, no. 5, pp. 813-821, 2011.

[31] I. Leibacher, P. Reichert, and J. Dual, "Microfluidic droplet handling by bulk acoustic wave (BAW) acoustophoresis," *Lab on a Chip,* 10.1039/C5LC00083A vol. 15, no. 13, pp. 2896-2905, 2015.

[32] B. Gol, M. E. Kurdzinski, F. J. Tovar-Lopez, P. Petersen, A. Mitchell, and K. Khoshmanesh, "Hydrodynamic directional control of liquid metal droplets within a microfluidic flow focusing system," *Applied Physics Letters,* vol. 108, no. 16, p. 164101, 2016.

[33] X. Niu, S. Gulati, J. B. Edel, and A. J. deMello, "Pillar-induced droplet merging in microfluidic circuits," *Lab on a Chip,* 10.1039/B813325E vol. 8, no. 11, pp. 1837-1841, 2008.

[34] Y.-C. Tan, Y. L. Ho, and A. P. Lee, "Droplet coalescence by geometrically mediated flow in microfluidic channels," *Microfluidics and Nanofluidics,* journal article vol. 3, no. 4, pp. 495-499, August 01 2007.

[35] M. Zagnoni and J. M. Cooper, "On-chip electrocoalescence of microdroplets as a function of voltage, frequency and droplet size," *Lab on a Chip,* 10.1039/B906298J vol. 9, no. 18, pp. 2652-2658, 2009.

[36] M. Zagnoni and J. M. Cooper, "A microdroplet-based shift register," *Lab on a Chip,* 10.1039/C0LC00219D vol. 10, no. 22, pp. 3069-3073, 2010.

[37] S. H. Jin, H.-H. Jeong, B. Lee, S. S. Lee, and C.-S. Lee, "A programmable microfluidic static droplet array for droplet generation, transportation, fusion, storage, and retrieval," *Lab on a Chip,* 10.1039/C5LC00651A vol. 15, no. 18, pp. 3677-3686, 2015.

[38] J. D. Tice, H. Song, A. D. Lyon, and R. F. Ismagilov, "Formation of Droplets and Mixing in Multiphase Microfluidics at Low Values of the

Reynolds and the Capillary Numbers," *Langmuir*, vol. 19, no. 22, pp. 9127-9133, 2003/10/01 2003.

[39] A. R. Abate, T. Hung, P. Mary, J. J. Agresti, and D. A. Weitz, "High-throughput injection with microfluidics using picoinjectors," *Proceedings of the National Academy of Sciences*, vol. 107, no. 45, pp. 19163-19166, November 9, 2010 2010.

[40] K. Maeda, H. Onoe, M. Takinoue, and S. Takeuchi, "Controlled Synthesis of 3D Multi-Compartmental Particles with Centrifuge-Based Microdroplet Formation from a Multi-Barrelled Capillary," *Advanced Materials*, vol. 24, no. 10, pp. 1340-1346, 2012.

[41] R. K. Shah, J.-W. Kim, and D. A. Weitz, "Janus Supraparticles by Induced Phase Separation of Nanoparticles in Droplets," *Advanced Materials*, vol. 21, no. 19, pp. 1949-1953, 2009.

[42] S.-H. Kim, A. Abbaspourrad, and D. A. Weitz, "Amphiphilic Crescent-Moon-Shaped Microparticles Formed by Selective Adsorption of Colloids," *Journal of the American Chemical Society*, vol. 133, no. 14, pp. 5516-5524, 2011/04/13 2011.

[43] Y. Zhao *et al.*, "Multifunctional photonic crystal barcodes from microfluidics," *NPG Asia Mater*, vol. 4, p. e25, 09/07/online 2012.

[44] S. Xu *et al.*, "Generation of Monodisperse Particles by Using Microfluidics: Control over Size, Shape, and Composition," *Angewandte Chemie International Edition*, vol. 44, no. 5, pp. 724-728, 2005.

[45] D. K. Hwang, D. Dendukuri, and P. S. Doyle, "Microfluidic-based synthesis of non-spherical magnetic hydrogel microparticles," *Lab on a Chip*, 10.1039/B805176C vol. 8, no. 10, pp. 1640-1647, 2008.

[46] A. Fang, C. Gaillard, and J.-P. Douliez, "Template-Free Formation of Monodisperse Doughnut-Shaped Silica Microparticles by Droplet-Based Microfluidics," *Chemistry of Materials*, vol. 23, no. 21, pp. 4660-4662, 2011/11/08 2011.

[47] K. Shin-Hyun, S. Jae Won, L. Jong-Min, L. Su Yeon, and Y. Seung-Man, "Microfluidic fabrication of microparticles with structural complexity

using photocurable emulsion droplets," *New Journal of Physics,* vol. 11, no. 7, p. 075014, 2009.

[48] Z. Nie, J. I. Park, W. Li, S. A. F. Bon, and E. Kumacheva, "An “Inside-Out” Microfluidic Approach to Monodisperse Emulsions Stabilized by Solid Particles," *Journal of the American Chemical Society,* vol. 130, no. 49, pp. 16508-16509, 2008/12/10 2008.

[49] H. Hwang, S.-H. Kim, and S.-M. Yang, "Microfluidic fabrication of SERS-active microspheres for molecular detection," *Lab on a Chip,* 10.1039/C0LC00125B vol. 11, no. 1, pp. 87-92, 2011.

[50] T. Konry, M. Dominguez-Villar, C. Baecher-Allan, D. A. Hafler, and M. L. Yarmush, "Droplet-based microfluidic platforms for single T cell secretion analysis of IL-10 cytokine," *Biosensors and Bioelectronics,* vol. 26, no. 5, pp. 2707-2710, 2011/01/15/ 2011.

[51] V. Chokkalingam *et al.*, "Probing cellular heterogeneity in cytokine-secreting immune cells using droplet-based microfluidics," *Lab on a Chip,* 10.1039/C3LC50945A vol. 13, no. 24, pp. 4740-4744, 2013.

[52] E. Brouzes *et al.*, "Droplet microfluidic technology for single-cell high-throughput screening," *Proceedings of the National Academy of Sciences,* vol. 106, no. 34, pp. 14195-14200, August 25, 2009 2009.

[53] L. Mazutis, J. Gilbert, W. L. Ung, D. A. Weitz, A. D. Griffiths, and J. A. Heyman, "Single-cell analysis and sorting using droplet-based microfluidics," *Nat. Protocols,* Protocol vol. 8, no. 5, pp. 870-891, 05//print 2013.

[54] M. Hosokawa, Y. Nishikawa, M. Kogawa, and H. Takeyama, "Massively parallel whole genome amplification for single-cell sequencing using droplet microfluidics," *Scientific Reports,* vol. 7, no. 1, p. 5199, 2017/07/12 2017.

[55] S. S. Terekhov *et al.*, "Microfluidic droplet platform for ultrahigh-throughput single-cell screening of biodiversity," *Proceedings of the National Academy of Sciences,* vol. 114, no. 10, pp. 2550-2555, March 7, 2017 2017.

[56] B. L. Wang *et al.*, "Microfluidic high-throughput culturing of single cells for selection based on extracellular metabolite production or consumption," *Nat Biotech,* Research vol. 32, no. 5, pp. 473-478, 05//print 2014.

[57] J. Pan *et al.*, "Quantitative tracking of the growth of individual algal cells in microdroplet compartments," *Integrative Biology,* 10.1039/C1IB00033K vol. 3, no. 10, pp. 1043-1051, 2011.

[58] Y. Zhan, J. Wang, N. Bao, and C. Lu, "Electroporation of Cells in Microfluidic Droplets," *Analytical Chemistry,* vol. 81, no. 5, pp. 2027-2031, 2009/03/01 2009.

[59] A. C. Madison *et al.*, "Scalable Device for Automated Microbial Electroporation in a Digital Microfluidic Platform," *ACS Synthetic Biology,* vol. 6, no. 9, pp. 1701-1709, 2017/09/15 2017.

[60] F. Chen, Y. Zhan, T. Geng, H. Lian, P. Xu, and C. Lu, "Chemical Transfection of Cells in Picoliter Aqueous Droplets in Fluorocarbon Oil," *Analytical Chemistry,* vol. 83, no. 22, pp. 8816-8820, 2011/11/15 2011.

[61] A. C. Larsen, M. R. Dunn, A. Hatch, S. P. Sau, C. Youngbull, and J. C. Chaput, "A general strategy for expanding polymerase function by droplet microfluidics," Article vol. 7, p. 11235, 04/05/online 2016.

[62] P.-Y. Colin *et al.*, "Ultrahigh-throughput discovery of promiscuous enzymes by picodroplet functional metagenomics," Article vol. 6, p. 10008, 12/07/online 2015.

[63] R. Zilionis *et al.*, "Single-cell barcoding and sequencing using droplet microfluidics," *Nature Protocols,* vol. 12, no. 1, pp. 44-73, 2017.

[64] A. Huebner *et al.*, "Quantitative detection of protein expression in single cells using droplet microfluidics," *Chemical Communications,* 10.1039/B618570C no. 12, pp. 1218-1220, 2007.

[65] M. S. Silverstein, "PolyHIPEs: Recent advances in emulsion-templated porous polymers," *Progress in Polymer Science,* vol. 39, no. 1, pp. 199-234, 1// 2014.

[66] Y. Li *et al.*, "Cellulose Sponge Supported Palladium Nanoparticles as Recyclable Cross-Coupling Catalysts," *ACS Applied Materials & Interfaces*, vol. 9, no. 20, pp. 17155-17162, 2017/05/24 2017.

[67] H. Zhang *et al.*, "Piezoresistive Sensor with High Elasticity Based on 3D Hybrid Network of Sponge@CNTs@Ag NPs," *ACS Applied Materials & Interfaces*, vol. 8, no. 34, pp. 22374-22381, 2016/08/31 2016.

[68] Y.-h. Wu *et al.*, "Channel Crack-Designed Gold@PU Sponge for Highly Elastic Piezoresistive Sensor with Excellent Detectability," *ACS Applied Materials & Interfaces*, vol. 9, no. 23, pp. 20098-20105, 2017/06/14 2017.

[69] L. Xu *et al.*, "Breathing Demulsification: A Three-Dimensional (3D) Free-Standing Superhydrophilic Sponge," *ACS Applied Materials & Interfaces*, vol. 7, no. 40, pp. 22264-22271, 2015/10/14 2015.

[70] X.-c. Chen *et al.*, "Self-Healing Spongy Coating for Drug “Cocktail” Delivery," *ACS Applied Materials & Interfaces*, vol. 8, no. 7, pp. 4309-4313, 2016/02/24 2016.

[71] M. C. Ford *et al.*, "A macroporous hydrogel for the coculture of neural progenitor and endothelial cells to form functional vascular networks invivo," *Proceedings of the National Academy of Sciences of the United States of America*, vol. 103, no. 8, pp. 2512-2517, February 21, 2006 2006.

[72] C. Ji, N. Annabi, A. Khademhosseini, and F. Dehghani, "Fabrication of porous chitosan scaffolds for soft tissue engineering using dense gas CO2," *Acta Biomaterialia*, vol. 7, no. 4, pp. 1653-1664, 2011/04/01/ 2011.

[73] N. Kobayashi, H. Miyaji, T. Sugaya, and M. Kawanami, "Bone Augmentation by Implantation of an FGF2-loaded Collagen Gel-sponge Composite Scaffold," *Journal of Oral Tissue Engineering*, vol. 8, no. 2, pp. 91-101, 2010.

[74] X. Yang, L. Tan, L. Xia, C. D. Wood, and B. Tan, "Hierarchical Porous Polystyrene Monoliths from PolyHIPE," *Macromolecular Rapid Communications,* vol. 36, no. 17, pp. 1553-1558, 2015.

[75] Q. Wang, Y. Liu, J. Chen, Z. Du, and J. Mi, "Control of Uniform and Interconnected Macroporous Structure in PolyHIPE for Enhanced CO2 Adsorption/Desorption Kinetics," *Environmental Science & Technology,* vol. 50, no. 14, pp. 7879-7888, 2016/07/19 2016.

[76] M. Alikhani and M. R. Moghbeli, "Ion-exchange polyHIPE type membrane for removing nitrate ions: Preparation, characterization, kinetics and adsorption studies," *Chemical Engineering Journal,* vol. 239, no. Supplement C, pp. 93-104, 2014/03/01/ 2014.

[77] S. Huš, M. Kolar, and P. Krajnc, "Separation of heavy metals from water by functionalized glycidyl methacrylate poly (high internal phase emulsions)," *Journal of Chromatography A,* vol. 1437, no. Supplement C, pp. 168-175, 2016/03/11/ 2016.

[78] E. Yüce *et al.*, "Photocatalytic Activity of Titania/Polydicyclopentadiene PolyHIPE Composites," *Macromolecular Materials and Engineering,* vol. 302, no. 10, pp. 1700091-n/a, 2017, Art. no. 1700091.

[79] C. Zhao, E. Danish, N. R. Cameron, and R. Kataky, "Emulsion-templated porous materials (PolyHIPEs) for selective ion and molecular recognition and transport: applications in electrochemical sensing," *Journal of Materials Chemistry,* 10.1039/B700929A vol. 17, no. 23, pp. 2446-2453, 2007.

[80] U. M. Patil *et al.*, "PolyHIPE Derived Freestanding 3D Carbon Foam for Cobalt Hydroxide Nanorods Based High Performance Supercapacitor," Article vol. 6, p. 35490, 10/20/online 2016.

[81] E. Erhan, E. Yer, G. Akay, B. Keskinler, and D. Keskinler, "Phenol degradation in a fixed-bed bioreactor using micro-cellular polymer-immobilized Pseudomonas syringae," *Journal of Chemical Technology & Biotechnology,* vol. 79, no. 2, pp. 195-206, 2004.

[82] R. Moglia, M. Whitely, M. Brooks, J. Robinson, M. Pishko, and E. Cosgriff-Hernandez, "Solvent-Free Fabrication of polyHIPE Microspheres for Controlled Release of Growth Factors," *Macromolecular Rapid Communications,* vol. 35, no. 14, pp. 1301-1305, 2014.

[83] M. Costantini *et al.*, "Highly ordered and tunable polyHIPEs by using microfluidics," *Journal of Materials Chemistry B,* 10.1039/C3TB21227K vol. 2, no. 16, pp. 2290-2300, 2014.

[84] E. K. Sackmann, A. L. Fulton, and D. J. Beebe, "The present and future role of microfluidics in biomedical research," *Nature,* Review vol. 507, no. 7491, pp. 181-189, 03/13/print 2014.

[85] W. Yang, Y. G. Nam, B.-K. Lee, K. Han, T. H. Kwon, and D. S. Kim, "Fabrication of a Hydrophilic Poly (dimethylsiloxane) Microporous Structure and Its Application to Portable Microfluidic Pump," *Japanese Journal of Applied Physics,* vol. 49, no. 6S, p. 06GM01, 2010.

[86] K. J. Cha and D. S. Kim, "A portable pressure pump for microfluidic lab-on-a-chip systems using a porous polydimethylsiloxane (PDMS) sponge," *Biomedical Microdevices,* journal article vol. 13, no. 5, p. 877, June 23 2011.

[87] S.-J. Choi *et al.*, "A Polydimethylsiloxane (PDMS) Sponge for the Selective Absorption of Oil from Water," *ACS Applied Materials & Interfaces,* vol. 3, no. 12, pp. 4552-4556, 2011/12/28 2011.

[88] X. Zhao, L. Li, B. Li, J. Zhang, and A. Wang, "Durable superhydrophobic/superoleophilic PDMS sponges and their applications in selective oil absorption and in plugging oil leakages," *Journal of Materials Chemistry A,* vol. 2, no. 43, pp. 18281-18287, 2014.

[89] D. N. H. Tran, S. Kabiri, T. R. Sim, and D. Losic, "Selective adsorption of oil-water mixtures using polydimethylsiloxane (PDMS)-graphene sponges," *Environmental Science: Water Research & Technology,* 10.1039/C5EW00035A vol. 1, no. 3, pp. 298-305, 2015.

[90] A. Zhang, M. Chen, C. Du, H. Guo, H. Bai, and L. Li, "Poly(dimethylsiloxane) Oil Absorbent with a Three-Dimensionally Interconnected Porous Structure and Swellable Skeleton," *ACS Applied Materials & Interfaces,* vol. 5, no. 20, pp. 10201-10206, 2013/10/23 2013.

[91] C.-F. Wang and S.-J. Lin, "Robust Superhydrophobic/Superoleophilic Sponge for Effective Continuous Absorption and Expulsion of Oil Pollutants from Water," *ACS Applied Materials & Interfaces,* vol. 5, no. 18, pp. 8861-8864, 2013/09/25 2013.

[92] A. A. Chavan *et al.*, "Elastomeric Nanocomposite Foams for the Removal of Heavy Metal Ions from Water," *ACS Applied Materials & Interfaces,* vol. 7, no. 27, pp. 14778-14784, 2015/07/15 2015.

[93] J.-W. Han, B. Kim, J. Li, and M. Meyyappan, "Flexible, compressible, hydrophobic, floatable, and conductive carbon nanotube-polymer sponge," *Applied Physics Letters,* vol. 102, no. 5, p. 051903, 2013.

[94] W. Liu *et al.*, "3D Porous Sponge-Inspired Electrode for Stretchable Lithium-Ion Batteries," *Advanced Materials,* vol. 28, no. 18, pp. 3578-3583, 2016.

[95] S. Liang *et al.*, "3D Stretchable, Compressible, and Highly Conductive Metal-Coated Polydimethylsiloxane Sponges," *Advanced Materials Technologies,* vol. 1, no. 7, pp. 1600117-n/a, 2016, Art. no. 1600117.

[96] S. Liang *et al.*, "Liquid metal sponges for mechanically durable, all-soft, electrical conductors," *Journal of Materials Chemistry C,* vol. 5, no. 7, pp. 1586-1590, 2017.

[97] K. Jiao, C. L. Graham, J. Wolff, R. G. Iyer, and P. Kohli, "Modulating molecular and nanoparticle transport in flexible polydimethylsiloxane membranes," *Journal of membrane science,* vol. 401-402, pp. 25-32, 2012.

[98] K. Zimny, A. Merlin, A. Ba, C. Aristégui, T. Brunet, and O. Mondain-Monval, "Soft Porous Silicone Rubbers as Key Elements for the

Realization of Acoustic Metamaterials," *Langmuir,* vol. 31, no. 10, pp. 3215-3221, 2015/03/17 2015.

[99] J. Li and Y. Zhang, "Porous Polymer Films with Size-Tunable Surface Pores," *Chemistry of Materials,* vol. 19, no. 10, pp. 2581-2584, 2007/05/01 2007.

[100] Q. Li *et al.,* "Engineering of carbon nanotube/polydimethylsiloxane nanocomposites with enhanced sensitivity for wearable motion sensors," *Journal of Materials Chemistry C,* 10.1039/C7TC03434B 2017.

[101] S. Hong *et al.*, "Magnetoactive sponges for dynamic control of microfluidic flow patterns in microphysiological systems," *Lab on a Chip,* 10.1039/C3LC51076J vol. 14, no. 3, pp. 514-521, 2014.

CHAPTER 2: Porous PDMS structures for the storage and release of aqueous solutions into fluidic environments

2.1 Abstract

Typical microfluidic systems take advantage of multiple storage reservoirs, pumps and valves for the storage, driving and release of buffers and other reagents. However, the fabrication, integration, and operation of such components can be difficult. In particular, the reliance of such components on external off-chip equipment limits their utility for creating self-sufficient, stand-alone microfluidic systems. This chapter demonstrates a porous sponge made of polydimethylsiloxane (PDMS), which is fabricated by templating micro-scale water droplets using a T-junction microfluidic structure. High-resolution microscopy reveals that this sponge contains a network of pores, interconnected by small holes. This unique structure enables the sponge to passively release stored solutions very slowly. Proof-of-concept experiments demonstrate that the sponge can be used for the passive release of stored solutions into narrow channels and circular well plates, with the latter used for inducing intracellular calcium signaling of immobilised endothelial cells. The release rate of stored solutions can be controlled by varying the size of interconnecting holes, which can be easily achieved by changing the flow rate of the water injected into the T-junction. The active release of stored liquids into a fluidic channel upon the manual compression of the sponge is also demonstrated. The developed PDMS sponge can be easily integrated into complex micro/macro fluidic systems and prepared with a wide array of reagents, representing a new building block for self-sufficient microfluidic systems.

2.2 Introduction

Microfluidic systems are generally equipped with multiple reservoirs for storing buffers, reagents and drugs. These reservoirs are interconnected to the main channel via narrow channels, which can be opened and closed on-demand using micro-valves. The flow through the main channel is provided by means of a pumping mechanism. While various active mechanisms can be used to actuate the valves and pumps [1, 2, 20], the reliance of active mechanisms on off-chip equipment might limit the effectiveness of the entire microfluidic system to research laboratories. A logical way to address this limitation is to use passive or hand-operated (manual) mechanisms for driving and control of flow through the microfluidic system, which can be fabricated, integrated, replaced and operated with minimum complexities, leading to self-sufficient microfluidic systems [3]. Interconnected porous structures enabling the storage and release of liquids into the surrounding fluidic environment hold a great promise for realising such self-contained microfluidic systems [4, 5].

Polydimethylsiloxane (PDMS) is a silicon elastomer, which is widely used for the fabrication of microfluidic structures [6]. PDMS is generally biocompatible, transparent, flexible, and chemically stable. While PDMS is a gas permeable material [7] it is not porous to liquids. Highly porous PDMS sponges have been created by templating and the subsequent removal of self-assembled colloidal micro/nano particles [8], gas foaming [9], and sugar cubes [10]. Other crystal structured materials such as salt [11], citric acid monohydrate [12], and ice [13] have also been used as a template for making porous PDMS sponges. Among these methods, sugar templating has become very popular due to its simplicity and accessibility. Sugar templated PDMS sponges have been used for selective

adsorption of oil from water [10, 14-16] or adsorption of water for filtering heavy metal ions [14]. Incorporation of conductive materials such as carbon nanotubes [17], metals [18, 19] and liquid metals [20] into the sugar templated porous sponges has been also used for making flexible electrical components and circuits. More interestingly, sugar templated porous sponges have been utilised for the active release of stored solutions upon manual compression [4, 21], enabling a portable pressure pump suitable for self-contained microfluidic systems. However, the utility of sugar templated sponges for the passive release of liquids has not been investigated in these works.

Alternatively, templating of high internal phase emulsions (HIPEs) has been demonstrated as a route for generating highly porous polymers, known as polyHIPEs [22]. Such emulsions are made by dispersing droplets (internal phase) into a polymer solution (external phase). Polymerisation of external phase and the subsequent removal of the internal phase droplets lead to the formation of a highly porous structure with interconnected pores [22], in which the pore size can vary from sub-microns to hundreds of microns [23, 24]. PolyHIPE sponges have been utilised for selective adsorption of liquids [25] and gasses [26], separation of ions [27] and heavy metals [28], chemical sensing [29], energy storage [30] as well as chemical and biochemical reactions [31, 32]. Using microfluidic droplet generation systems, uniformly sized droplets can be continuously generated within a carrier fluid (e.g. water droplets in styrene) [33, 34]. The collection of droplets and carrier fluid inside a chamber leads to formation of an emulsion of droplets in carrier fluid. The polymerisation of carrier fluid (external phase) and the subsequent extraction of the liquid encapsulated within the droplets (internal phase) results in the formation of a

highly ordered polyHIPE. This technique, also known as microfluidic foaming, has been used for making highly porous sponges made of polymers such as dextran-methacrylate [35], alginate [36] and polystyrene [37]. However, the utility of microfluidic foaming for making highly porous PDMS sponges has not been investigated in these works. More importantly, the utility of these sponges for the storage and passive release of liquids have not been studied.

This chapter presents a porous PDMS sponge for the storage and passive release of aqueous solutions into the surrounding liquid environment. The sponge is fabricated by continuous generation of micro-scale water droplets in uncured PDMS using a microfluidic droplet generation system. The PDMS was supplemented with hydroxy group terminations to avoid the coalescence of water droplets. The polymerisation of PDMS and evaporation of water leads to formation of a porous PDMS sponge. High-resolution microscopy indicates that the pores of the sponge are only interconnected via small holes. This unique structure enables the sponge to passively release the stored solutions at a controllable rate, which is governed by the size of the interconnecting holes. Proof-of-concept experiments demonstrate the capability of this PDMS sponge for the passive release of aqueous solutions into narrow channels and circular well plates. The latter is used to induce intracellular calcium signalling of endothelial cells upon the release of chemicals. Furthermore, the active release of dye solution into a microfluidic system upon manual compression was demonstrated. The PDMS sponge can be easily integrated within more complex micro/macro fluidic systems, and thus represents a new building block for PDMS lab-on-a-chip systems.

2.3 Materials and Methods

2.3.1 Fabrication process of the PDMS sponge

In order to fabricate a porous PDMS sponge, a microfluidic droplet generation system (**Figure 2.1a**), as briefly described here was utilised. The droplet generation system consists of a T-junction with cross-sectional dimensions of 300 µm × 300 µm (**Figure 2.1b**) imprinted into PDMS (Sylgard® 184, 10:1 w/w base to curing agent) using soft lithography techniques. The PDMS structure was then peeled off the master, trimmed to size, and punched with 600 µm diameter ports for liquid interfacing. The PDMS structure was then plasma bonded to a glass microscope slide.

Similar to other microfluidic droplet generation systems, this system relies on a discrete liquid to make droplets along with a carrier liquid to pinch off the discrete liquid into small droplets. The discrete liquid was prepared by mixing deionized water with a non-ionic surfactant (Polysorbate 20, Sigma-Aldrich) with a volumetric ratio of 19:1. A small amount of blue dye was then added for producing visual contrast of droplets. The carrier liquid was made of PDMS composite, composed of PDMS base, PDMS curing agent, and monohydroxy terminated PDMS with a molar weight of 4670 (all from Sigma-Aldrich) with a weight ratio of 15:2:5 respectively, and mixed manually for 5 minutes. The PDMS composite was allowed to degas for 30 minutes at room temperature to remove air bubbles introduced by mixing.

A pair of 2 ml syringes (Braun, Germany) were then filled with discrete and carrier liquids and connected to the microfluidic droplet generation system via stainless steel liquid interfaces (21.5 gauge hypodermic needles) and Tygon®

tubing (inner diameter = 0.51 mm). The carrier liquid was applied into the main channel at 20 µl/min while the discrete liquid was applied into the narrow channel at 4 µl/min using two syringe pumps (Harvard Pico Plus). The produced water droplets have a diameter of ~300 µm.

The water droplets and the carrying PDMS composite were discharged from the droplet generation system via Tygon® tubing (**Figure 2.1c**) to be collected in a collection chamber made of poly(methyl methacrylate) (**Figure 2.1d**). It should be noted that while droplets can be generated using standard PDMS, the produced droplets will coalesce shortly after leaving the T-junction. In contrast, the monohydroxy terminated PDMS, used here has ionic charged hydroxy (OH) group terminations, which migrate to the water/PDMS interface forming a negatively charged barrier protecting against droplet coalescence [38-41].

The PDMS composite was then allowed to cure at room temperature for 48 hours. It should be noted that the sample should be cured in a high humidity environment to reduce the effects of water evaporation from the droplets and subsequent shrinkage of the pores. To maintain humidity, the sample was cured in a sealed plastic container that was partially filled with water. During the curing process, the droplets were dispersed randomly within the surrounding PDMS composite (**Figure 2.1e-f**). The droplets rose during the curing process and accumulated at the top free surface of PDMS composite (**Figure 2.1g**), forming a dense network of droplets. The sponge was then squeezed manually to eject the water droplets trapped within the cured sponge, and allowed to dry in the room temperature for 60 minutes. This left a porous PDMS sponge with a dense network of air voids (**Figure 2.1h**).

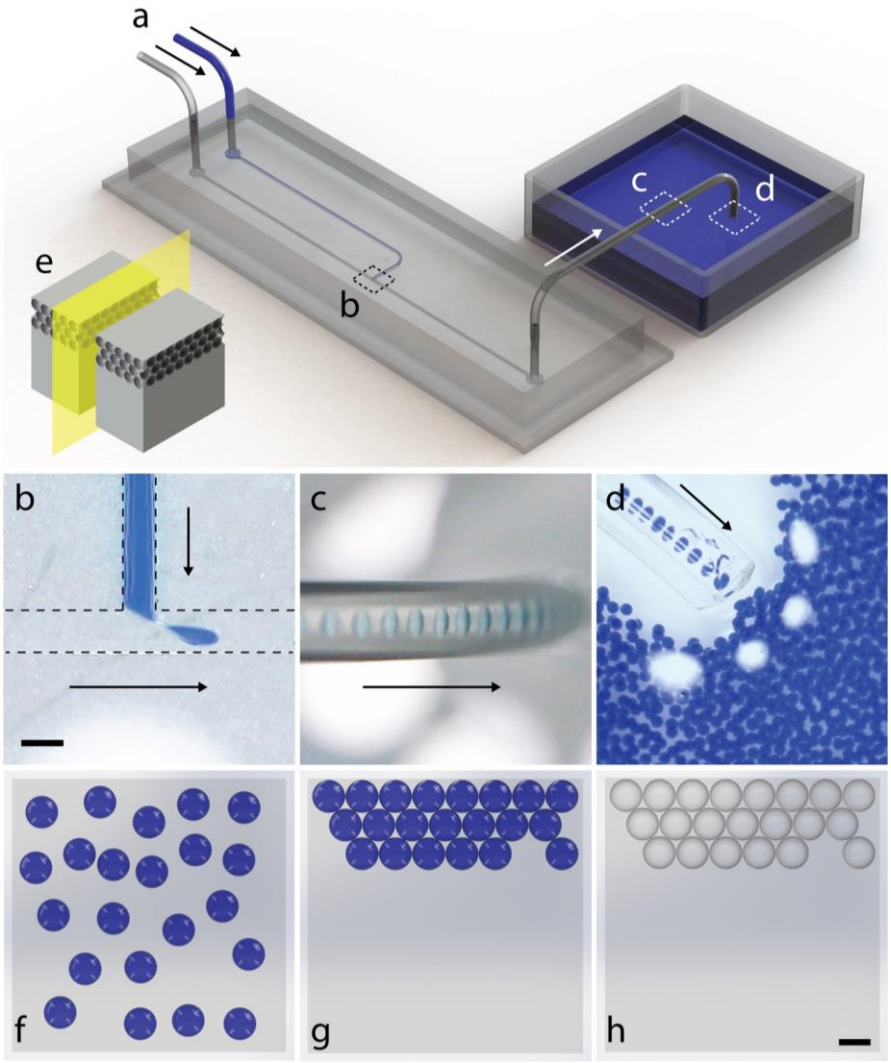

Figure 2.1: Continuous generation of water droplets for the fabrication of porous PDMS structures. **a)** Illustration of the microfluidic droplet generation system. **b)** Microscope image of formation of water droplets within modified PDMS carrier fluid using a microfluidic T-junction with arrows representing flow direction. **c)** Microscope image of continuous flow of water droplets in PDMS through Tygon® tubing. **d)** Microscope image of collection of water droplets in PDMS in the curing reservoir. **e)** A rendering of a section of sponge after curing and drying. **f)** Random arrangement of the droplets within the PDMS. **g)** Illustration of droplet accumulation during the curing process. **h)** Illustration of dried sponge after curing and cleaning. Scale bars are 300 µm.

2.3.2 Characterisation of the PDMS sponge

To characterise the PDMS sponge, a section of the sponge with a diameter of 6 mm and a height of 8 mm was isolated using a biopsy punch (Harris Uni-core, Sigma-Aldrich). It was hypothesised that the pores within the PDMS sponge were interconnected. To validate this hypothesis, a simple experiment was conducted. The PDMS sponge was loaded with food dye. In doing so, the sponge was placed in a glass container filled with blue food dye. The sponge was squeezed using a plastic spatula to approximately 50% of its height for 3-5 times. This enabled the sponge pores to be saturated with the dye within 30 seconds (**Figure 2.2a**). To examine if the stored dye can be released the sponge was placed on absorbent paper and squeezed using the same plastic spatula to approximately 50% of its height. This caused the dye to be released from the sponge and absorbed by the paper (**Figure 2.2b**). Owing to its elasticity, once the plastic spatula was removed the sponge returns to its original shape (**Figure 2.2c**). The sponge could be repeatedly squeezed to release the remaining dye. Experiments indicated that the process of loading and unloading of the sponge can be repeated without changing the elastic or releasing characteristics of the sponge.

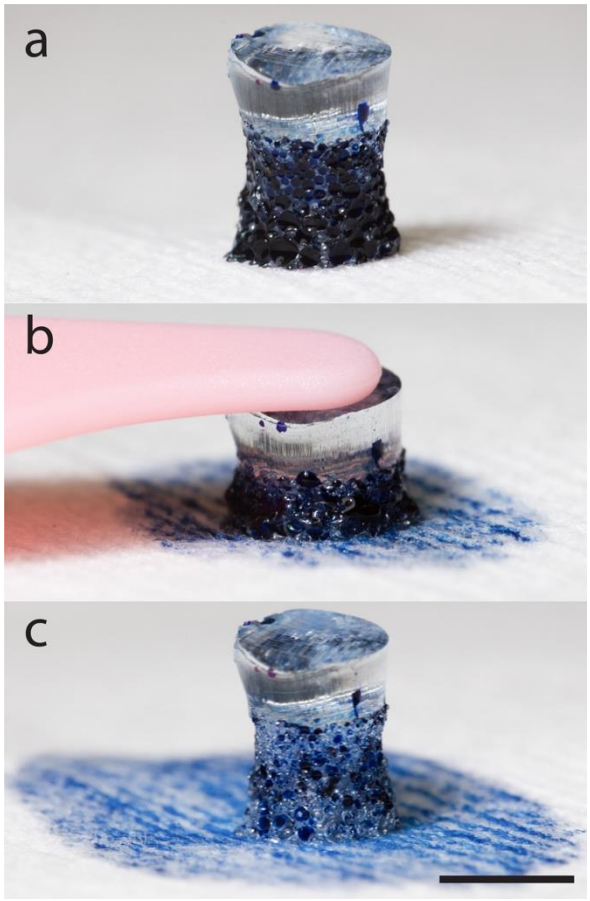

Figure 2.2: Qualitative characterisation of PDMS porous sponge, confirming that the pores are interconnected. **a)** PDMS sponge loaded with blue dye. **b)** The stored dye is then released via elastic compression of the sponge, and **c)** The sponge returns to its original shape. Scale bar is 6 mm.

The volume of the pores was calculated by comparing the weight of wet (water-loaded) and dry sponges, as follows: $V_{pores} = \frac{m_{wet} - m_{dry}}{\rho_{water}}$, and the porosity of sponge as follows: $Porosity = \frac{V_{pores}}{V_{sponge}}$. Using this method, the porosity of the sponge was obtained as 64.1%.

The porous structure of the sponge was analysed using scanning electron microscopy (SEM). In doing so, the sponge was coated with a 20 nm layer of gold and analysed using a FEI Quanta ESEM, equipped with a back-scattered secondary electron Everhart-Thornley detector. The SEM images were taken in high-voltage, high-vacuum mode (**Figure 2.3**). Measurements based on 15 pores indicated the pores have a diameter of D_{pore} = 356 ± 74 µm (average ± standard deviation). More importantly, SEM imaging confirms that the pores within the PDMS sponge are interconnected through smaller holes. Measurements based on 36 interconnecting holes indicated that these holes have a diameter of d_{hole} = 23.5 ± 11.2 µm.

It is hypothesised that the small holes that interconnect the larger pores are formed when the cured sponge is squeezed for the first time. This causes the very thin walls between the droplet-templated pores to collapse, forming the smaller interconnects.

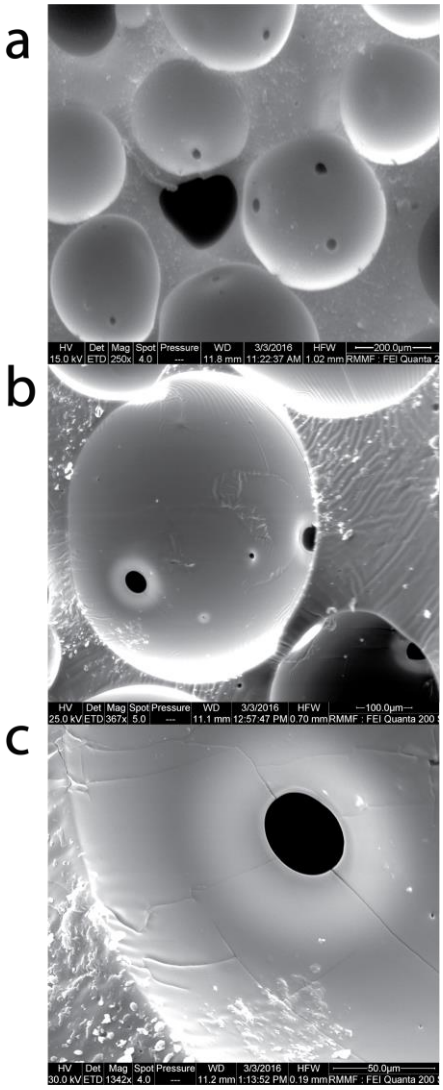

Figure 2.3: Quantitative characterisation of PDMS porous sponge. SEM images confirm the interconnection of pores with small holes, shown at different magnifications of **a)** 100×. **b)** 367×. and **c)** 1342×.

Characterisation of the porous structure of a sugar templated sponge fabricated as introduced in [4]. SEM imaging showed that the sugar template sponges have a pore size of D_{pore} = 410 ± 85 µm (**Figure 2.4**), which is similar to the values that were obtained for the droplet templated sponge. However, unlike the droplet templated sponge that consists of an array of isolated pores interconnected by small holes, the sugar template sponge consists of an open network of pores (similar to hydrogel scaffolds used for tissue engineering applications [42-44]).

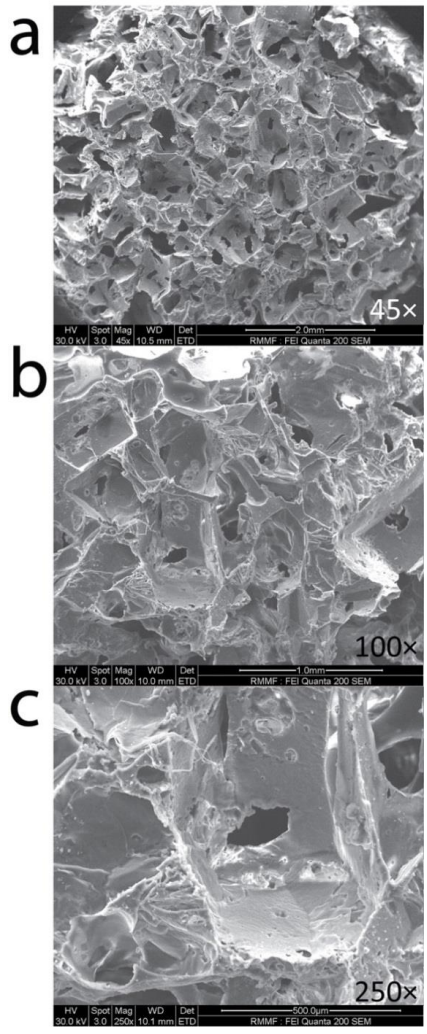

Figure 2.4: SEM imaging of a sugar templated PDMS sponge, shown at various magnifications of **a)** 45×, **b)** 100×, and **c)** 250×.

2.3.3 Cell culture, live cell imaging of intracellular calcium and data analysis

Human Umbilical Vein Endothelial Cells (HUVECs) were grown in EGMTM-2 media supplemented with SingleQuots kit (Lonza, Walkersville, USA) according to the supplier instruction. HUVECs were seeded at the density of 1,000,000 cells per well onto a 6-well plate, and cultured for 24 hours. Cells were then washed with HBSS (Hank's Balanced Salt Solution) buffer at 37 °C, and loaded with the calcium sensitive dye, Fluo4-AM ester (2 μM) to quantify their intracellular calcium signalling ($[Ca^{2+}]_i$) following stimulation with Ca^{2+} ionophore ionomycin (Sigma-Aldrich). Following loading with Fluo4-AM, the cells were kept at 37°C and 5% CO_2 in the dark for 30 min, before being washed twice with HBSS buffer.

The loaded cells were excited with a 488 nm laser using the Nikon A1 laser scanning confocal microscope (Nikon Instruments Inc., Melville, USA). Changes in the fluorescent intensity of individual cells were measured using NIS-Elements software. Details of calcium imaging and image analysis are reported elsewhere [45, 46]. Data are shown as mean ± standard deviation of at least three independent experiments, and at least 20 cells have been analysed in each experiment.

2.4 Results and Discussions

2.4.1 Passive release of stored liquids

Having shown that the interconnected porous structure of the PDMS sponge enables the sponge to be manually loaded with liquid solutions, as presented in **Figure 2.2**, the utility of these features were further explored for practical applications. As a first step, it was hypothesised that the sponge could be used for the passive release of stored liquids into the surrounding liquid.

A simple proof-of-concept experiment was conducted, as briefly explained here. The experimental setup consisted of a straight channel (Length × Width × Height = 24 mm × 2 mm × 9 mm) cut into a poly-methyl methacrylate (PMMA) slab with two 6 mm wells at each end of the channel. The channel was prefilled with water to a depth of 2 mm. A PDMS sponge (Diameter × Height = 6 mm × 8 mm) preloaded with ~145 µl of red food dye was then placed into one of the wells (**Figure 2.5a**). The colour change of the water along the channel following the release of dye was recorded using a Canon 6D camera equipped with a 100 mm macro lens, over a period of 20 min (**Figure 2.5b** + **Movie 2.1** (Clickable online video)). Under these conditions, the amount of time required for the red dye to cross the 24 mm long channel is obtained as 12.5 ± 0.7 min (average ± standard deviation, based on 15 independent experiments), which is referred to as 'crossing time' in the manuscript (**Figure 2.5c**), based on which the average velocity of dye progression is calculated as 31.5 ± 3.6 µm/s. Analysis of the intensity of the red colour at multiple segments along the channel with 2.25 mm gap in between using ImageJ software (**Figure 2.5c-inset**).

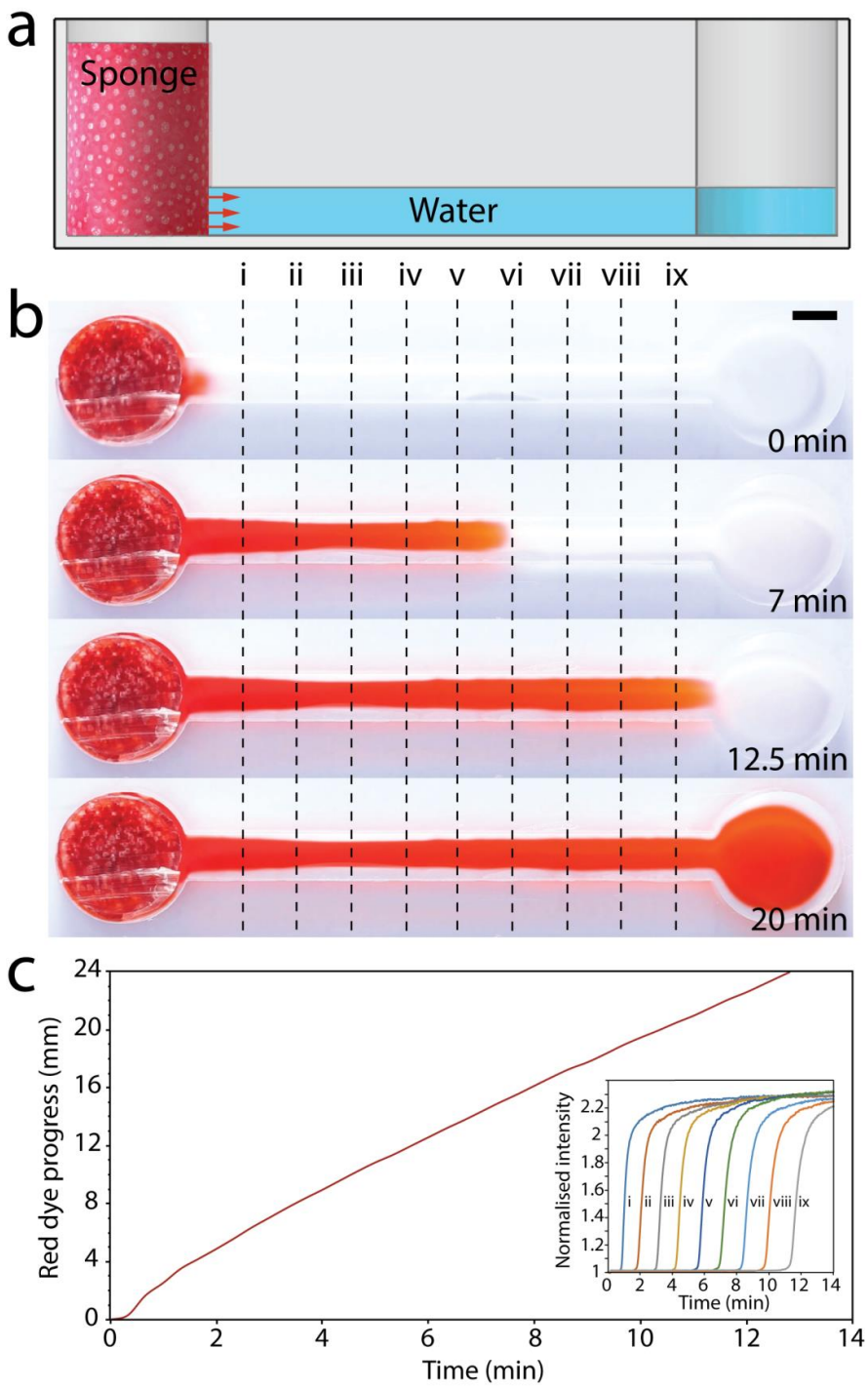

Figure 2.5: Passive release of stored food dye within the PDMS sponge into a narrow channel prefilled with water over a 20 minute period. **a)** Experimental setup. **b)** Gradual colour change within the channel captured over 20 minutes, and **c)** Normalised intensity of red food dye at sampling lines **i** to **ix** which are 2.25 mm apart. Scale bar is 2 mm.

To further analyse the release characteristics of the sponge, Various volumes of red dye ranging from 145 to 1.45 µl was directly pipetted into the well and monitored the release of red dye through the channel (**Figure 2.6** + **Movie 2.2**). The amount of time required for the red dye to advance along the channel was obtained as 0.05, 1.87, 2.97, 6.03, 7.37 and 9.33 min when pipetting 145, 14.5, 7.2, 3.6, 1.8 and 1.45 µl of red dye into the channel inlet well, respectively. This clearly demonstrated that the diffusive velocity of the dye through the channel reduces by reducing the volume (concentration) of the dye. Despite this, even after reducing the volume of pipetted red dye to 1.45 µl the progression velocity of the red was ~25% faster compared to the porous PDMS sponge prefilled with 145 µl of dye. This suggests that the sponge enables the slow release of stored liquids.

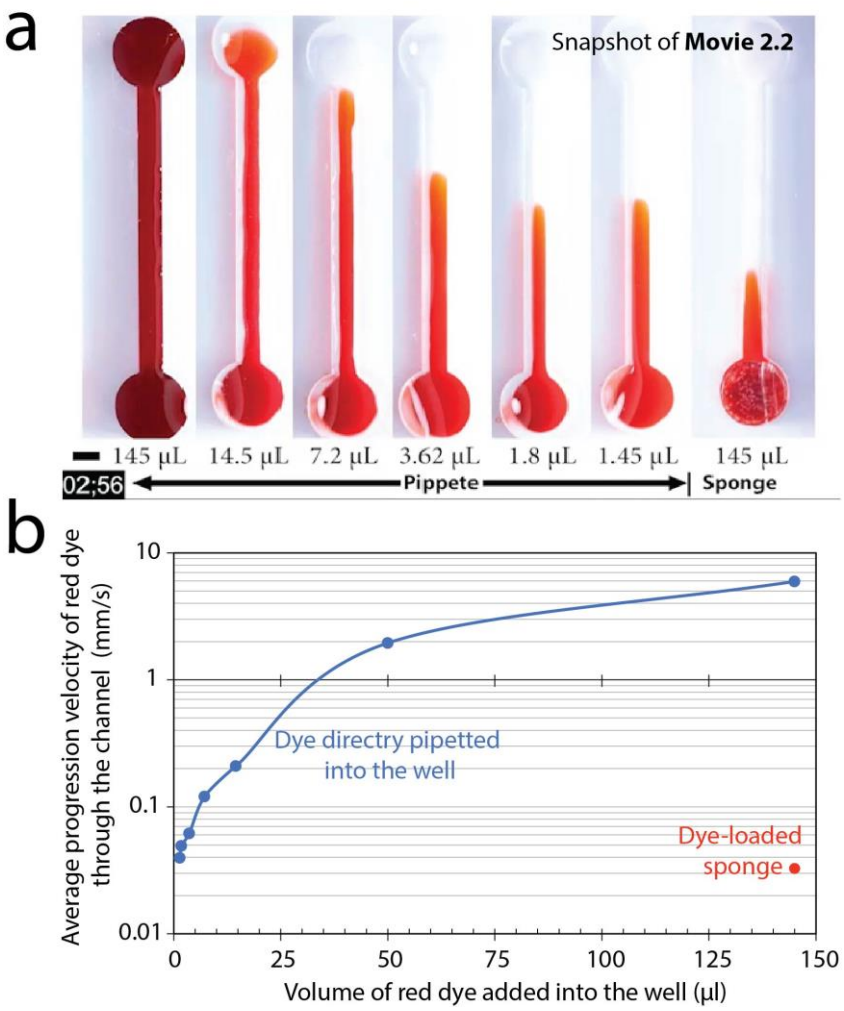

Figure 2.6: Comparing the velocity of red dye released into the channel when red dye pipetted directly into the channel and when loaded into the sponge. **a)** various volumes of directly pipetted dye injected into a straight channel. **b)** Average progression of dye though the channel. Snapshot image extracted from **Movie 2.2** (Clickable online video).

The passive release characteristics of droplet and sugar [4] templated sponges (**Figure 2.7** + **Movie 2.3**) was also compared. Under similar conditions, the dye released from the sugar templated sponge filled the channel in 3 ± 0.12 min (based on 15 independent experiments using 3 different sponges), which is ~4.1 times faster than the droplet templated sponge. This was further illustrated by comparing the release characteristics of droplet and sugar templated sponges placed at the opposite wells of the channel (**Figure 2.8** + **Movie 2.4**). The slower release characteristics of the droplet templated sponge can be attributed to the small interconnecting holes between the pores (**Figure 2.3**), which restricts the diffusion of stored dye through the sponge, as compared to the open network of pores in the sugar template sponge (**Figure 2.4**).

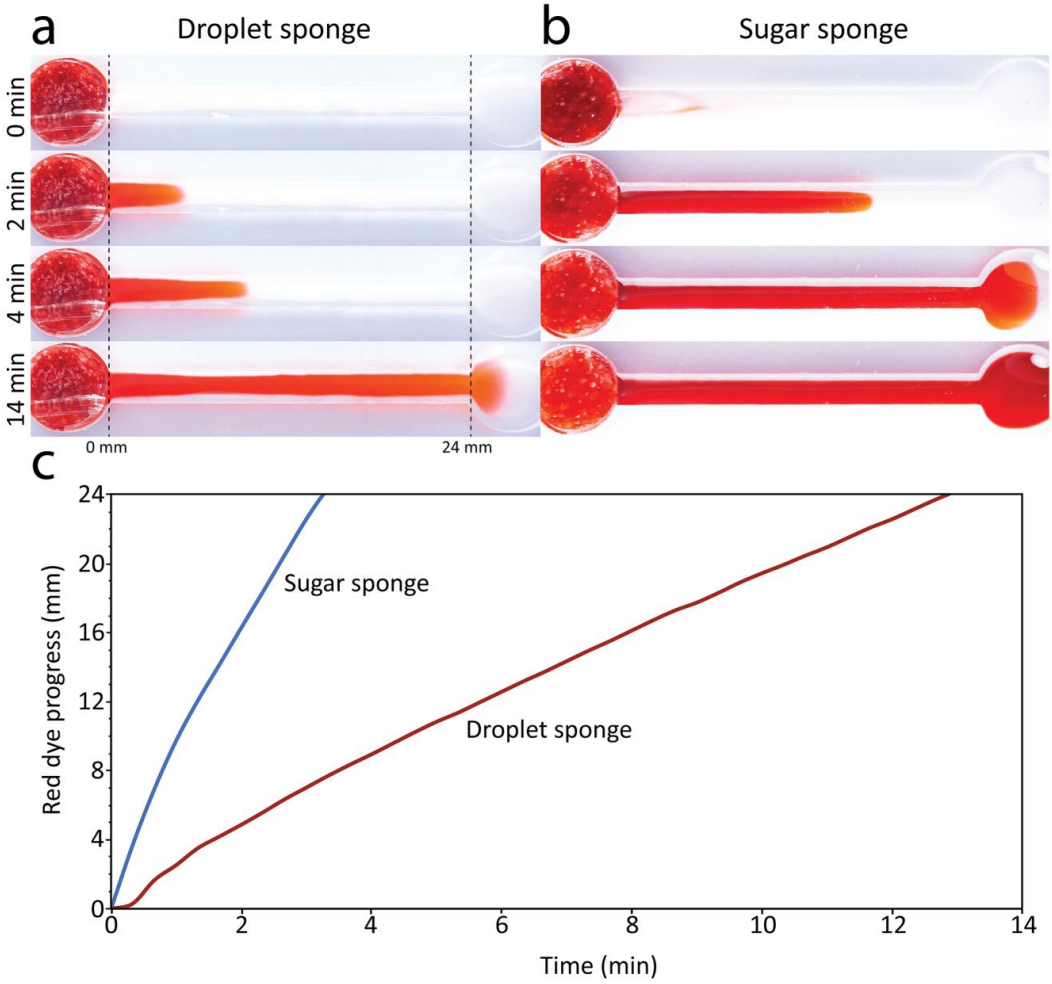

Figure 2.7: Comparison of the passive release of stored food dye into a narrow channel using: **a)** Reference droplet sponge. **b)** Sugar templated PDMS sponges. **c)** Shows the progress of the red food dye though the narrow channel over time. Snapshot images are extracted from **Movie 2.3** (Clickable online video).

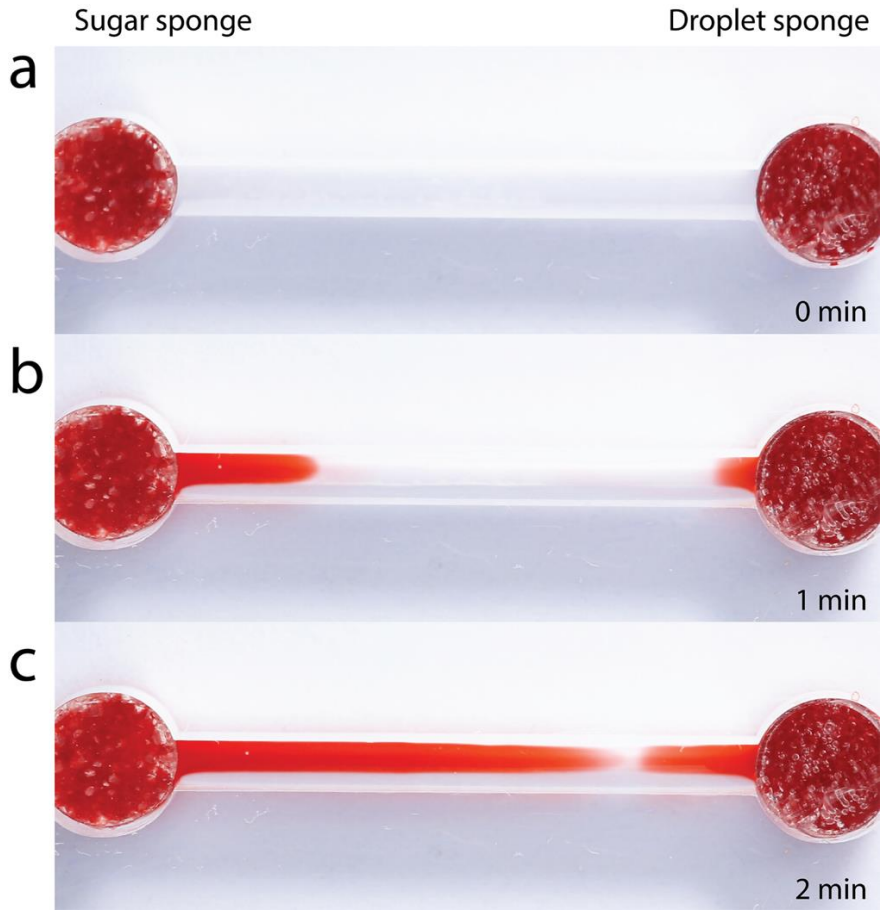

Figure 2.8: Comparison of the passive release of stored food dye into a narrow channel using: **(left)** Sugar and **(right)** Droplet templated PDMS sponges placed at the opposite wells of a 22 mm channel. **a)** 0 min. **b)** 1 min. **c)** 2 min. Snapshot images are extracted from **Movie 2.4** (Clickable online video).

To examine whether the droplet template PDMS sponge can be passively loaded with solutions, a wet (water-saturated) and dry sponge was inserted onto a channel prefilled with red dye solution. These experiments showed the passive penetration of dye into the wet sponge, whereas the dye did not penetrate into the dry sponge even after 18 hours (**Figure 2.9**). This can be attributed to the surface tension at the interface of the dry pores and the dye solution, which limits the diffusive penetration of dye into the pores. The passive loading of the wet PDMS sponge enables loading multiple liquid solutions onto a single sponge (**Figure 2.10**), and more interestingly allows for the passive mixing of multiple liquids (**Figure 2.11**).

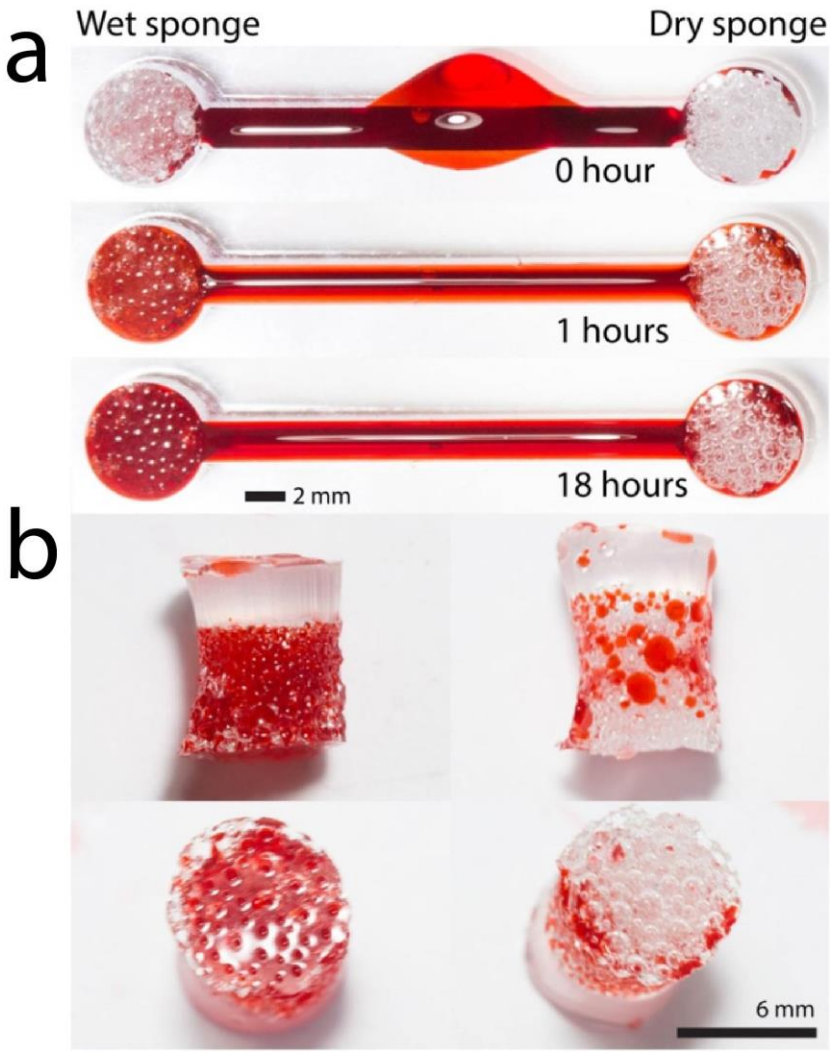

Figure 2.9: Left column: A wet sponge (prefilled with water) can be passively loaded with red food dye. Right column: In contrast, a dry sponge is not loaded with red dye. **a)** Sponges in a straight channel. **b)** Sponges removed from the channel after 18 hours.

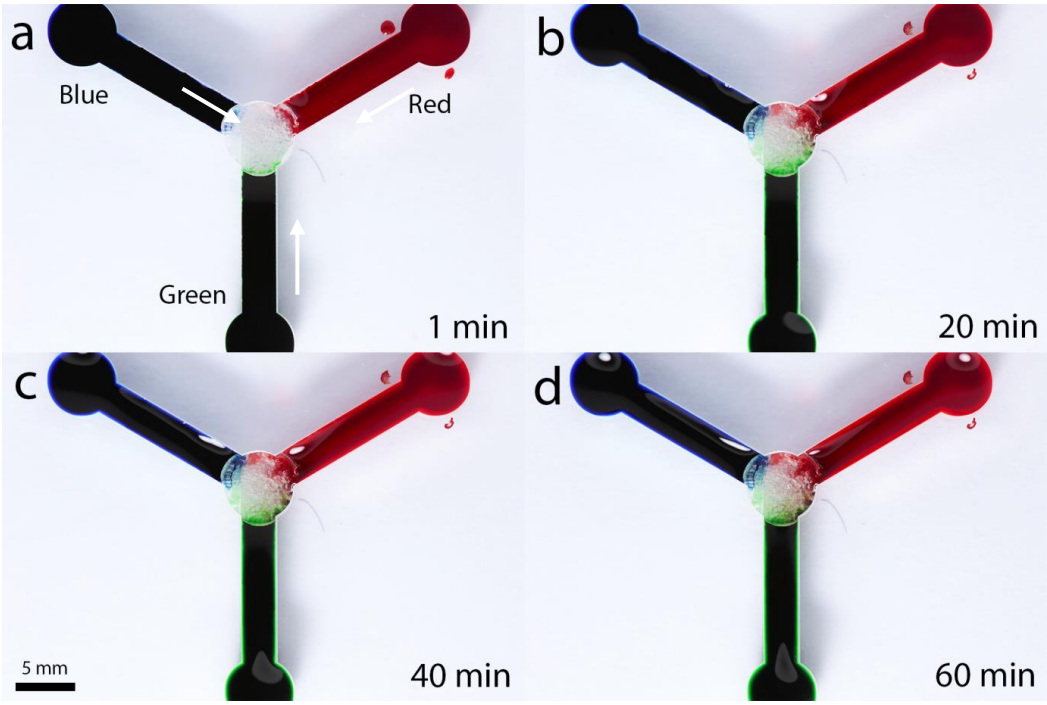

Figure 2.10: Passive loading of multiple liquid solutions, demonstrated by loading blue, red and green dyes into the droplet templated PDMS sponge over a period of 60 minutes. **a)** 1 min. **b)** 20 min. **c)** 40 min. **d)** 60 min.

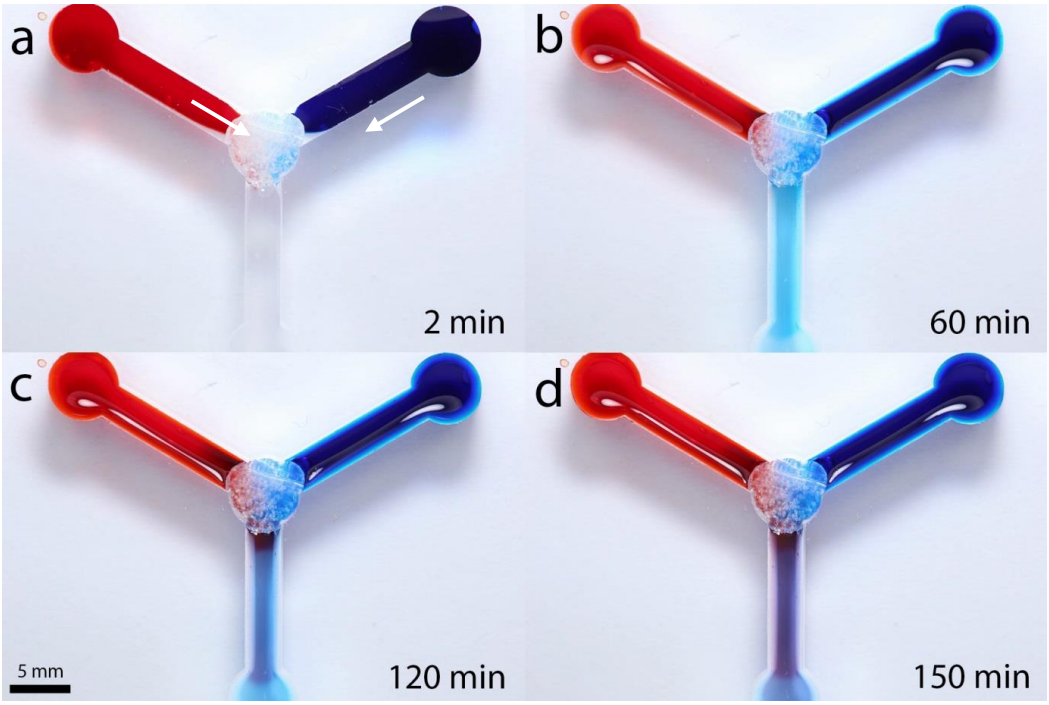

Figure 2.11: Passive loading and mixing of multiple liquid solutions, demonstrated by loading blue and red dyes into the droplet templated PDMS sponge followed by the passive release of mixed dye from the outlet channel over a period of 150 minutes. **a)** 2 min. **b)** 60 min. **c)** 120 min. **d)** 150 min.

In addition, a control experiment was conducted to examine whether the adsorption of dye into the wet sponge is due to the terminal hydroxyl groups or the pores. In doing so, three PDMS structures, including an ordinary PDMS, an OH terminated PDMS, and a droplet templated PDMS sponge were placed into a 35 mm Petri dish, which was prefilled with red dye solution. Time lapse imaging indicated that only the droplet templated sponge absorbed the dye. Extended experiments up to 24 hours led to similar results (**Figure 2.12**).

This experiment clearly shows that the porous PDMS sponge can be used for the storage and passive release of liquids into fluidic systems. These results show that a controlled diffusion profile can be seen in a narrow channel. The sponges are durable and can be washed, dried and subsequently reused. It is also possible to load the sponges mechanically or passively via diffusion.

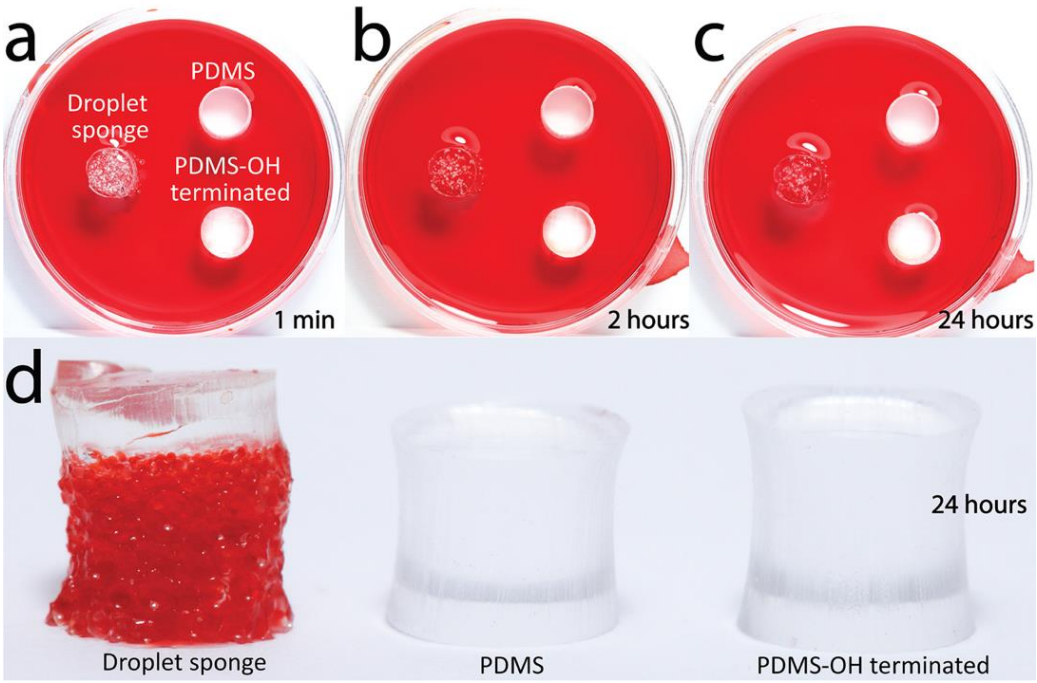

Figure 2.12: Comparison of adsorption of dye into cylindrical structures made of ordinary PDMS, OH terminated PDMS, and the droplet templated sponge, shown: **a)** 1 minute. **b)** 2 hours. **c-d)** 24 hours after placing into a 35 mm Petri dish.

2.4.2 Characterisation of the release rate of droplet templated PDMS sponges

Additional experiments were conducted to study how the size of interconnecting holes influences the diffusion rate of the droplet templated porous sponges. Extensive SEM characterisation indicated that the average diameter of the interconnecting holes is proportional to the average diameter of the pores (**Figure 2.13**), which can be expressed as $\bar{d}_{hole} \propto 0.0474\, \bar{D}_{pore}$. This creates opportunities to vary the diameter of interconnecting holes, as described below.

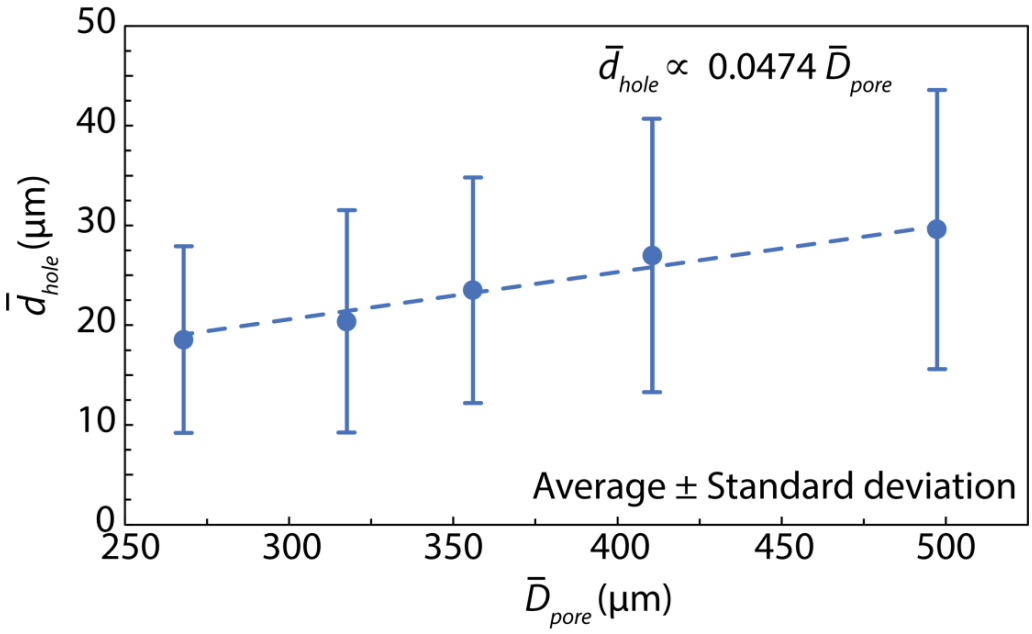

Figure 2.13: Variations of the average diameter of interconnecting holes versus the average diameter of pores, obtained from SEM imaging of droplet templated PDMS sponges.

In a T-junction, the length of the discrete phase slug is proportional to the ratio of discrete to carrier flow rates, which can be expressed as $L_{discrete} / W_{discrete} = 1 + \alpha\, Q_{discrete} / Q_{carrier}$ (in which $L_{discrete}$ is the length of discrete phase slug, $W_{discrete}$ is the width of the discrete phase inlet channel at the T-junction while $Q_{discrete}$ and $Q_{carrier}$ are the flow rates of the discrete and carrier liquids), as comprehensively discussed in [47]. Therefore, by varying the ratio of water to PDMS flow rates (Q_{water} / Q_{PDMS}), the length of water slugs was varied and consequently the diameter of the pores and holes. Using this strategy, porous sponges with larger pores (D_{pore}= 497.3 ± 94.7 µm, d_{hole} = 29.6 ± 13.9 µm) were fabricated as well as smaller pores (D_{pore} = 267.9 ± 55.1 µm, d_{hole} = 19.1 ± 9.2 µm) in comparison to the reference sponge discussed previously, as presented in **Figure 2.14**.

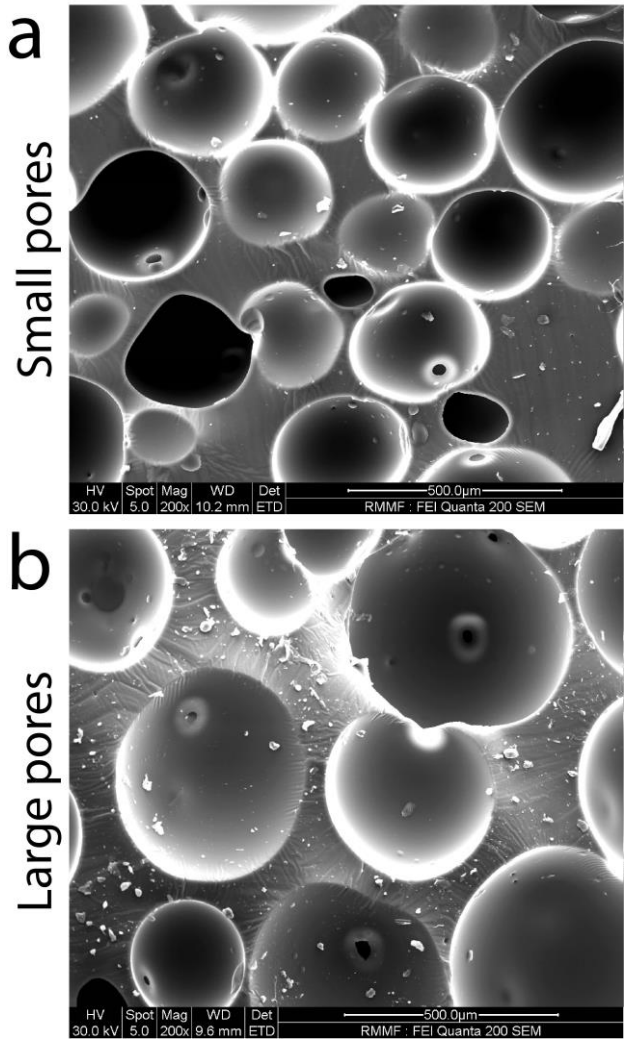

Figure 2.14: SEM imaging of droplet templated PDMS sponges shown at 200× with different pore sizes. **a)** Small pores, the pore size is measured as 267.9 ± 59.1 µm (average ± standard deviation) and interconnecting holes as 19.1 ± 9.2 µm. **b)** Large pores, the pore size is measured as 497.3 ± 94.7 µm and interconnecting holes as 29.6 ± 13.9 µm.

Next, the release characteristics of these two sponges were analysed in a 24 mm long channel, as presented in **Movie 2.5** + **Figure 2.15**. The slope of these curves, which correspond to the velocity of diffused dye, is proportional to the diameter of interconnecting holes (**Figure 2.16a**). Using these curves, the amount of time required for the released dye to reach the end of the channel (crossing time) was measured as 8.23 ± 0.4 and 19.85 ± 1.1 minutes for the sponges with the larger and smaller holes, respectively. **Figure 2.16b** presents the variations of crossing time with respect to the diameter of interconnecting holes, which can be expressed as $\text{crossing time} \propto \bar{d}_{hole}^{-2.07}$.

Theoretically, the diffusion rate of dye through the sponge can be defined as $J_{dye} = \frac{D\Delta c}{\sum(A/t)_{holes}}$, in which D is the diffusion coefficient of dye in water, c is the concentration of dye, while A_{hole} and t_{hole} are the cross sectional area and the thickness of interconnecting holes, respectively [48]. $A_{hole} \propto \bar{d}_{hole}^{2}$ and therefore, this equation can be simplified as $J_{dye} \propto \bar{d}_{hole}^{2}$, based on which $crossing\ time \propto \bar{d}_{hole}^{-2}$. Experimental analysis suggests $\text{crossing time} \propto \bar{d}_{hole}^{-2.07}$, which matches well with theory.

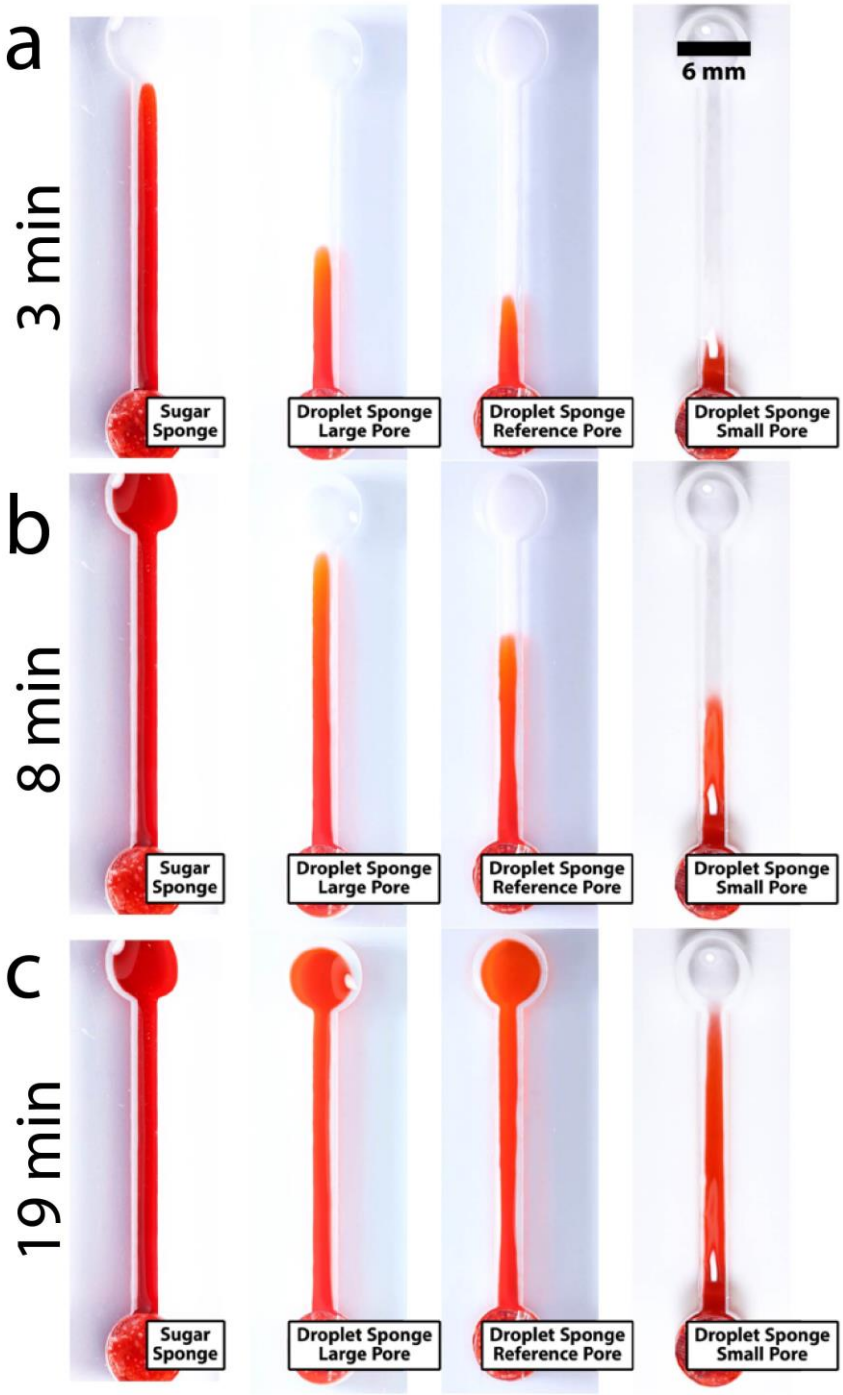

Figure 2.15: Qualitative comparison of the passive release of stored food dye into a 24 mm channel using sugar sponge, droplet sponge with large pores, droplet sponge with reference pores, and droplet sponge with small pores. **a)** 3 min. **b)** 8 min. **c)** 19 min. Snapshot images are extracted from **Movie 2.5** (Clickable online video).

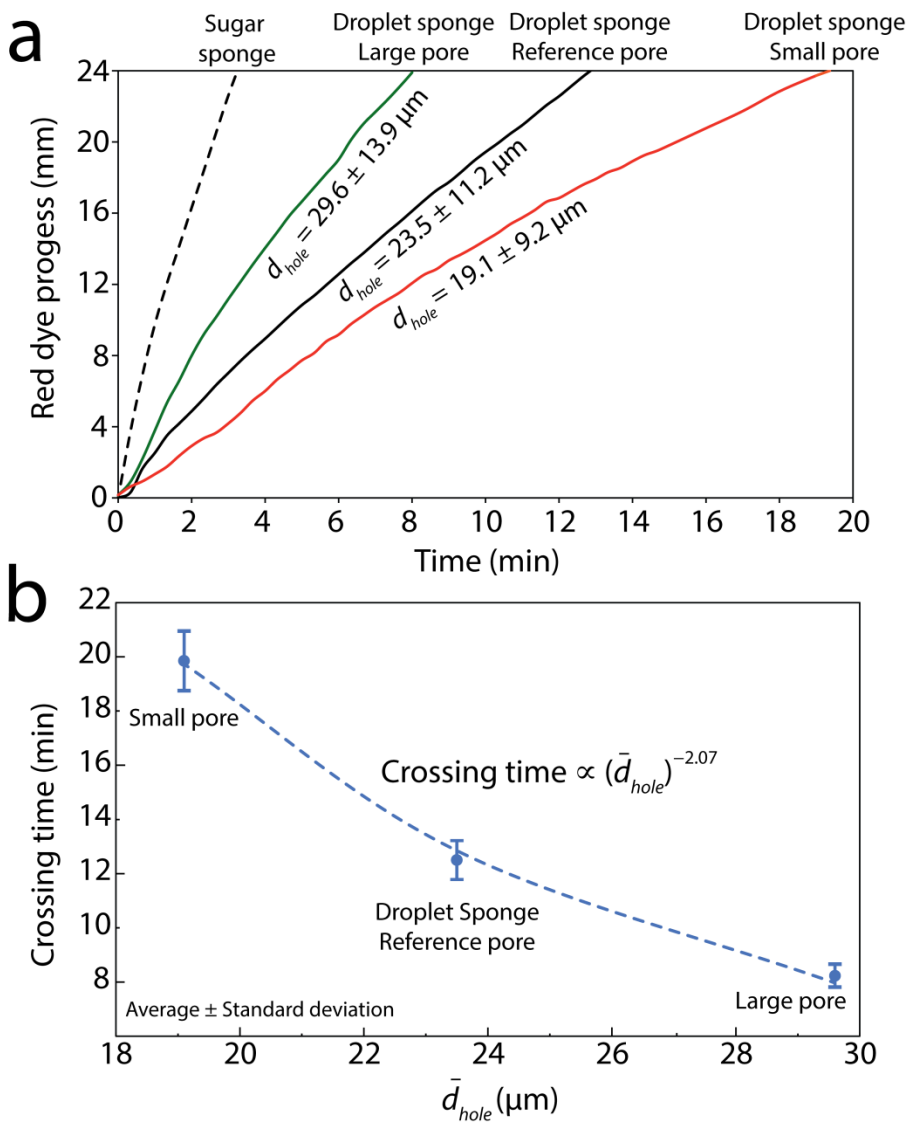

Figure 2.16: Quantitative analysis of the passive release of stored dye with respect to the average diameter of interconnecting holes. **a)** Dye progress along the 24 mm channel using droplet sponges with large, reference and small pores and a sugar sponge, extracted from **Movie 2.5** (Clickable online video). **b)** Crossing time of various droplet sponges with respect to the average diameter of their interconnecting holes.

Furthermore, numerical simulations to study the effect of the size of the interconnecting holes on the release rate of the sponge was conducted. The simple model consisted of three pores interconnected by small holes (**Figure 2.17**). The diameter of the pores was set to 350 µm while the size of interconnecting holes was varied as 15, 25 and 50 µm.

Simulations are performed using ANSYS Fluent software by solving the differential equation governing the transport of species in liquid environments: $\frac{\partial c}{\partial t} = D\,\nabla^2 c$, in which c is the concentration, t is time, and D is the diffusion coefficient of dye in water.

Simulations clearly indicate a faster diffusion rate for the sponge with larger holes (**Figure 2.18**), which is in line with experimental results. Extended simulations by setting the size of interconnecting holes to 25 µm but variable pore sizes of 300, 350 and 400 µm did not change the release rate of sponges significantly.

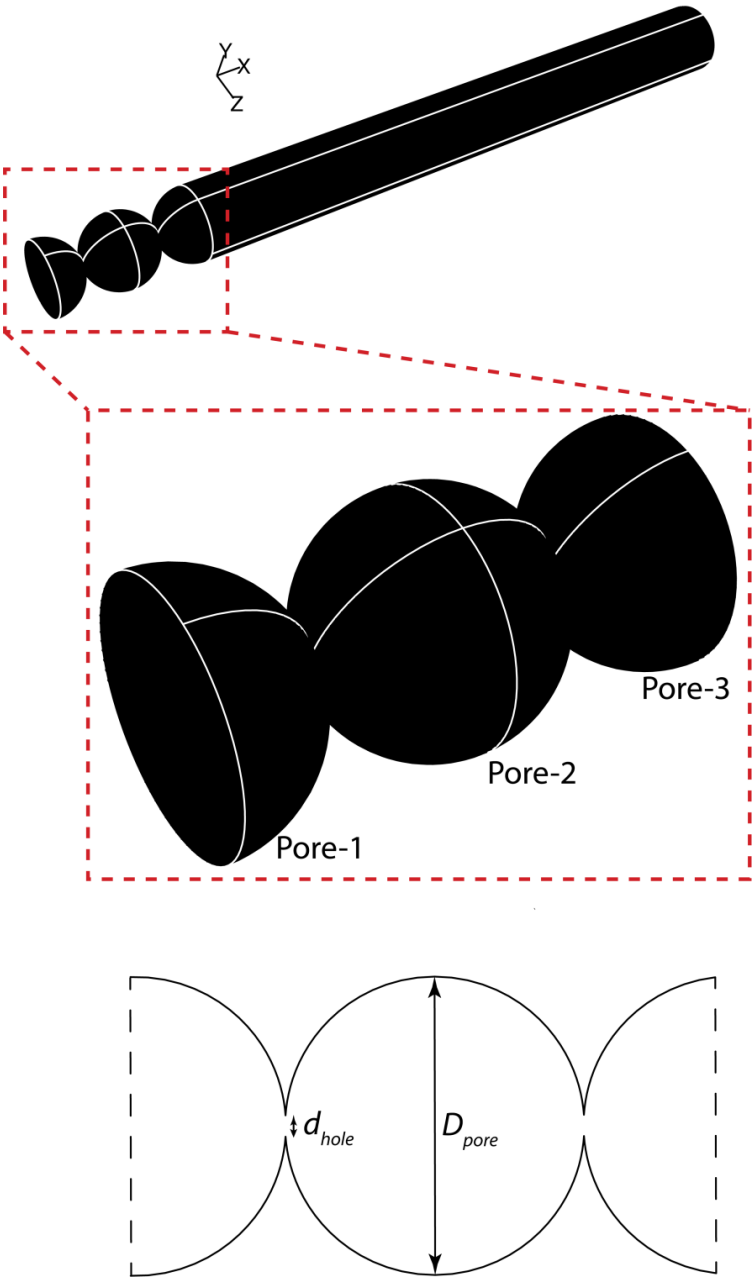

Figure 2.17: Geometry of the numerical model used for studying the effect of interconnecting hole dimensions on diffusion rate of stored liquids. Geometry consists of three interconnected pores (shown as pores 1 to 3 in the inset), which are connected to a longer channel, which represents the liquid filled container. In the simulation, the pore diameter, D_{pore} is set to 350 µm, whereas the width of the interconnecting holes, $d_{inter\text{-}pore}$ is varied as 15, 25, and 50 µm. Mesh generation is conducted using Gambit software.

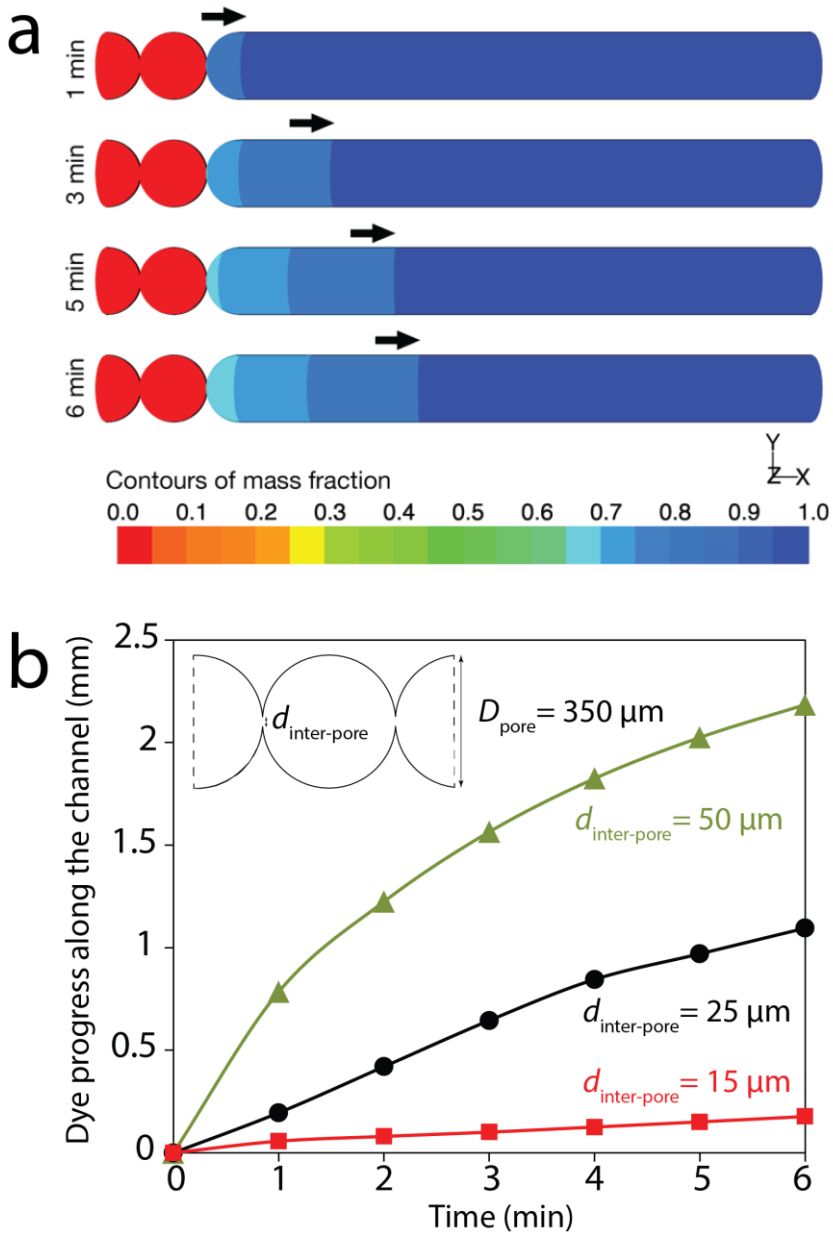

Figure 2.18: Results of numerical simulations. **a)** Contours of mass fraction obtained by numerical simulations over 6 minutes, showing the diffusion rate of food dye through the channel for the model with D_{pore}= 350 µm and $d_{inter\text{-}pore}$ = 25 µm. **b)** the diffusion rate of dye from sponges over 6 minutes with various $d_{inter\text{-}pore}$ of 15, 25 and 50 µm, obtained from numerical model. In all cases, D_{pore}= 350 µm.

2.4.3 Passive release of chemicals to induce intracellular calcium signalling of endothelial cells

The utility of the porous PDMS sponge for the storage and slow release of liquids into a narrow channel passively has been shown (**Figures 2.5** and **2.16**). To extend this and demonstrate the utility of the sponge in an experimental environment, It was hypothesised that the sponge could be utilised for the slow release of chemicals/drugs into a cell culture system. However, the majority of cell culture systems consist of circular structures such as Petri dishes or well plates rather than narrow channels. Therefore, the release of chemicals in a 6-well plate (with a well diameter of 24 mm) was studied. In doing so, a reference droplet sponge was manually loaded with red dye, and inserted it close to the sidewalls of the well plate, which was prefilled with water up to the height of 2 mm. The release of red dye was monitored over a period of 95 min, as demonstrated in the **Movie 2.6**. This experiment indicated the ordered progression of released dye up to the middle plane of the well plate followed by the more chaotic progression of released dye after passing the middle plane, caused by the converging cross section of the well plate.

The passive release characteristics of the reference droplet and sugar [4] templated sponges was also compared in a 24 mm well. Under similar conditions, dye released from the sugar templated sponge filled the well in 12.5 ± 0.7 min (based on 12 independent experiments using 3 different sponges), which is ~7.6 times faster than the droplet templated sponge (**Figure 2.19** + **Movie 2.7**). The release characteristics of these two sponges was further compared by inserting them into the opposite sides of a 24 mm well (**Figure 2.20** + **Movie 2.8**).

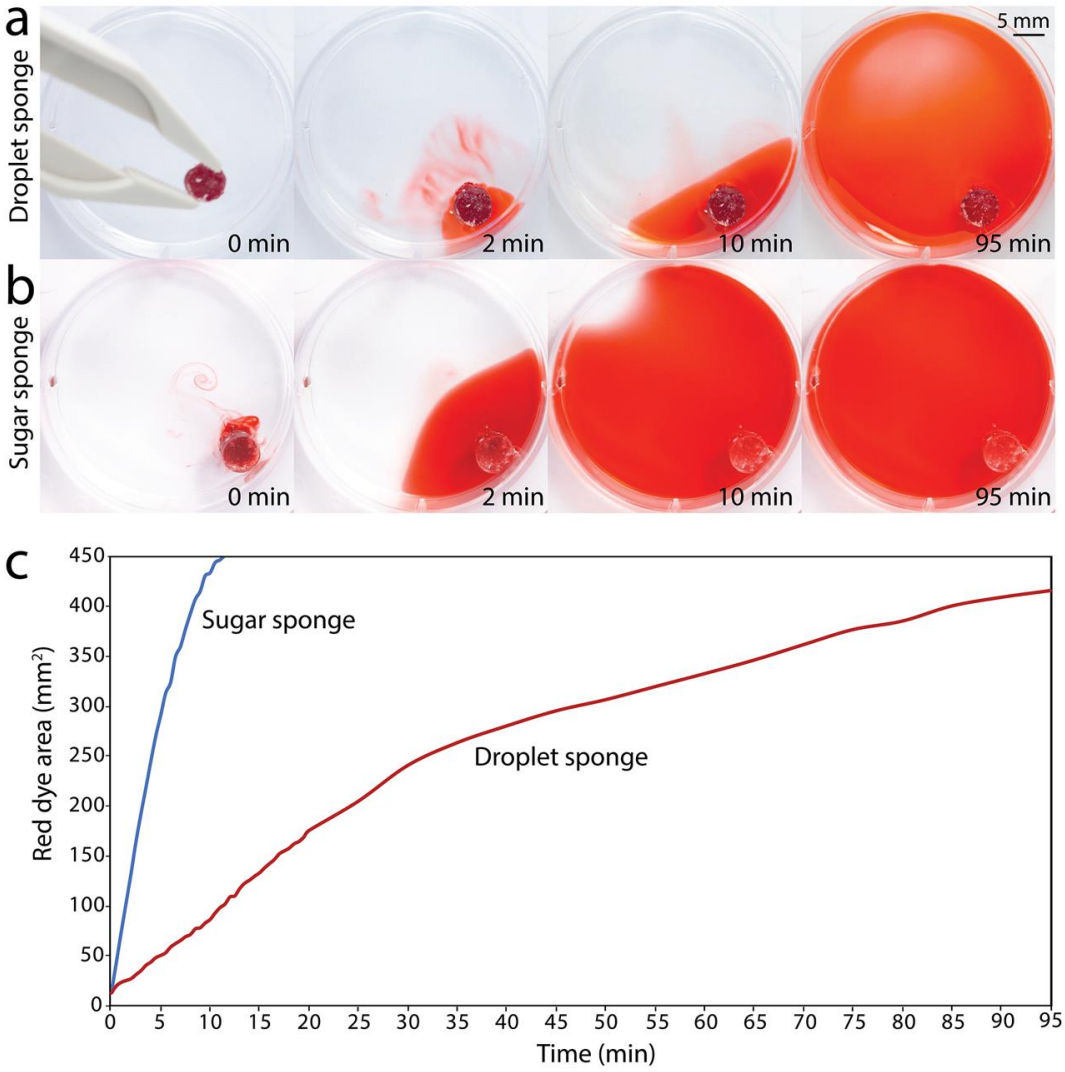

Figure 2.19: Comparison of the passive release of stored food dye into a 24 mm well. **a)** Reference droplet templated PDMS sponge. **b)** Sugar templated PDMS sponge. **c)** Compares the area of the red food dye into the well plate over time. Snapshot images are extracted from **Movie 2.6** (Clickable online video).

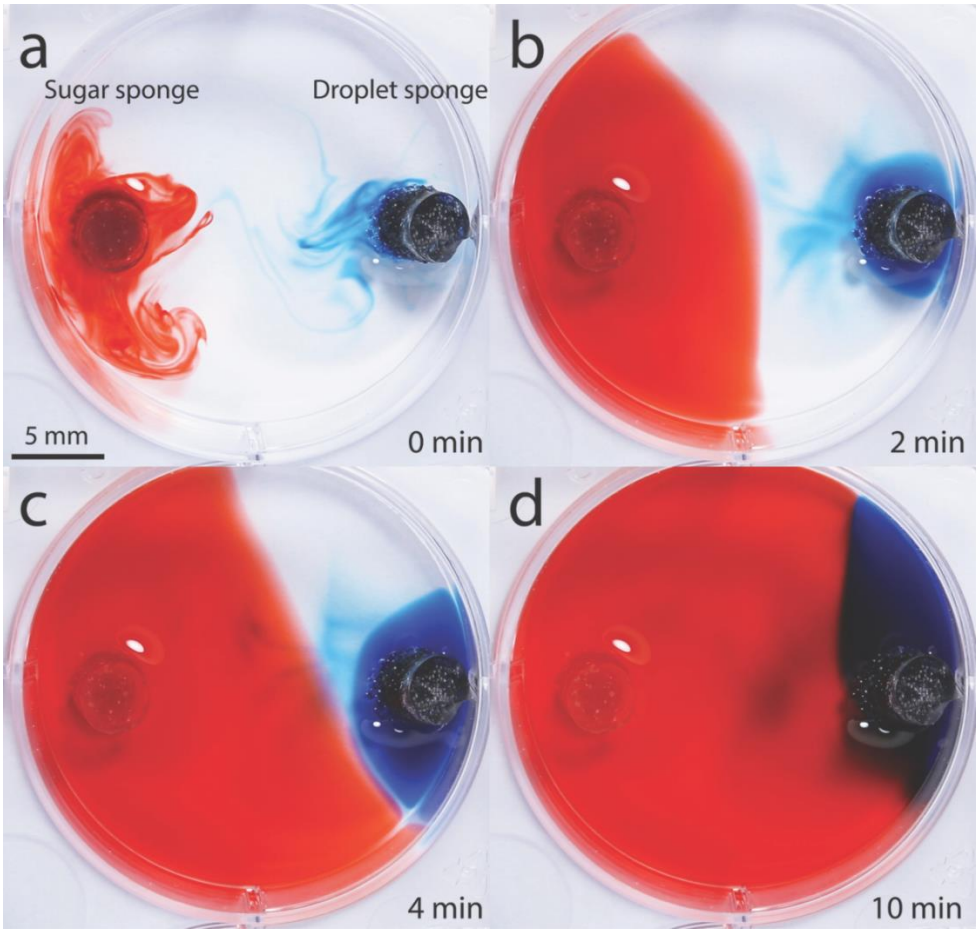

Figure 2.20: Comparison of the passive release of stored food dye into a 24 mm well using: **(left**) Sugar and **(right)** Droplet templated PDMS sponges, placed at the opposite sides of the well. The sponges were loaded with blue and red dyes for better visual comparison. **a)** 0 min **b)** 2 min. **c)** 4 min. **d)** 10 min. Snapshot images are extracted from **Movie 2.8** (Clickable online video).

Proof-of-concept experiments were conducted to assess the ability of the PDMS sponge for the chemical stimulation of cultured HUVEC endothelial cells, as detailed in Materials and Methods. The cells were loaded with calcium sensitive dye, Fluo-4AM, to quantify their intracellular calcium signalling ($[Ca^{2+}]_i$) following stimulation with ionomycin. The well plate was filled with cell culture medium up to a height of 2 mm. A PDMS sponge (Diameter × Height = 6 mm × 8 mm) was manually loaded with 2 µg/ml ionomycin, and inserted close to the sidewall of the well plate (**Figure 2.21a**).

Changes in the $[Ca^{2+}]_i$ of cells in response to stimulation with ionomycin were measured using confocal microscopy. The response of cells was monitored across a square region close to the sponge (**Figure 2.21b**). The selected region was located before the middle plane of the well plate to ensure the ordered progression of released ionomycin. It had an area of 1.27 mm × 1.27 mm, accommodating more than 100 cells. **Figure 2.21c-f** show the changes in the fluorescent intensity of endothelial cells when exposed to 2 µg/ml ionomycin over a 10-minute period.

Figure 2.21g presents the changes in the $[Ca^{2+}]_i$ of 20 individual cells. The calcium response of cells increased until reaching a peak value, after which it remained almost constant. The slow release of ionomycin from the sponge led to the delayed response of cells depending on their location relative to the sponge. Based on 20 randomly selected cells, the maximum fold increase of $[Ca^{2+}]_i$ in response to 2 µg/ml ionomycin was obtained as 4.2 ± 0.4 fold. Control negative group (without ionomycin) did not show any change in $[Ca^{2+}]_i$, confirming the selectivity and sensitivity of the proposed assay.

To quantify the velocity of released ionomycin, five cells (designated with ***i*** to ***v*** in **Figure 2.21h**) were selected, which were located along the radial axis of the well plate. Using these five cells, the velocity of released ionomycin was obtained as 3.96 μm/s (**Movie 2.9**).

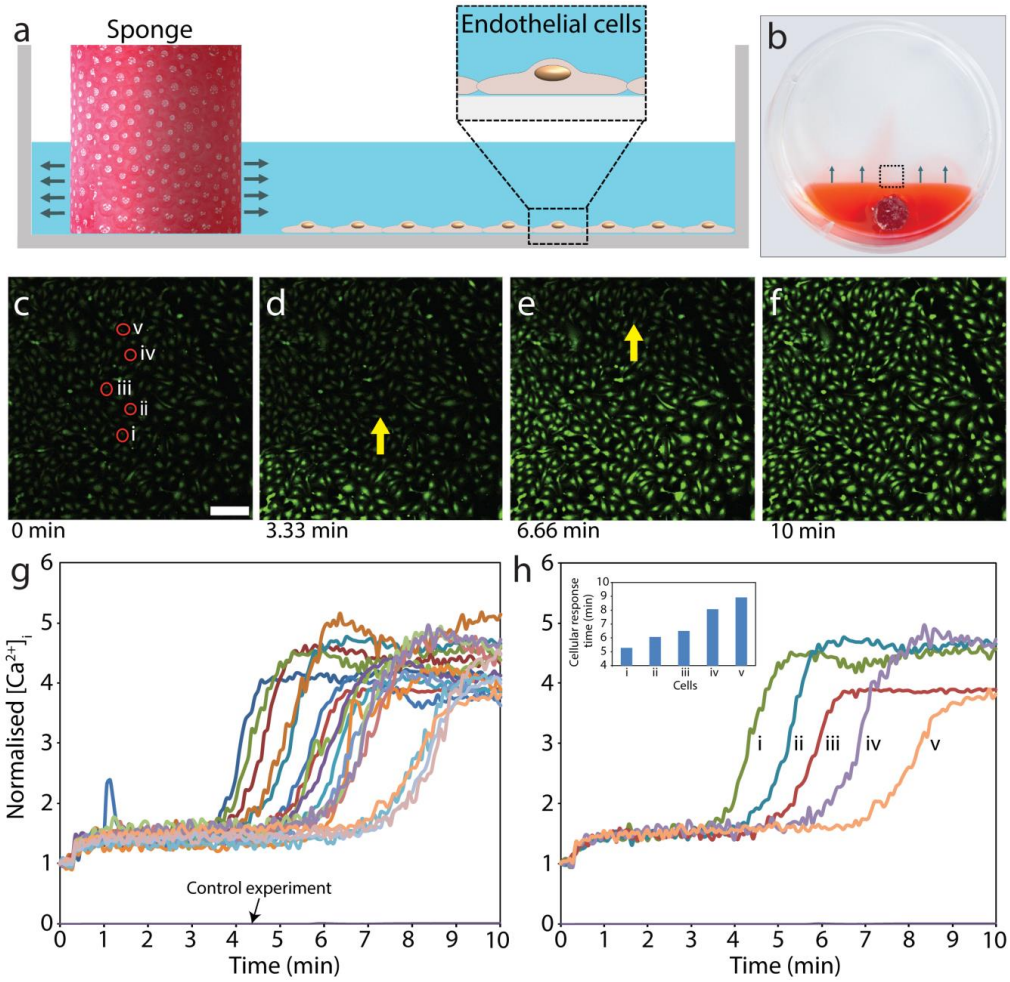

Figure 2.21: Passive release of 2 µg/ml ionomycin from the PDMS sponge into a 6-well plate to induce intracellular calcium signalling of endothelial cells. **a)** Experimental setup comprising of ionomycin-loaded sponge inserted into one of the wells which is pre-coated with endothelial cells and pre-filled with cell culture medium. **b)** Release pattern of ionomycin into the well visualised by using red food dye with the observational region shown as a dashed square. **c-f)** Intracellular calcium signalling of endothelial cells in response to the passive release of 2 µg/ml ionomycin over a 10 minute period. **g)** Normalised intensity profiles for 30 randomly selected cells. **h)** Normalised intensity profiles for five cells designated with **i** to **iv** in **Figure 2.21c** located radially with respect to the sponge with inset showing the response time of each cell. Scale bar is 200 µm.

The calcium response of cells when stimulated with 1 µg/ml ionomycin (**Figure 2.22** + **Movie 2.10**) was also investigated. The calcium response of cells increased until reaching a peak value, after which it reduced, which is expected at low concentrations of ionomycin [45, 49]. The maximum fold increase of $[Ca^{2+}]_i$ reduced to 2.5 ± 0.4 fold. The velocity of ionomycin release reduced to 2.26 µm/s compared to 3.96 µm/s obtained at a concentration of 2 µg/ml.

This experiment showed the utility of a porous PDMS sponge for the passive release of stored chemicals/drugs into a cell culture system. The calcium signalling response of endothelial cells was investigated for two different concentrations of ionomycin. This system can also be used for investigation of the response of cells to various drugs such as apoptosis inducer drugs [50]. More complicated cellular assays can be designed by implementing several sponges, which can be loaded with desired reagents/buffers/drugs.

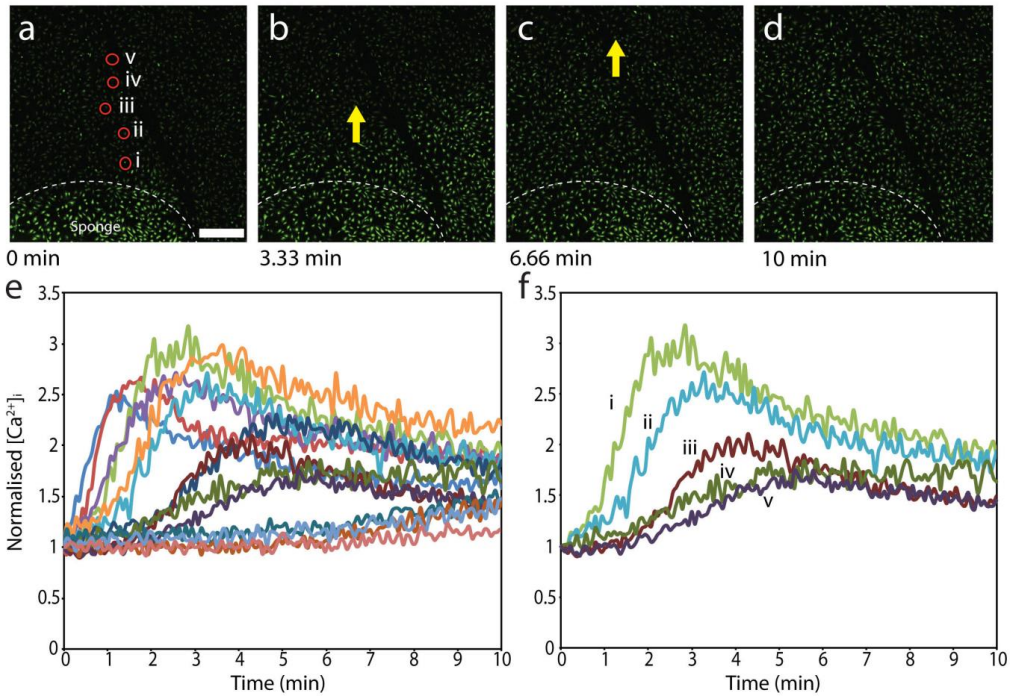

Figure 2.22: Passive release of 1 µg/ml ionomycin from the PDMS sponge into a 6-well plate to induce intracellular calcium signalling of endothelial cells. **a-d)** Intracellular calcium signalling of endothelial cells in response to the passive release of 1 µg/ml ionomycin over a 10 minute period. **e)** Normalised intensity profiles for 30 randomly selected cells. f) Normalised intensity profiles for five cells designated with **i** to **iv** in **Figure 2.22a** located radially with respect to the sponge. Scale bar is 600 µm.

2.4.4 Active release of stored liquids into a microfluidic channel

The utility of the sponge for the active release of stored liquids into the surrounding environment is investigated in this section.

The experimental setup consisted of a U-shaped fluidic channel (Width × Height = 2 mm × 2 mm) with a large inlet reservoir imprinted into a PDMS slab using soft lithography (**Figure 2.23a**). A cylindrical well was punched over the channel using a biopsy punch (diameter = 8 mm) to accommodate a reference PDMS sponge (Diameter × Height = 6 mm × 8 mm). The sponge was pre-loaded with red food dye before being placed into the well. The active release mechanism consisted of an M4 screw thread to convert the rotational into axial movement to enable the controlled compressing of the PDMS sponge (**Figure 2.23b**). Water was extracted through the outlet port of the channel using a syringe pump (Harvard Pico Plus) at 180 µl/min. This allowed water to flow around the sponge and carry away the released dye. The Péclet number of the system, describing the ratio of convective to diffusive release, is defined as $Pe = d_{sponge}.\overline{U}/D$ (where d_{sponge} is the diameter of sponge, $\overline{U}$ is the average velocity of water through the channel and *D* is the mass diffusion coefficient of food dye in water, which is taken as 10^{-9} m^2/s [51]). At the flow rate of 180 µl/min the Péclet number was obtained as ~4,800 indicating the dominance of convective release at such a high flow rate.

Using this setup, the active release of red dye over 5 consecutive release cycles was investigated over a 25-minute period. Each release cycle corresponded to a full turn on the M4 threaded screw, causing a 700 µm compression of the sponge. The consequent compression of the sponge led to the active release of dye from

the sponge into the surrounding water flow (**Figure 2.23c-e**). The experiment was recorded using a Canon 6D camera equipped with a 100 mm macro lens. The resulting video was then processed and the intensity of the red dye was extracted at cross section **iii** of the channel using ImageJ (**Figure 2.23a**).

Analysis indicated that the red dye reaches peak intensity ~1.5 minutes after each turn. For example, **Figure 2.23c-e** show the second release cycle starting at 5 minutes (**Figure 2.23c**) reaching peak intensity at 6.5 minutes (**Figure 2.23d**) followed by the beginning of the third cycle at 10 minutes (**Figure 2.23e**). This process is presented in **Movie 2.11**.

The results also indicated a slight increase of dye release over the consecutive cycles. For example, the peak intensity of cycles one to five was measured as 1.35, 1.37, 1.42, 1.44 and 1.45, respectively. Accordingly, the area under intensity curves one to five was calculated as 6.090, 6.217, 6.484, 6.472 and 6.433, respectively suggesting the increased release of dye. This could be due to the non-linear compression of the sponge due to its flexible properties. The duration of release cycle, and accordingly the amount of released dye can be varied by changing the amount of sponge compression. Similar trends were observed in five independent experiments.

Experiments clearly indicated that the active release of stored solutions from the sponge was at least one order of magnitude higher than the passive release. To minimise the effect of the passive release, the sponges could be inserted in side channels of a microfluidic chip, rather than in the main channel. This could significantly reduce the passive release of stored solutions into the main channel.

This experiment clearly shows that the porous PDMS sponge can be used for the active release of liquids into microfluidic systems. The system can be easily adapted for the use of different sponge and channel sizes. More importantly, the system is adaptable into parallel systems with multiple sponges/channels. The system could also be automated using stepper motors for automation or complex squeezing patterns.

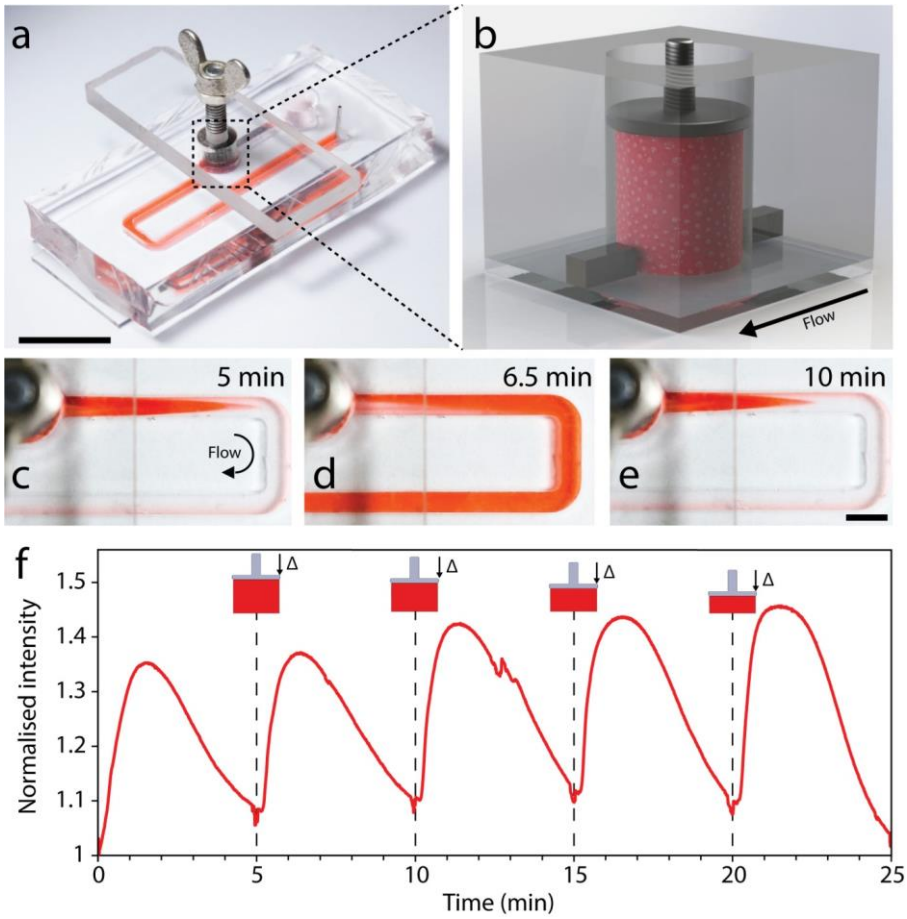

Figure 2.23: Active release of stored liquids into a microfluidic channel using a porous PDMS sponge. **a)** Experimental setup comprising of a microfluidic U-shaped channel integrated with a PDMS sponge and the active release mechanism. **b)** A rendering view of the sponge assembly showing the sponge secured in the well with the screw mechanism (M4 thread, 700 µm pitch) allowing water to flow around the sponge. **c-e)** Show the release of red dye into the water channel at different stages of active release cycle: **c)** Start of release cycle after 1 turn (700 µm). **d)** Peak intensity of the release cycle. **e)** Beginning of the next cycle. **f)** Relative intensity of red dye in the microfluidic channel as a response to the actuation of the screw mechanism as measured over cross section iii over five consecutive cycles of screw compression. Scale bar is 20 mm for **a)** and 4 mm for **c-e)**.

2.5 Summary

In summary, A highly porous PDMS sponge that is fabricated using a microfluidic droplet generation system has been demonstrated. The application of hydroxy terminated PDMS reduces the hydrophobicity of PDMS, facilitating the loading of sponge with aqueous solutions. The elasticity of PDMS along with its interconnected porous structure enables the quick loading of the sponge with liquids upon manual compression. The PDMS sponge consists of large pores, which act as miniaturised reservoirs to store liquids. These pores are interconnected by small holes, which act as miniaturised diffusion barriers that restrict the release rate of stored liquids into surrounding fluidic environments. The ability to tailor the size of these holes allowed us to control the diffusion rate of dye through the sponge, expressed as $J_{dye} \propto \bar{d}_{hole}^{2.07}$. By varying the average size of the interconnecting holes from 19.1 to 29.6 μm it was possible to increase the diffusion rate of dye into a narrow channel by a factor of 2.4. This enables the sponge to act as a passive yet controllable reservoir, which allows the user to control the duration and rate of release of stored solutions.

Furthermore, the utility of the porous PDMS sponge for the passive release of stored chemicals into cell culture systems has been demonstrated. This feature is used to investigate the intracellular calcium signalling of endothelial cells in response to two different concentrations of ionomycin. Finally, the porous sponge can be used for the active release of stored liquids upon compression. This feature is demonstrated by cyclic release of stained water into the surrounding flow through compressing the sponge using a screw mechanism. The process of loading and unloading of the sponge can be repeated without changing the elastic or releasing characteristics of the sponge.

The PDMS sponge can be loaded with various drugs to investigate the response of cultured cells [50] or interaction between different cell populations [52]. More complicated cellular assays can also be designed by implementing multiple sponges to enable consequent preparation, stimulation and washing of cells with desired buffers, reagents, chemicals and drugs. The system can be equipped with stepper motors or solenoid actuators [53] to automate the active release of liquids from the sponge, also enabling more complex compression patterns.

Using this fabrication approach, the sponges created by introducing the stabilised water droplets into an unstructured volume of PDMS which was cured. It would be possible instead to introduce the water droplets into local regions of a more complex cast PDMS structure [54] to achieve a composite with solid and porous regions adding a new building block for lab-on-a-chip microfluidics.

2.6 References

[1] W. O. Kwang and H. A. Chong, "A review of microvalves," *Journal of Micromechanics and Microengineering,* vol. 16, no. 5, p. R13, 2006.

[2] D. J. Laser and J. G. Santiago, "A review of micropumps," *Journal of Micromechanics and Microengineering,* vol. 14, no. 6, p. R35, 2004.

[3] M. Boyd-Moss, S. Baratchi, M. Di Venere, and K. Khoshmanesh, "Self-contained microfluidic systems: a review," *Lab on a Chip,* 10.1039/C6LC00712K vol. 16, no. 17, pp. 3177-3192, 2016.

[4] K. J. Cha and D. S. Kim, "A portable pressure pump for microfluidic lab-on-a-chip systems using a porous polydimethylsiloxane (PDMS) sponge," (in eng), *Biomed Microdevices,* vol. 13, no. 5, pp. 877-83, Oct 2011.

[5] V. Rastogi, K. P. Velikov, and O. D. Velev, "Microfluidic characterization of sustained solute release from porous supraparticles," *Physical Chemistry Chemical Physics,* vol. 12, no. 38, pp. 11975-11983, 2010.

[6] J. C. McDonald *et al.*, "Fabrication of microfluidic systems in poly(dimethylsiloxane)," (in eng), *Electrophoresis,* vol. 21, no. 1, pp. 27-40, Jan 2000.

[7] K. Berean *et al.*, "The effect of crosslinking temperature on the permeability of PDMS membranes: evidence of extraordinary CO 2 and CH 4 gas permeation," *Separation and Purification Technology,* vol. 122, pp. 96-104, 2014.

[8] J. Li and Y. Zhang, "Porous Polymer Films with Size-Tunable Surface Pores," *Chemistry of Materials,* vol. 19, no. 10, pp. 2581-2584, 2007/05/01 2007.

[9] K. Jiao, C. L. Graham, J. Wolff, R. G. Iyer, and P. Kohli, "Modulating molecular and nanoparticle transport in flexible polydimethylsiloxane membranes," *Journal of Membrane Science,* vol. 401–402, pp. 25-32, 5/15/ 2012.

[10] S.-J. Choi *et al.*, "A Polydimethylsiloxane (PDMS) Sponge for the Selective Absorption of Oil from Water," *ACS Applied Materials & Interfaces,* vol. 3, no. 12, pp. 4552-4556, 2011/12/28 2011.

[11] X. Zhao, L. Li, B. Li, J. Zhang, and A. Wang, "Durable superhydrophobic/superoleophilic PDMS sponges and their applications in selective oil absorption and in plugging oil leakages," *Journal of Materials Chemistry A,* 10.1039/C4TA04406A vol. 2, no. 43, pp. 18281-18287, 2014.

[12] C. Yu *et al.*, "Facile Preparation of the Porous PDMS Oil-Absorbent for Oil/Water Separation," *Advanced Materials Interfaces,* vol. 4, no. 3, pp. n/a-n/a, 2017.

[13] S. Chatterjee, S. Sen Gupta, and G. Kumaraswamy, "Omniphilic Polymeric Sponges by Ice Templating," *Chemistry of Materials,* vol. 28, no. 6, pp. 1823-1831, 2016/03/22 2016.

[14] A. A. Chavan *et al.*, "Elastomeric Nanocomposite Foams for the Removal of Heavy Metal Ions from Water," *ACS Applied Materials & Interfaces,* vol. 7, no. 27, pp. 14778-14784, 2015/07/15 2015.

[15] D. N. H. Tran, S. Kabiri, T. R. Sim, and D. Losic, "Selective adsorption of oil-water mixtures using polydimethylsiloxane (PDMS)-graphene sponges," *Environmental Science: Water Research & Technology,* 10.1039/C5EW00035A vol. 1, no. 3, pp. 298-305, 2015.

[16] A. Zhang, M. Chen, C. Du, H. Guo, H. Bai, and L. Li, "Poly(dimethylsiloxane) Oil Absorbent with a Three-Dimensionally Interconnected Porous Structure and Swellable Skeleton," *ACS Applied Materials & Interfaces,* vol. 5, no. 20, pp. 10201-10206, 2013/10/23 2013.

[17] J.-W. Han, B. Kim, J. Li, and M. Meyyappan, "Flexible, compressible, hydrophobic, floatable, and conductive carbon nanotube-polymer sponge," *Applied Physics Letters,* vol. 102, no. 5, p. 051903, 2013.

[18] W. Liu *et al.*, "3D Porous Sponge-Inspired Electrode for Stretchable Lithium-Ion Batteries," *Advanced Materials*, vol. 28, no. 18, pp. 3578-3583, 2016.

[19] S. Liang *et al.*, "3D Stretchable, Compressible, and Highly Conductive Metal-Coated Polydimethylsiloxane Sponges," *Advanced Materials Technologies*, vol. 1, no. 7, pp. n/a-n/a, 2016.

[20] S. Liang *et al.*, "Liquid metal sponges for mechanically durable, all-soft, electrical conductors," *Journal of Materials Chemistry C*, 10.1039/C6TC05358K vol. 5, no. 7, pp. 1586-1590, 2017.

[21] W. Yang, Y. G. Nam, B.-K. Lee, K. Han, T. H. Kwon, and D. S. Kim, "Fabrication of a Hydrophilic Poly (dimethylsiloxane) Microporous Structure and Its Application to Portable Microfluidic Pump," *Japanese Journal of Applied Physics*, vol. 49, no. 6S, p. 06GM01, 2010.

[22] N. R. Cameron, "High internal phase emulsion templating as a route to well-defined porous polymers," *Polymer*, vol. 46, no. 5, pp. 1439-1449, 2/14/ 2005.

[23] G. Akay, M. A. Birch, and M. A. Bokhari, "Microcellular polyHIPE polymer supports osteoblast growth and bone formation in vitro," *Biomaterials*, vol. 25, no. 18, pp. 3991-4000, 8// 2004.

[24] M. S. Silverstein, "PolyHIPEs: Recent advances in emulsion-templated porous polymers," *Progress in Polymer Science*, vol. 39, no. 1, pp. 199-234, 1// 2014.

[25] X. Yang, L. Tan, L. Xia, C. D. Wood, and B. Tan, "Hierarchical Porous Polystyrene Monoliths from PolyHIPE," *Macromolecular Rapid Communications*, vol. 36, no. 17, pp. 1553-1558, 2015.

[26] Q. Wang, Y. Liu, J. Chen, Z. Du, and J. Mi, "Control of Uniform and Interconnected Macroporous Structure in PolyHIPE for Enhanced CO2 Adsorption/Desorption Kinetics," *Environmental Science & Technology*, vol. 50, no. 14, pp. 7879-7888, 2016/07/19 2016.

[27] M. Alikhani and M. R. Moghbeli, "Ion-exchange polyHIPE type membrane for removing nitrate ions: Preparation, characterization,

kinetics and adsorption studies," *Chemical Engineering Journal,* vol. 239, pp. 93-104, 3/1/ 2014.

[28] S. Hus, M. Kolar, and P. Krajnc, "Separation of heavy metals from water by functionalized glycidyl methacrylate poly (high internal phase emulsions)," (in eng), *J Chromatogr A,* vol. 1437, pp. 168-75, Mar 11 2016.

[29] C. Zhao, E. Danish, N. R. Cameron, and R. Kataky, "Emulsion-templated porous materials (PolyHIPEs) for selective ion and molecular recognition and transport: applications in electrochemical sensing," *Journal of Materials Chemistry,* 10.1039/B700929A vol. 17, no. 23, pp. 2446-2453, 2007.

[30] U. M. Patil *et al.*, "PolyHIPE Derived Freestanding 3D Carbon Foam for Cobalt Hydroxide Nanorods Based High Performance Supercapacitor," *Scientific Reports,* Article vol. 6, p. 35490, 10/20/online 2016.

[31] V. V. Ordomsky, J. C. Schouten, J. van der Schaaf, and T. A. Nijhuis, "Foam supported sulfonated polystyrene as a new acidic material for catalytic reactions," *Chemical Engineering Journal,* vol. 207–208, pp. 218-225, 10/1/ 2012.

[32] E. Erhan, E. Yer, G. Akay, B. Keskinler, and D. Keskinler, "Phenol degradation in a fixed-bed bioreactor using micro-cellular polymer-immobilized Pseudomonas syringae," *Journal of Chemical Technology & Biotechnology,* vol. 79, no. 2, pp. 195-206, 2004.

[33] S.-Y. Teh, R. Lin, L.-H. Hung, and A. P. Lee, "Droplet microfluidics," *Lab on a Chip,* 10.1039/B715524G vol. 8, no. 2, pp. 198-220, 2008.

[34] B. Gol, M. E. Kurdzinski, F. J. Tovar-Lopez, P. Petersen, A. Mitchell, and K. Khoshmanesh, "Hydrodynamic directional control of liquid metal droplets within a microfluidic flow focusing system," *Applied Physics Letters,* vol. 108, no. 16, p. 164101, 2016.

[35] M. Costantini *et al.*, "Highly ordered and tunable polyHIPEs by using microfluidics," *Journal of Materials Chemistry B,* 10.1039/C3TB21227K vol. 2, no. 16, pp. 2290-2300, 2014.

[36] M. Costantini *et al.*, "Microfluidic Foaming: A Powerful Tool for Tailoring the Morphological and Permeability Properties of Sponge-like Biopolymeric Scaffolds," (in eng), *ACS Appl Mater Interfaces,* vol. 7, no. 42, pp. 23660-71, Oct 28 2015.

[37] A. Quell, J. Elsing, W. Drenckhan, and C. Stubenrauch, "Monodisperse Polystyrene Foams via Microfluidics – A Novel Templating Route," *Advanced Engineering Materials,* vol. 17, no. 5, pp. 604-609, 2015.

[38] T. M. Obey and B. Vincent, "Novel Monodisperse "Silicone Oil"/Water Emulsions," *Journal of Colloid and Interface Science,* vol. 163, no. 2, pp. 454-463, 1994/03/15 1994.

[39] Z. Gao, J. Schulze Nahrup, J. E. Mark, and A. Sakr, "Poly(dimethylsiloxane) coatings for controlled drug release. I. Preparation and characterization of pharmaceutically acceptable materials," *Journal of Applied Polymer Science,* vol. 90, no. 3, pp. 658-666, 2003.

[40] C. I. Zoldesi and A. Imhof, "Synthesis of Monodisperse Colloidal Spheres, Capsules, and Microballoons by Emulsion Templating," *Advanced Materials,* vol. 17, no. 7, pp. 924-928, 2005.

[41] J. MacMullen, Z. Zhang, J. Radulovic, H. N. Dhakal, and N. Bennett, "An investigation of hydroxyl end-terminated polydimethylsiloxane (PDMS) in exterior oil-in-water (O/W) emulsion treatments," *Construction and Building Materials,* vol. 37, pp. 283-290, 12// 2012.

[42] M. C. Ford *et al.*, "A macroporous hydrogel for the coculture of neural progenitor and endothelial cells to form functional vascular networks invivo," *Proceedings of the National Academy of Sciences of the United States of America,* vol. 103, no. 8, pp. 2512-2517, February 21, 2006 2006.

[43] C. Ji, N. Annabi, A. Khademhosseini, and F. Dehghani, "Fabrication of porous chitosan scaffolds for soft tissue engineering using dense gas CO2," (in eng), *Acta Biomater,* vol. 7, no. 4, pp. 1653-64, Apr 2011.

[44] N. Annabi *et al.*, "Controlling the porosity and microarchitecture of hydrogels for tissue engineering," (in eng), *Tissue Eng Part B Rev*, vol. 16, no. 4, pp. 371-83, Aug 2010.

[45] S. Baratchi, J. G. Almazi, W. Darby, F. J. Tovar-Lopez, A. Mitchell, and P. McIntyre, "Shear stress mediates exocytosis of functional TRPV4 channels in endothelial cells," *Cellular and Molecular Life Sciences*, journal article vol. 73, no. 3, pp. 649-666, 2016.

[46] S. Baratchi *et al.*, "Examination of the role of transient receptor potential vanilloid type 4 in endothelial responses to shear forces," *Biomicrofluidics*, vol. 8, no. 4, p. 044117, 2014.

[47] P. Garstecki, M. J. Fuerstman, H. A. Stone, and G. M. Whitesides, "Formation of droplets and bubbles in a microfluidic T-junction-scaling and mechanism of break-up," (in eng), *Lab on a Chip*, vol. 6, no. 3, pp. 437-46, Mar 2006.

[48] D. P. D. F. P. Incropera, *Fundamentals of Heat and Mass Transfer*. John Wiley & Sons, 2002.

[49] R. Soffe, S. Baratchi, S.-Y. Tang, A. Mitchell, P. McIntyre, and K. Khoshmanesh, "Concurrent shear stress and chemical stimulation of mechano-sensitive cells by discontinuous dielectrophoresis," *Biomicrofluidics*, vol. 10, no. 2, p. 024117, 2016.

[50] K. Khoshmanesh *et al.*, "Dynamic Analysis of Drug-Induced Cytotoxicity Using Chip-Based Dielectrophoretic Cell Immobilization Technology," *Analytical Chemistry*, vol. 83, no. 6, pp. 2133-2144, 2011/03/15 2011.

[51] K. Khoshmanesh *et al.*, "Mixing characterisation for a serpentine microchannel equipped with embedded barriers," 2008, vol. 7270, pp. 727005-727005-11.

[52] Y. Lei *et al.*, "An on-chip model for investigating the interaction between neurons and cancer cells," *Integrative Biology*, 10.1039/C5IB00309A vol. 8, no. 3, pp. 359-367, 2016.

[53] S. Elizabeth Hulme, S. S. Shevkoplyas, and G. M. Whitesides, "Incorporation of prefabricated screw, pneumatic, and solenoid valves into microfluidic devices," *Lab on a Chip*, 10.1039/B809673B vol. 9, no. 1, pp. 79-86, 2009.

[54] C. Szydzik *et al.*, "Fabrication of complex PDMS microfluidic structures and embedded functional substrates by one-step injection moulding," *RSC Advances,* vol. 6, no. 91, pp. 87988-87994, 2016.

CHAPTER 3: A self-sufficient micro-droplet generation system using porous sponges: enabling simple and quick cellular assays

3.1 Abstract

Microfluidic droplet generation systems enable the production of micro-scale droplets. However, such systems generally rely on microfluidic structures, bulky and rather expensive supporting equipment such as pumps, specialised training and time-consuming processes, which limit their usage in biological laboratories. This chapter presents a self-sufficient droplet generation system by simply squeezing a porous polydimethylsiloxane (PDMS) structure filled with aqueous solutions into oil. This enables the generation of hundreds of isolated micro-scale droplets containing cells and desired chemicals inside a well. The number of encapsulated cells is proportional to the volume of the droplets, allowing for generating customised small, medium and large cell clusters. The droplets are chemically isolated, mechanically stable, and do not evaporate due to the presence of oil in the well. This sponge based droplet generation system facilitates customised cellular and molecular assays in a simple, quick and parallel manner suitable for biological laboratories with minimum supportive equipment and microfluidic skills.

3.2 Introduction

Microfluidic droplet generation systems enable the continuous formation of micro-scale droplets using a pair of immiscible liquids such as water and oil [1-3]. The size, shape and generation rate of the droplets depends on the flow rate and viscosity of the accompanying liquids as well as the interfacial tension between them [4]. Each droplet carries a very small amount of liquid, which can be loaded with multiple liquid solutions or desired micro/nano particle suspensions. This facilitates studying various chemical and biochemical reactions inside a stream of isolated droplets [5-9]. Recirculation of flow inside the droplets facilitates rapid mixing of the stored materials [10]. These reactions can also be triggered by optical, electrical or thermal stimuli [11, 12].

Encapsulation of single cells inside droplets has provided unprecedented opportunities for studying various cellular and molecular reactions in a high throughput manner. Cells need to be ordered along the inlet channel to ensure the droplets carry a single cell [13, 14]. The droplets can be loaded with desired reagents, chemicals, fluorescent probes, and functionalised beads to enable the stimulation of encapsulated cells and consequent detection of cellular responses. Such materials can be added into the cell suspension prior to injection into the microfluidic device [15-17] or be injected into the cell suspension on-chip [18-20]. The droplets can be sorted, deflected, trapped and released using various passive and active mechanisms [21, 22]. The droplets can be collected for a predetermined period to enable cellular reactions to occur [16] and re-injected into secondary microfluidic devices for further investigation [23, 24]. The chemical content of these droplets can be changed by combining two neighbouring droplets [23, 25, 26] or by injection of chemicals into moving

droplets [27]. The droplets can also be broken to measure the fluorescent response of chemically stimulated cells using flow cytometry [28] or to process the nucleic acids released from lysed cells using various sequencing technologies [29, 30].

Despite these advantages, current microfluidic droplet generation systems strongly rely on external bulky equipment such as multiple syringe pumps to drive the carrier and discrete fluids through the microfluidic structures. The operation of such systems requires general training and skills in microfluidics, and is rather time-consuming due to degassing, tubing and leakage. These drawbacks limit the widespread application of such systems in biological laboratories. Self-sufficient, stand-alone droplet generation systems, which could be operated with minimum reliance on external equipment and specialised training could facilitate the utilisation of this technology by biomedical researchers.

Porous sponges exhibit unique properties such as permeability and high surface area. They can be made from different materials such as cellulose [31-33], hydrogels [34], and polymers [35, 36] while their physical properties can be changed following synthesis with various chemicals or functionalisation with different nanomaterials [31-33]. In particular, polymeric porous sponges made of polydimethylsiloxane (PDMS) are suitable for microfluidic applications due to their biocompatibility, stability, transparency, and elasticity. PDMS sponges have been utilised for the active storage and release of solutions [37, 38]. In general, PDMS sponges are made by templating and the subsequent removal of crystal structured materials such as sugar cubes [39]. Alternatively, highly porous polymeric sponges can be made by injecting micro-scale droplets of water into

uncured polymers [40, 41]. Curing of the polymer and subsequent evaporation of the encapsulated water droplets leads to the formation of a network of interconnected air voids within a polymer scaffold. Using this method, highly porous PDMS sponges were fabricated, consisting of large pores that are interconnected by very small holes (presented in detail in **Chapter 2**), which has been utilised for the passive chemical stimulation of immobilised endothelial cells as well as the active release of solutions into microfluidic environments. Despite these advantages, PDMS sponges have not been used for generation of micro-scale droplets.

In this chapter, a novel approach was presented for generating micro-droplets by squeezing highly porous PDMS sponges loaded with aqueous solutions into a cell culture well filled with oil. Experiments indicate that upon squeezing, hundreds of micro-droplets are generated inside the well. The capability of this droplet generation system for encapsulating THP-1 human monocytic leukemia cells inside droplets was demonstrated. Measurements indicate that the number of encapsulated cells is proportional to the volume of droplets as well as the concentration of cells in the cell suspension. Furthermore, cytotoxicity assays were conducted using this encapsulation method. As a proof-of-concept, the response of encapsulated THP-1 cells to hydrogen peroxide using fluorescent microscopy was studied. The ability to generate droplets with different chemical contents into the same well was also demonstrated. The cells settle at the lowest surface of the droplets without using any secondary immobilisation mechanisms. This sponge based droplet generation system enables highly parallel cellular assays in a very simple, versatile and quick manner without the need for rather expensive supporting equipment or any expertise in microfluidics.

3.3 Materials and Methods

3.3.1 Fabrication of the porous PDMS sponge

The PDMS sponge is fabricated using a microfluidic T-junction droplet generation system imprinted into a PDMS slab, as presented in detail in **Chapter 2** and briefly summarised in **Figure 3.1**. Deionised water mixed with a surfactant (polysorbate 20, Sigma-Aldrich) (19:1 v/v) is injected into a continuous phase consisting of PDMS base, PDMS curing agent (Sylgard 184, Dow Corning) and monohydroxy terminated PDMS (Sigma-Aldrich) (15:2:5 v/v) to create droplets of water in uncured PDMS. The resulting emulsion is then collected and cured in a high humidity environment at room temperature. The water is then squeezed out of the sponge leaving a porous PDMS sponge consisting of a network of large pores ($D_{pore} = 356 \pm 74$ μm) which are interconnected via small holes ($d_{hole} = 23.5 \pm 11.2$ μm) with an overall porosity of 64.1%. SEM imaging presented in **Figure 3.1e** shows the non-uniform size of the pores with larger pores accumulating at the top section of the sponge during the curing process. This indicates the expansion or shrinkage of the droplets within the PDMS chamber, which could be due to the gas permeability of PDMS to water vapour as well as waters relatively low vapour point.

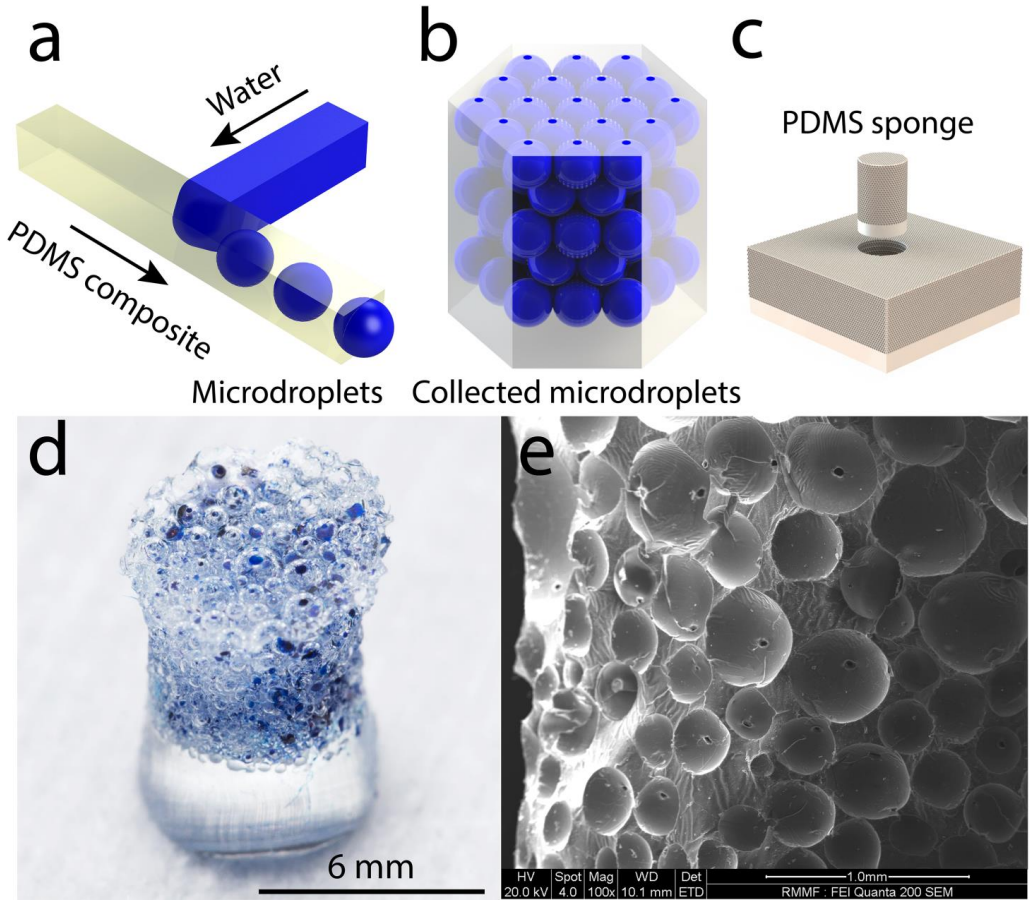

Figure 3.1: Fabrication process of the porous PDMS sponge, as explained in reference [42]. **a)** A microfluidic droplet generation system used for generating water droplets by injecting deionised water mixed with polysorbate surfactant (19:1 v/v) into a carrier fluid comprised of PDMS base, PDMS curing agent and monohydroxy terminated PDMS (15:2:5 v/v). The T-junction has cross-sectional dimensions of 300 µm × 300 µm, **b)** The emulsion is then collected in a container for curing, **c)** A 6 mm section of sponge is then isolated using a biopsy punch, **d)** Photograph of the PDMS sponge partially loaded with blue dye for visualisation. **e)** SEM image of the PDMS sponge showing the large pores interconnected by small holes.

3.3.2 Cell preparation

The human THP-1 monocytic leukemia cell line was grown in RPMI1640 medium supplemented with 10% fetal bovine serum, 50 U/ml of penicillin and 50 µg/ml of streptomycin at 37°C, 5% CO_2. Before each experiment, the cell suspension was diluted to the concentrations of 3×10^6 and 6×10^6 cells/ml using the growth media.

3.3.3 Microscopic imaging and Analysis

Microscopic images were acquired using a Nikon Eclipse Ti inverted fluorescence microscope (Nikon Corporation, Japan) equipped with a QuantEM:512SC electron-multiplying CCD camera (Photometrics, USA) using objective lenses 4×, 10×, 20× (Nikon). Fluorescence images were obtained using an Intensilight C-HGFI UV light source (Nikon) set to ND8 in conjunction with a Nikon G-2A filter set to capture the response of propidium iodide (ex/em 536/617 nm) stained THP-1 cells. Automated time-lapse image acquisition was acquired using NIS-Elements software (Advanced Research, Nikon Instruments) at 5 second intervals with an exposure time of 400 ms with an electron-multiplier gain of 200× to minimise photo bleaching. Fluorescence intensities were extracted using NIS-Elements software, and subsequently normalised in Microsoft Excel. Results shown are representatives of three independent experiments. Counting and measurement of droplets were performed using ImageJ (https://imagej.nih.gov/ij/).

3.4 Results and discussion

3.4.1 Droplet generation using PDMS porous sponge

The process of droplet generation consists of both loading and squeezing steps, as schematically shown in **Figure 3.2**. During loading step, the sponge is placed in a cell culture well filled with aqueous solutions, and gently squeezed two to three times to be filled (**Figures 3.2a-c**). The loaded sponge is then gently placed into the second well filled with olive oil, and gently squeezed to release the stored solution into the surrounding oil (**Figures 3.2d-e**). This leads to generation of hundreds of micro-scale droplets which settle at the bottom surface of the well (**Figures 3.2f**). The manual squeezing of the sponge is principally similar to deformation of elastomeric membranes used in ref. [43] for discretisation of stored liquid and consequent generation of droplets.

Olive oil is 80 times more viscous than water ($\mu_{\text{olive oil}}$ = 80 mPa) yet is 8.55% less dense than water ($\rho_{\text{olive oil}}$ = 914.5 kg/m^3) [44]. The high viscosity of olive oil is essential to produce sufficient shear force to break the continuous water phase into micro-scale droplets upon leaving the sponge, while its low density facilitates the settling of produced water droplets onto the surface of the well. In comparison, fluorinated oils which are commonly used in microfluidic droplet generation systems [17, 19, 21, 30], are less viscous yet denser than water, which makes them unsuitable for this approach.

The sponge can then be removed from the well for further analysis of droplets (**Figure 3.2g**). The resulting droplet pattern shown here is obtained by inserting a PDMS sponge with a diameter of 6 mm and a height of 8 mm loaded with a solution of deionised water stained with red dye into a 6-well plate (Corning®

Costar® 3516, diameter = 34.8 mm) containing 3 ml of olive oil. It should be noted that the surface of the well should be non-treated to avoid the adhesion of droplets to the well plate.

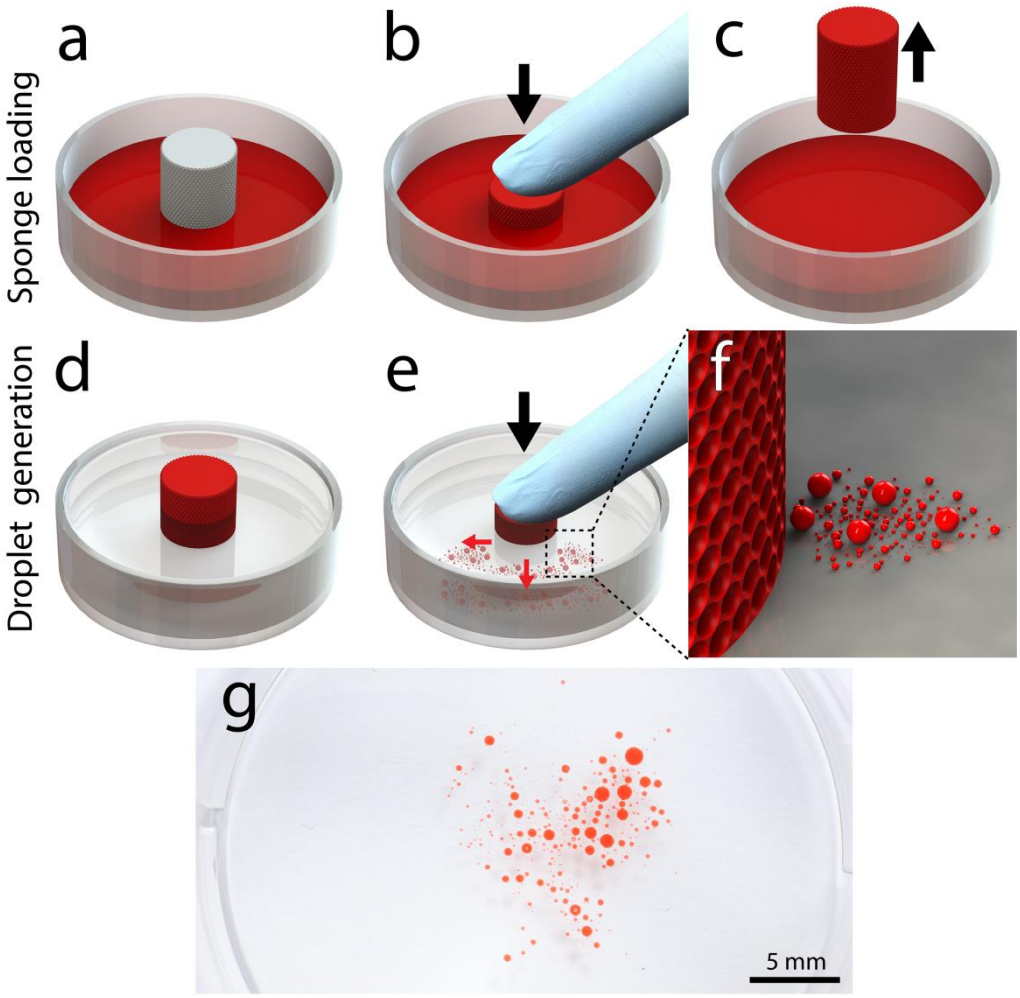

Figure 3.2: Generation of aqueous micro-droplets-in-oil emulsion using a porous PDMS sponge. **a)** Schematic of the droplet generation method, including a porous PDMS sponge placed into a well containing water with red dye. **b)** Manual compression of the sponge to load the aqueous solution. **c)** Removal of the saturated sponge. **d)** Placement of the sponge into the second well containing olive oil **e)** Generation of micro-droplets-in-oil via manual compression of the sponge. **f)** Droplets settling on the bottom of the well plate. **g)** Photograph of water droplets-in-oil settled on the surface of a well plate.

3.4.2 Principles of sponge based droplet generation

The ability of the PDMS sponge to generate a large quantity and variety of droplet sizes, as presented in **Figure 3.2g** lies in its unique structure, which consists of a network of large pores that are only interconnected via small holes (**Figure 3.1e**). The large pores ($D_{\text{pore}} = 356 \pm 74$ μm) facilitate the storage of aqueous solutions inside the sponge, whereas the small holes ($d_{\text{hole}} = 23.5 \pm 11.2$ μm) facilitate the passage of solution from one pore to another upon squeezing of the sponge. The small holes located at the interface of sponge and surrounding oil serve as micro-scale 'orifices', which facilitate the breaking (pinch off) of droplets by stationary viscous oil upon leaving the sponge, as schematically presented in **Figure 3.3**.

The shear stress induced at the interface of water-oil can be expressed as $\tau \propto \mu_{solution} U_{solution}/d_{hole}$ is, in which $\mu_{solution}$ is the viscosity of water, $U_{solution}$ is the average velocity of aqueous solution through the orifice induced by squeezing, which can be defined as $U_{solution} = \dot{Q}_{solution}/\sum A_{hole} = 4\, A_{sponge}\, \Delta\dot{h}/N_{hole}\, \pi d_{hole}^2$, where $\dot{Q}_{solution}$ is the average flow rate of water released from the sponge, A_{hole} is the area of orifices along the external surface of the sponge which are exposed to oil, A_{sponge} is the basal surface area of the sponge, $\Delta\dot{h}$ is the rate of sponge compression, N_{hole} is the total number of holes along the external surface of the sponge. This suggests that $\tau \propto d_{hole}^{-3}$.

Accordingly, the capillary number [4] of generated droplets ($Ca = \mu_{solution} U_{solution}/\gamma_{solution-oil}$) can be expressed as:

$$Ca = 4\, \mu_{solution}\, A_{sponge}\, \Delta\dot{h}/N_{hole}\, \pi d_{hole}^2\, \gamma_{solution-oil}.$$

It should be noted that the level of shear stress induced on encapsulated cells is minimal, as the cells are suspended inside the cell suspension.

SEM imaging characterisation indicates that $d_{hole} = 23.5 \pm 11.2$ μm [42], suggesting that for the majority of interconnecting holes lie between 12.3 to 35.7 μm. This suggests that the sponge acts as a droplet generation system with multiple orifices with varying sizes, which enables it to produce various droplet sizes simultaneously, as explored in **Section 3.4.3**.

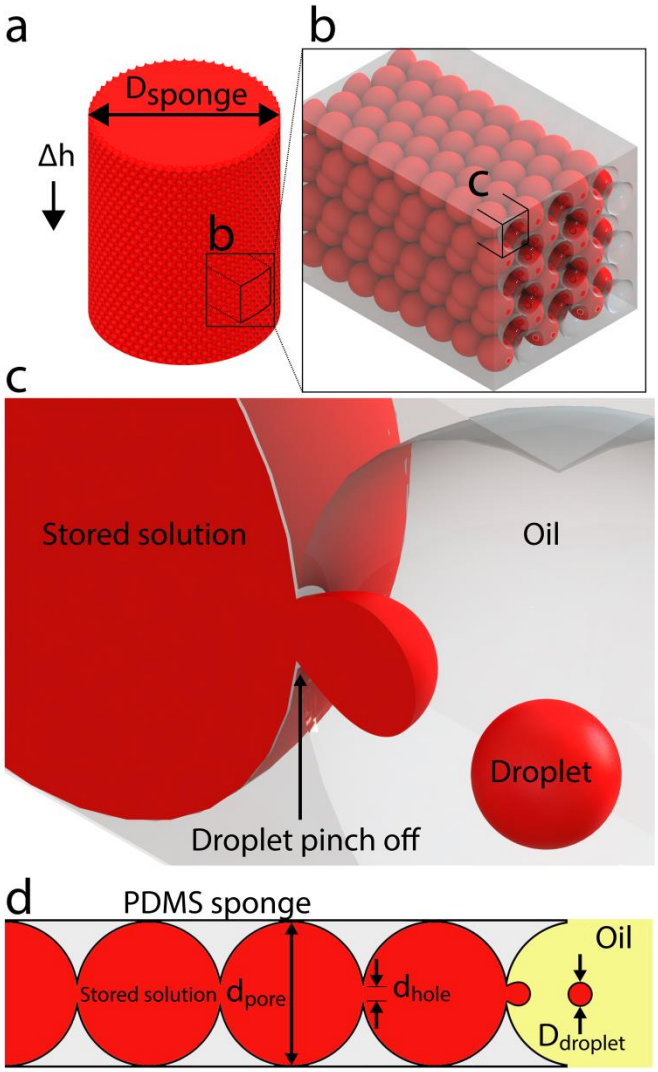

Figure 3.3: Schematics of micro-droplet generation using a porous PDMS sponge. **a)** Rendering of the PDMS Sponge filled with a red aqueous solution. **b)** Shows the internal interconnected porous structure of the filled sponge. **c)** Schematic of the process of droplet pinch off when squeezed into oil. **d)** A simplified schematic of the droplet generation system.

3.4.3 Size distribution of generated droplets

Figures 3.4a-d show the stitched microscopic images of generated droplets over successive squeezes. In this case, the sponge was loaded with cell culture medium and gently squeezed over four separate wells prefilled with olive oil, as described in **Figure 3.2**. The droplets were counted and measured using ImageJ to calculate their size and volume distributions, as shown in **Figures 3.4a′-d′**. The first squeeze produced 298 droplets in the range of 5-1600 µm in diameter (**Figures 3.4a′**). Smaller droplets were not counted, as they were smaller than the diameter of THP-1 cells investigated in this paper. A positively skewed normal distribution was obtained with 44.6% of droplets falling between 10-30 µm in diameter, and 89.9% falling between 10-200 µm. Similar trends are obtained for the volume distribution of droplets with 37.9% of droplets falling between 1-10 pL, and 94.3% of them below 10 nL (shown in the insets of **Figures 3.4a′-d′**).

Interestingly, successive squeezes produced similar size and volume distributions of droplets. However, the number of generated droplets increased over successive squeezes. For instance, 394, 815, and 1061 of droplets were counted within the range of 5-1600 µm produced in 2^{nd} to 4^{th} squeezes, respectively. Interestingly, this increase was observed mostly for droplets smaller than 100 µm, as shown in **Figure 3.4e**. This also coincided with a reduction in the number of droplets larger than 200 µm, which can be clearly seen in **Figures 3.4a-d**. This was associated with increasing the number of droplets with volumes less than 10 pL, as shown **Figure 3.4e-inset.** Similar trends were obtained in five independent experiments.

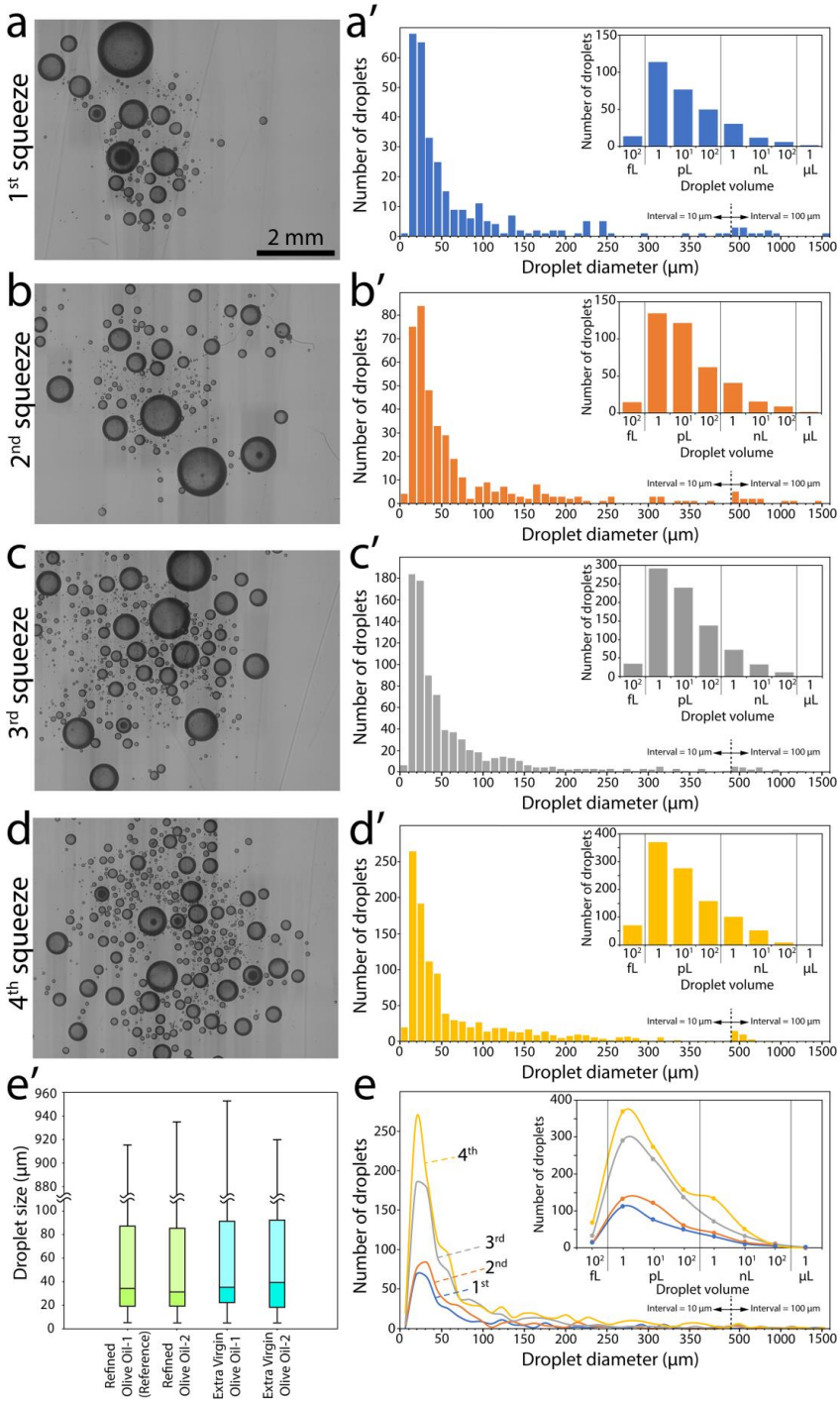

Figure 3.4: Characterisation of droplets generated by successive squeezes. **a-d)** Stitched microscopic images of four successive squeezes. **a´-d´)** The size distribution of micro-droplets for each squeeze with the inset showing the distribution of droplet volume. **e)** Comparison of droplet size and droplet volume with respect to each squeeze. **e´)** Comparison of droplet size distribution obtained at the 4th squeeze using various olive oils.

According to **Figures 3.4a′-d′**, 46.9% of droplets lie in the range of 12.3 to 35.7 µm, suggesting a very good correlation between the diameter of interconnecting holes and the diameter of droplets. It was hypothesised that the larger droplets are generated when the orifice is not directly exposed to oil, and instead is located at the upstream of a large pore which holds cell culture medium (**Figure 3.5**).

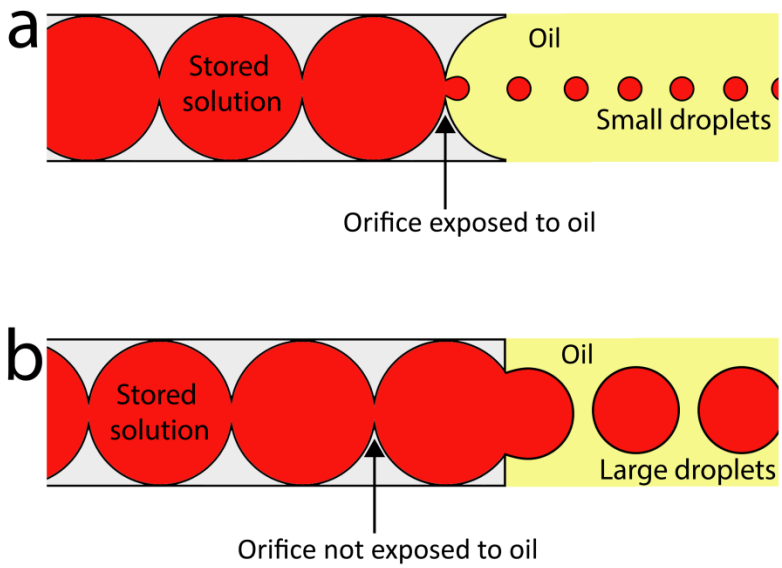

Figure 3.5: Varying the size of droplets according to the location of orifice with respect to surrounding oil. **a)** Orifice is exposed to oil leading to generation of small droplets. **b)** Orifice is not exposed to oil and is followed by a portion of a large pore leading to generation of large droplets.

The droplet size distribution was further investigated using two categories of olive oils, including ‘refined’ and ‘extra virgin’. Each category was provided from two independent Australian suppliers (Always Fresh and Moro). The ‘refined’ olive oil supplied from Always Fresh is the reference oil used throughout the manuscript. Similar size distribution trends were obtained using various olive oils (**Figure 3.4e′**), in which whiskers represent the 0^{th} and 100^{th} percentiles (corresponding to largest and smallest droplet sizes), and the boxes represent the 25^{th}, 50^{th} and 75^{th} percentiles. This is expected, as these oils have similar viscosities ranging from 75 to 83 mPa at room temperature [45], inducing similar shear stress levels at the interface of water-oil. These oils have also similar densities [45] facilitating the settling of droplets in the well.

3.4.4 Reducing the heterogeneity of droplet sizes

The possibility for improving the uniformity of droplets dimensions was investigated by sieving them using conventional cell strainers. In doing so, a cell strainer was submerged in oil above the well substrate. A sponge loaded with cell culture medium was then squeezed (four times) above the filter using tweezers. This enabled droplets smaller than the mesh size to pass through the strainer. The strainer was then gently removed from the well to facilitate the imaging process (**Figure 3.6**). **Figures 3.7a-d** present the stitched images of unfiltered cells, and filtered cells using nylon mesh cell strainers (pluriStrainer, Germany) with mesh sizes of 500, 200 and 100 µm, respectively. **Figure 3.7e** compares the size distribution of droplets with the whiskers representing the 0^{th} and 100^{th} percentiles (corresponding to largest and smallest droplet sizes), and the boxes representing the 25^{th}, 50^{th} and 75^{th} percentiles. It should be noted that the unfiltered case corresponds to the 4^{th} squeeze, as previously shown in **Figure 3.4d**. The size of the largest droplet reduced from 915 µm for the unfiltered case to 412, 164, and 94 µm for the filtered cases with 500, 200 and 100 µm mesh sizes. This in turn reduced the heterogeneity of droplets. The largest and median droplet sizes reduced proportional to the mesh size, as given in the inset. The filtering reduced the number of droplets settling in the well. This is because the large droplets block the mesh filter, reducing the chance of smaller droplets to pass through the filter. This also increases the median droplet size pushing them toward the centre of the box.

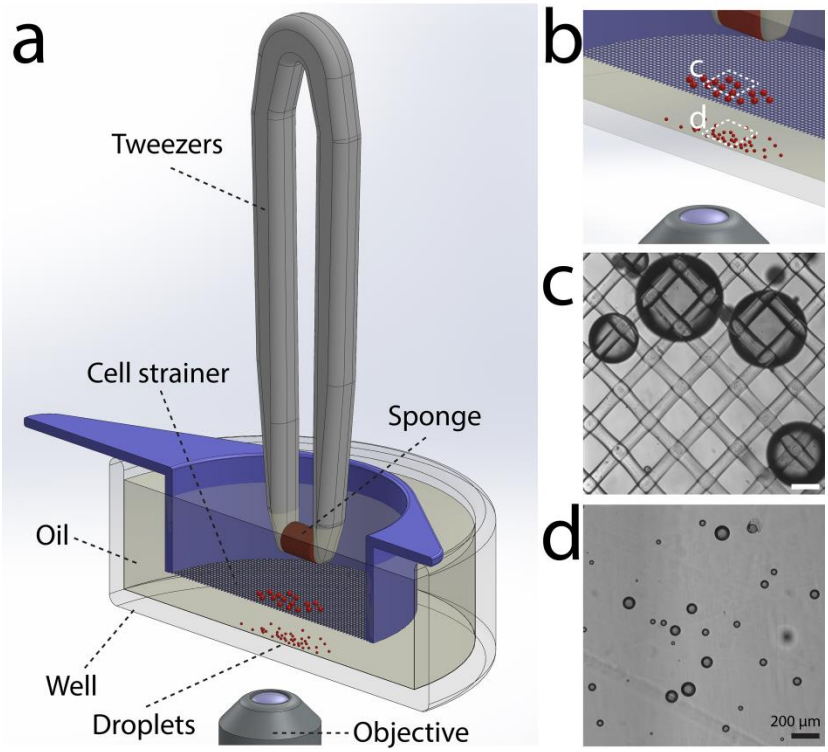

Figure 3.6: Schematics of size-based droplet filtering using a cell strainer: **a)** experimental setup, **b)** Close-up of experimental setup, **c)** Large droplets trapped by the cell strainer with a mesh size of 200 µm, **d)** Small droplets that have passed through the mesh and settled on the well substrate.

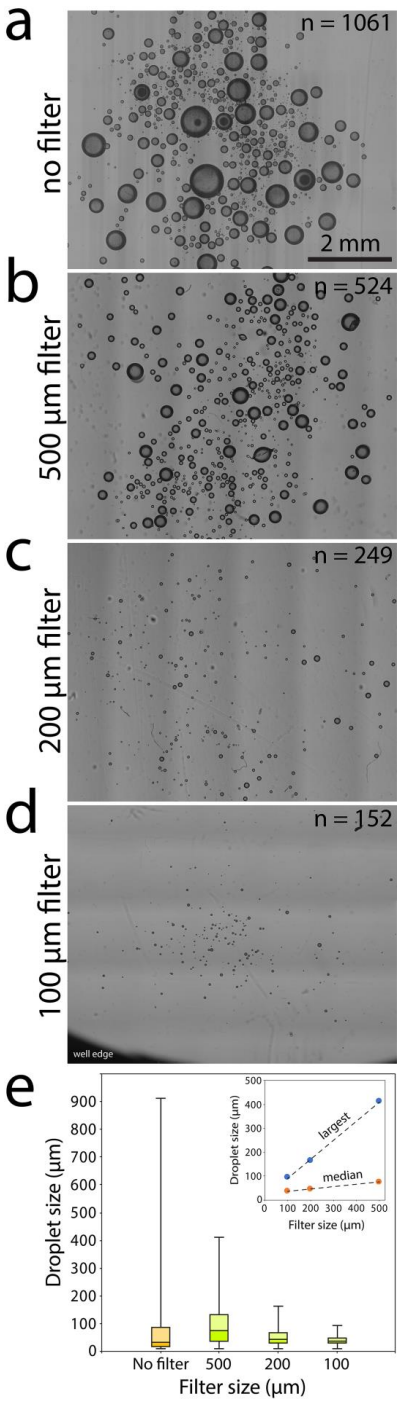

Figure 3.7: Improving the homogeneity of droplet dimensions by sieving using nylon mesh filters. **a-d)** Stitched images showing the distribution of unfiltered droplets at the 4th squeeze, and filtered droplets using 500, 200, and 100 µm mesh filters, respectively. **e)** Comparing the size distribution of droplets. The whiskers represent the minimum and maximum droplet sizes, and the boxes represent the 25th, 50th and 75th percentiles.

3.4.5 Encapsulation of cells inside droplets: enabling droplet-based cellular assays

Further experiments were conducted to investigate whether cells can be encapsulated inside the generated droplets. In doing so, the sponge was loaded with a cell suspension containing THP-1 cells, and squeezed in a well containing olive oil. Experiments indicated that the cells can indeed be encapsulated inside droplets (**Figure 3.8a**). The majority of encapsulated cells settled at the lowest surface of the droplet in contact with the well surface, which facilitated monitoring of cells using inverted microscopy.

Next, the number of cells inside each droplet was counted to investigate whether the population of encapsulated cells can be correlated to the size of droplets. Droplets with diameters ranging from 5 to 300 µm, which constituted ~95% of generated droplets. In doing so, the droplets were divided into six groups according to their diameter, as follows: $D_{droplet}$ = 25±2.5, 50±5, 100±10, 150±15, 200±20, and 250±25 µm. The number of encapsulated cells within each droplet group was counted using ImageJ. Counting was performed over four successive sponge squeezes with the droplets generated in each squeeze collected in separate wells. For example, **Figure 3.8b** presents the number of encapsulated cells against droplet diameter averaged over four successive squeezes. Measurements revealed that the average number of encapsulated cells can indeed be correlated with the diameter of droplets: $\bar{N}_{\mathrm{Cell}} \propto D_{\mathrm{Droplet}}^{3.06}\,(\mu\mathrm{m})$. This is significant, as it suggests that the average number of encapsulated cells is proportional to the volume of droplets: $\bar{N}_{\mathrm{Cell}} \propto V_{Droplet}$. A similar trend was obtained for 1st to 4th sponge squeezes with a maximum ~10% standard deviation observed between them (**Figure 3.8c**). Reducing the concentration of THP-1

cells in the cell suspension reduced the number of encapsulated cells (**Figure 3.8d + Figure 3.9**). Similar trends were observed in three independent experiments.

These findings suggest that this droplet generation method enables the creation of hundreds of isolated droplets inside a well with a single squeeze, which accommodate small, medium and large cell clusters depending on the size of droplets. These cell clusters are isolated and several can be observed in the same field of view. This provides unique opportunities for studying various cellular responses using different categories of cell populations.

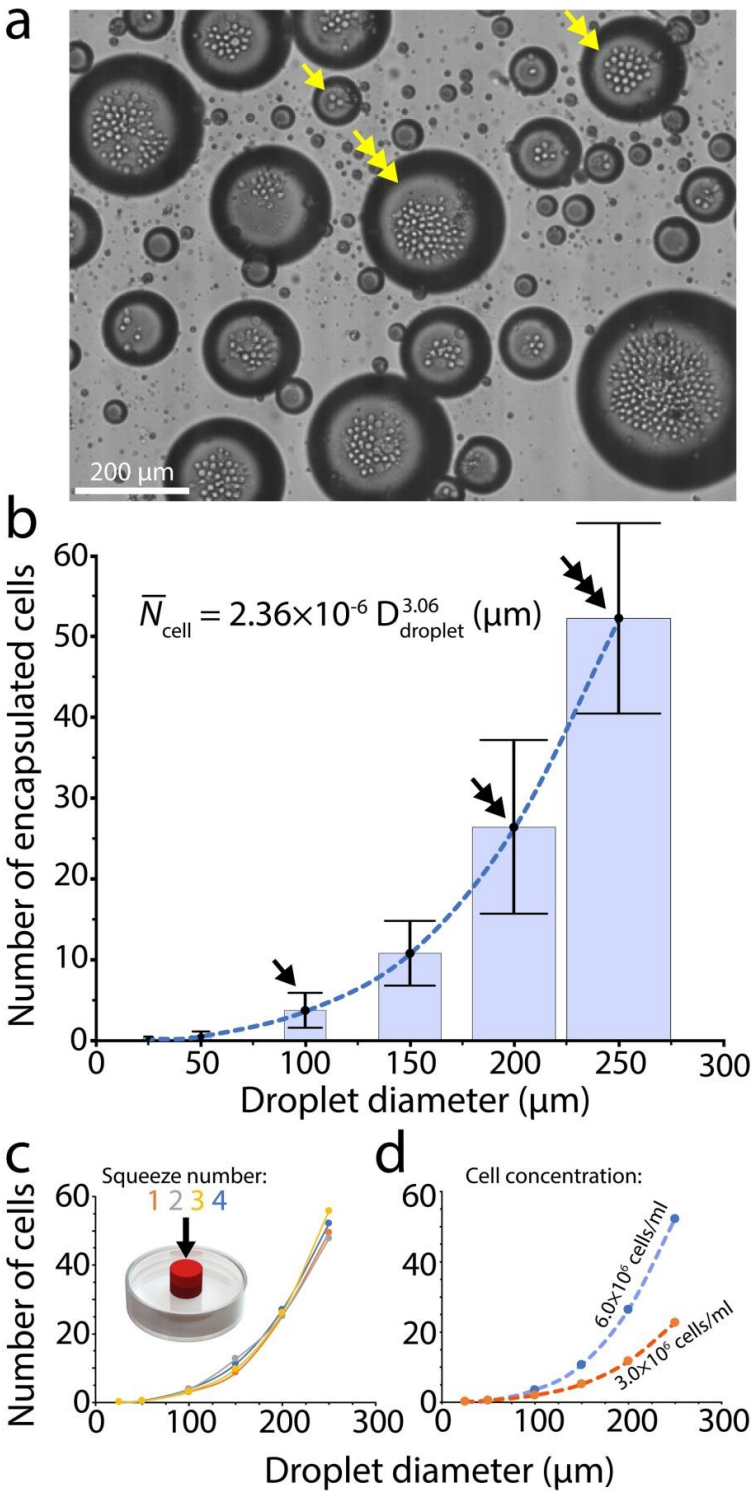

Figure 3.8: Encapsulation of cells inside the micro-droplets. **a)** A snapshot of THP-1 cells encapsulated in micro-droplets. **b)** The number of encapsulated cells against the diameter of droplets. **c)** The number of encapsulated cells over successive squeezes. **d)** The number of encapsulated cells at two cell concentrations.

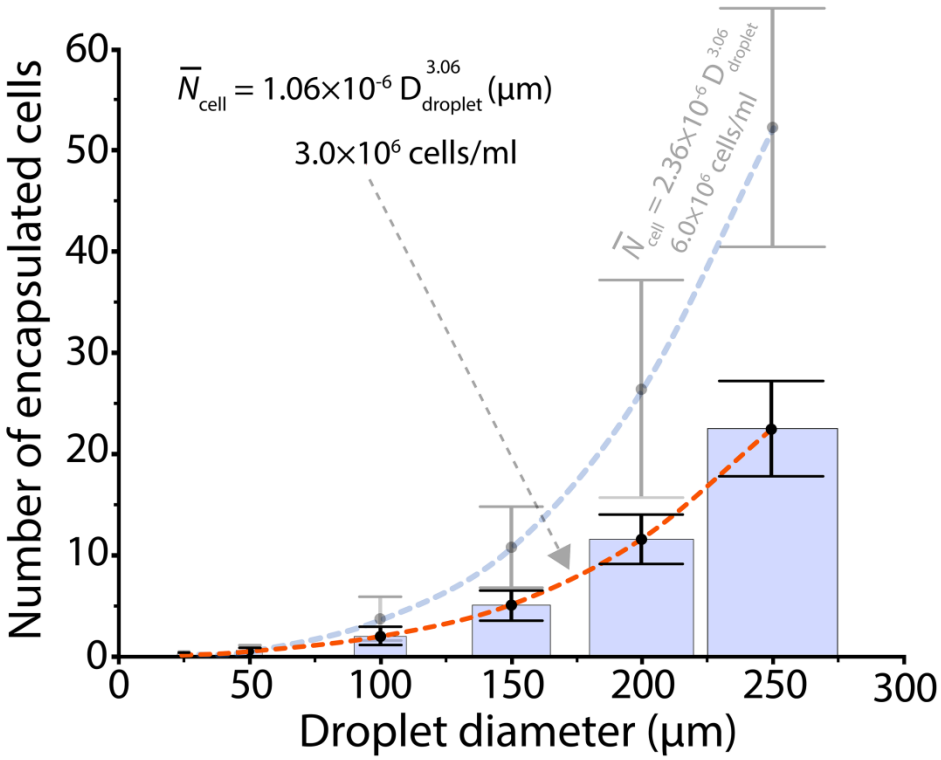

Figure 3.9: The number of encapsulated cells against the diameter of droplets shown for the cell concentrations of 3.0×10^6 and 6×10^6 cells/ml.

3.4.6 Analysing the viability of encapsulated cells

To ensure the process of encapsulating cells within droplets does not damage the cells, viability tests were conducted. THP-1 cells in culture medium were treated with 25 µg/ml of propidium iodide (PI), which is a fluorescent stain, which infiltrates into the plasma membrane of damaged cells and stains their cell nucleus. PI-treated cells were loaded into the PDMS sponge to be encapsulated within droplets. The viability of the encapsulated cells was monitored over a 3 hour period. In doing so, images at 5 minute intervals were extracted, and measured the normalised fluorescent intensity of cells using NIS Elements software (**Figure 3.10a** + **Movie 3.1** (Clickable online video)). Using this data, viability curves of the encapsulated cells were obtained (**Figure 3.10c**). An off-chip viability assay was also conducted by treating cells with PI and directly applying them into a well (**Figure 3.11 + Movie 3.2)** Similar viability curves were obtained from on-chip (droplet encapsulated) and off-chip assays, suggesting that this sponge droplet generation system does not damage cells over a 3 hour period (**Figure 3.10c**).

Proof-of-concept cytotoxicity experiment were also conducted by treating cells with hydrogen peroxide (H_2O_2) [46, 47]. THP-1 cells were treated with 20 mM H_2O_2 following which PI was added to the cell culture medium. These cells were then loaded into the PDMS sponge to be encapsulated within droplets. The viability of the encapsulated cells was monitored over a 3-hour period (**Figure 3.10b** + **Movie 3.3**), using which the viability curve was obtained for the H_2O_2 treated cells (**Figure 3.10c**). Stitched microscopic images confirmed the death of >98% of the cells, which were encapsulated inside a total number of 693 droplets after 3 hours (**Figure 3.13**). Similar viability curves were obtained with off-chip

assays (**Figure 3.12** + **Movie 3.4**). Furthermore, analysing the size of H_2O_2 containing droplets indicated similar trends presented in **Figure 3.4e**, suggesting that the incorporation of cell suspension, H_2O_2 or the by-products of treated cells does not influence the size distribution of droplets.

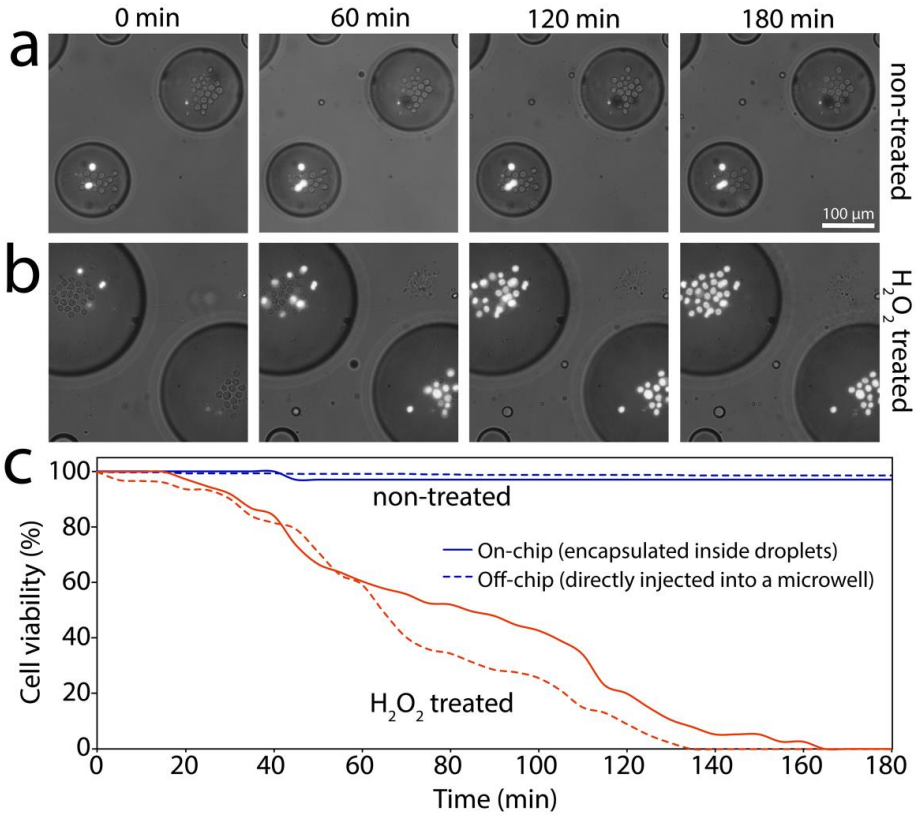

Figure 3.10: Analysis of cell viability for THP-1 cells encapsulated in droplets. **a)** Control experiment comprising of cells suspended in cell culture media and PI fluorescent probe encapsulated in droplets. **b)** Cytotoxicity experiment comprising of cells suspended in cell culture media and PI fluorescent probe treated with 20 mM H_2O_2 encapsulated in droplets. **c)** Viability curves showing the response of control and H_2O_2 treated cells indicating similar responses for off-chip (petri dish) and on-chip (encapsulated in droplets) experiments over 180 minute period.

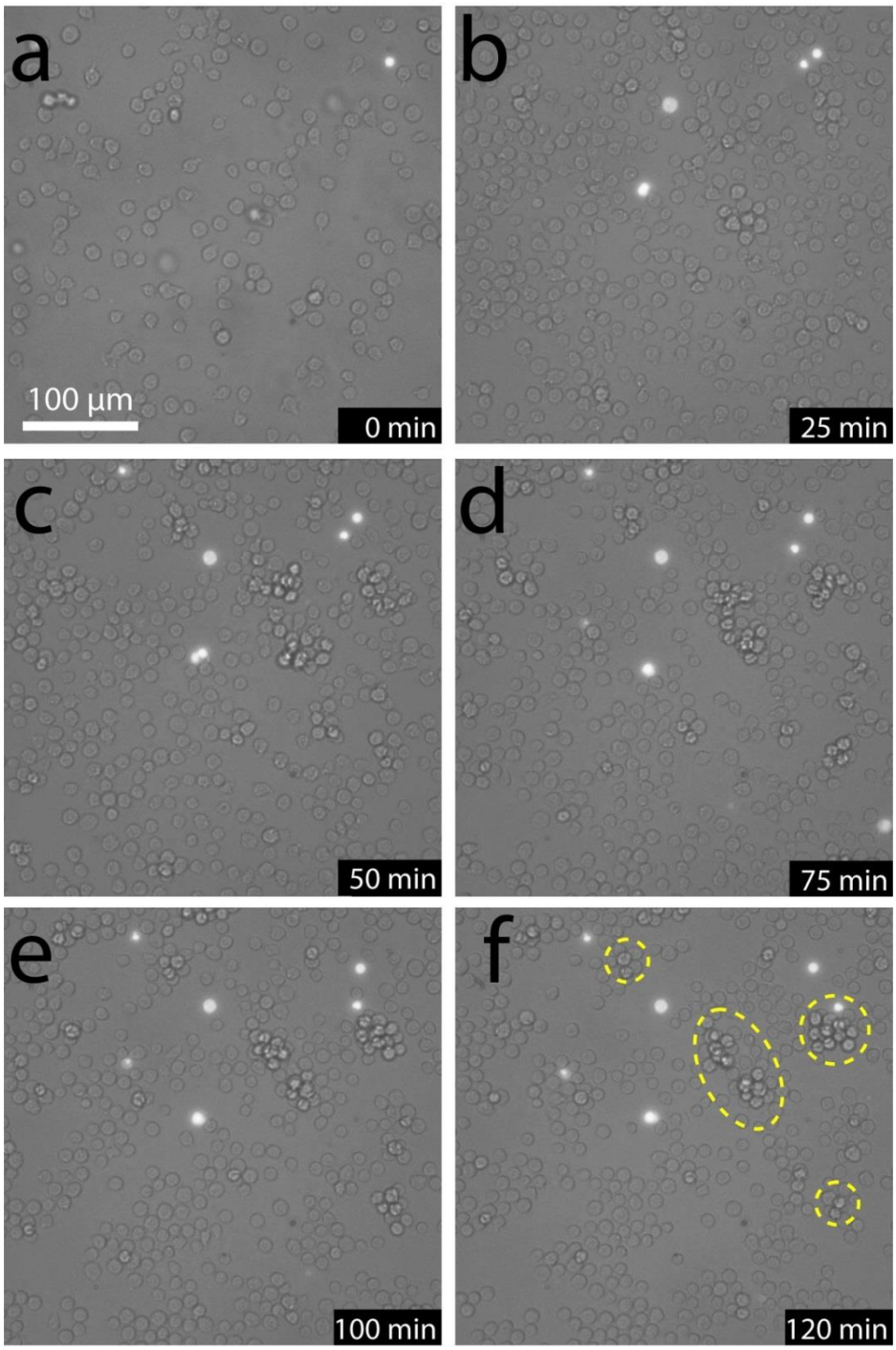

Figure 3.11: Snapshot images captured over a period of 120 minutes to demonstrate the motility of THP-1 cells following injection into a 24 mm diameter well. The images clearly show the crawling and swarming of cells even after 120 minutes, which makes it challenging for tracking individual cells. Highly motile cell clusters are highlighted with dashed lines.

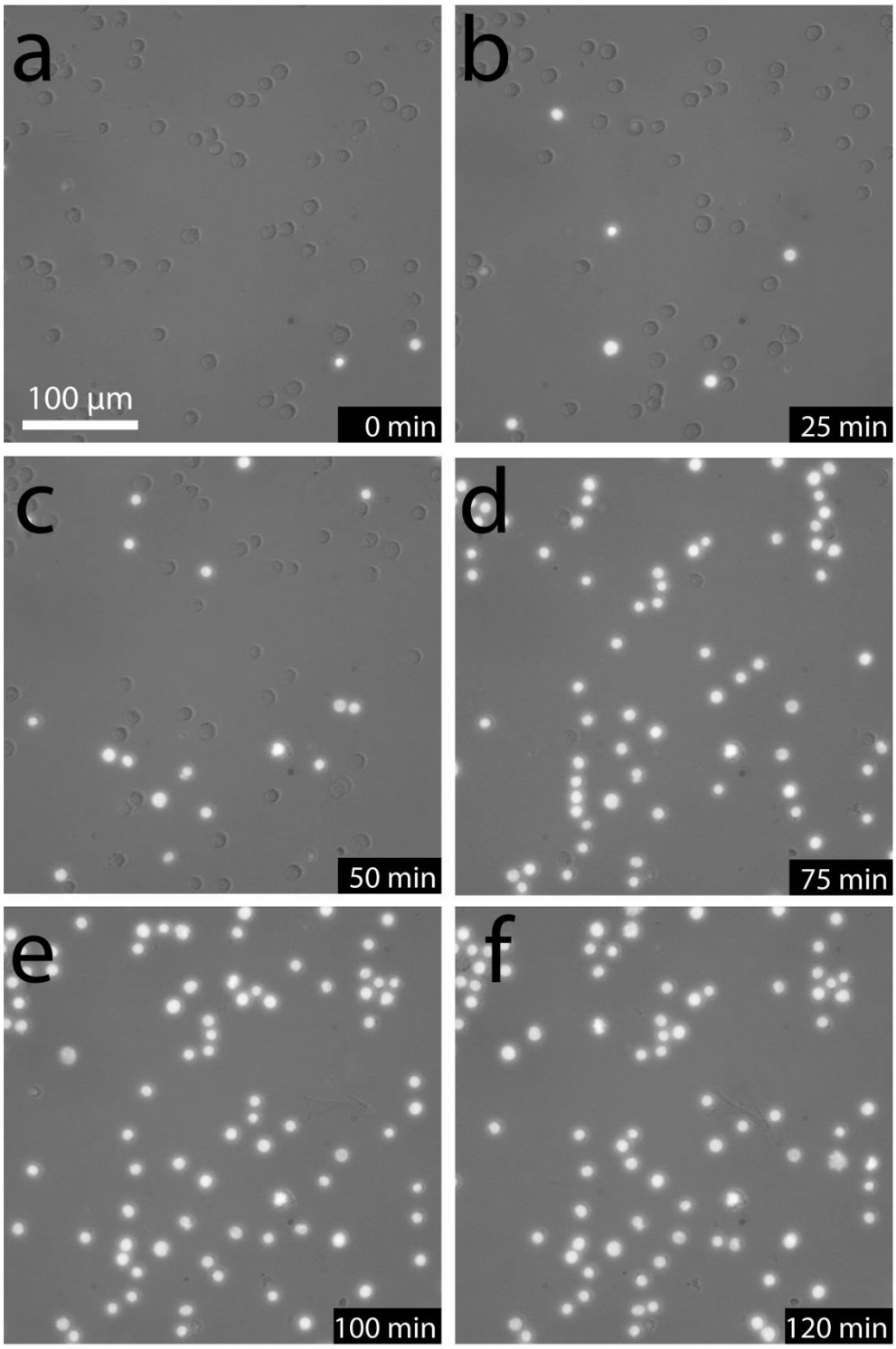

Figure 3.12: Snapshot images captured over a period of 120 minutes to demonstrate the motility of H_2O_2 treated THP-1 cells following injection into a 24 mm diameter well.

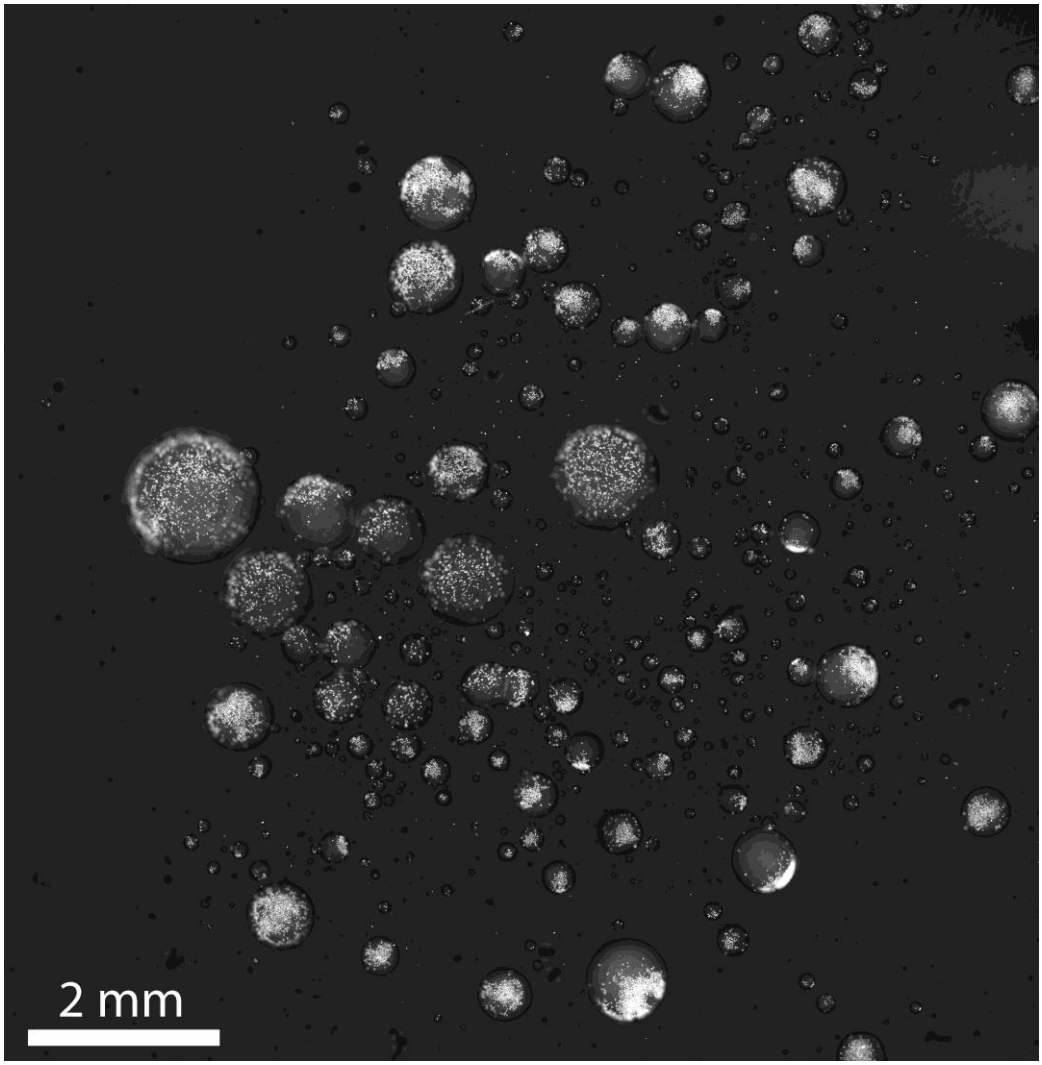

Figure 3.13: A large image of H_2O_2 stimulated/PI stained cells encapsulated inside droplets. This image is obtained by stitching an array of 7×7 images captured with a 4× Nikon objective.

3.4.7 Parallel viability assays

Considering that the droplets are isolated this allows for parallel cytotoxicity assays to be conducted using various chemical stimuli simultaneously. A simple experiment was carried out by loading two sponges with red and blue dye solutions and squeezing them in the same well (**Figure 3.14a**). Only two droplets merged in this process. Extended experiments indicated that the droplets smaller than 150 µm are very stable and do not merge due to dominance of surface tension.

Based on this, a proof-of-concept parallel cytotoxicity assay was conducted utilising two sponges. The first sponge was loaded with a suspension of THP-1 cells containing PI. The second sponge was loaded with a suspension of THP-1 cells containing PI and treated with 20 mM H_2O_2. The sponges were placed in the same well at approximately 5 mm apart, and squeezed simultaneously. A location of the well was selected, where multiple droplets generated by the first and second sponges were settled in close proximity (**Figure 3.14b**). The droplets were easily differentiated due to addition of blue dye solution into the H_2O_2 treated THP-1 cell suspension. This allowed us to monitor the response of non-treated and H_2O_2 treated cells over a 120 minute period in the same field of view (**Figure 3.14c-e** + **Movie 3.5**). The viability curves based on a small population of 16 cells is presented in **Figure 3.14f**. The results matched very well with the results presented in **Figure 3.10**, where the viability of cells in the presence and absence of H_2O_2 was studied in two separate experiments.

This experiment further proves the ability of this sponge based droplet generation system for formation of isolated cell clusters that are pre-stimulated with various

chemicals in close proximity of each other, paving the way for conducting highly parallel cellular assays in a simple, quick, and inexpensive manner.

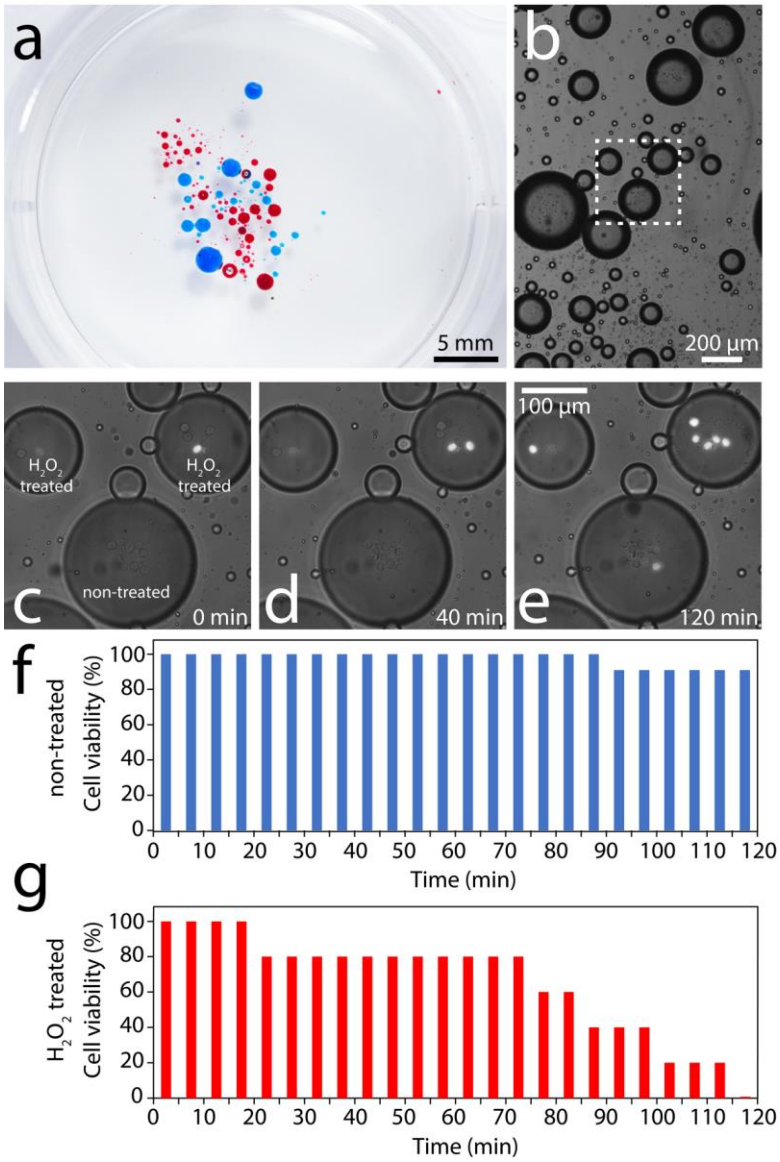

Figure 3.14: Simultaneous analysis of cell viability for non-treated and H_2O_2 treated cells encapsulated in droplets in one field of view. **a)** Red and blue water droplets generated by squeezing two separated sponges in a single well. **b)** Microscope image showing the monitored cells. **c-e)** Snapshot images over a 120 minute period showing the fluorescent response of non-treated (bottom droplet) and H_2O_2 treated cells (top two droplets). **f-g)** Cell viability bar charts for the non-treated and H_2O_2 treated cells encapsulated in separate droplets.

3.4.8 Analysing the dynamic response of encapsulated cells

Experiments demonstrate that the encapsulated cells settle at the bottom area of droplets almost immediately, and remain stable (**Movie 3.1**). In contrast, off-chip experiments demonstrate that the cells directly injected into a well require up to 30 minutes to settle at the bottom area of the well. Even after settling, the cells remain highly motile and can crawl and swarm [48], which makes it difficult to track individual cells (**Movie 3.3** with snapshot images presented in **Figure 3.11**). The reduced motility of cells encapsulated within droplets enables the dynamic response of non-adherent and motile cells to various stimuli to be monitored almost immediately without the need for secondary immobilisation mechanisms such as conventional surface modification [49], or other techniques commonly used in microfluidics such as hydrodynamic traps [50], dielectrophoresis [51], magnetophoresis [52], and optical tweezing [53].

This reduced motility was taken advantage of to study the dynamic response of encapsulated cells against 20 mM H_2O_2 by recording the normalised fluorescent intensity of cells in 5 second intervals (**Figure 3.15a-b**). Interestingly, the results revealed two distinct patterns of cellular responses, which will be referred to as 'slow' and 'fast' response, respectively (**Figures 3.15c-d**). These responses were further investigated by analysing the normalised fluorescent intensity of 14 individual cells over a period of three hours (**Figures 3.15e**) with the location of cells presented in (**Figure 3.16**). Using these dynamic curves the initial response time of cells was measured (the time at which the cells start to fluoresce) and the peak response time of cells (the time at which the cell fluorescence reaches its peak and becomes saturated). It should be noted that the initial and peak response times are widely used for quantifying the intracellular calcium signalling of cells

induced by shear stress or chemicals [49, 54]. Using these two parameters, the dynamic response time of stimulated cells was measured, defined as the difference between the initial and peak response times. The dynamic response time of 'slow' responding cells was measured as 32.84 ± 3.60 minutes, which reduced to 3.94 ± 1.80 minutes for 'fast' responding cells.

Furthermore, the average normalised fluorescent intensity of those 14 individual cells was calculated, which is presented as a dashed line in **Figure 3.15e**. Using this curve, the dynamic cell viability was calculated, defined as $Cell\ viability\ (t) = (f(t) - f_{min})/(f_{max} - f_{min}) \times 100\%$, in which f is the normalised fluorescent intensity, f_{min} = 1 (as the data is normalised) and f_{max}= 3.67, as shown in **Figure 3.17**. Interestingly, the dynamic cell viability matches very well with the viability curves presented in **Figure 3.8c**. A similar concept is used in fluorescence microplate readers to measure the viability or other cellular responses after stimulation with desired drugs [55].

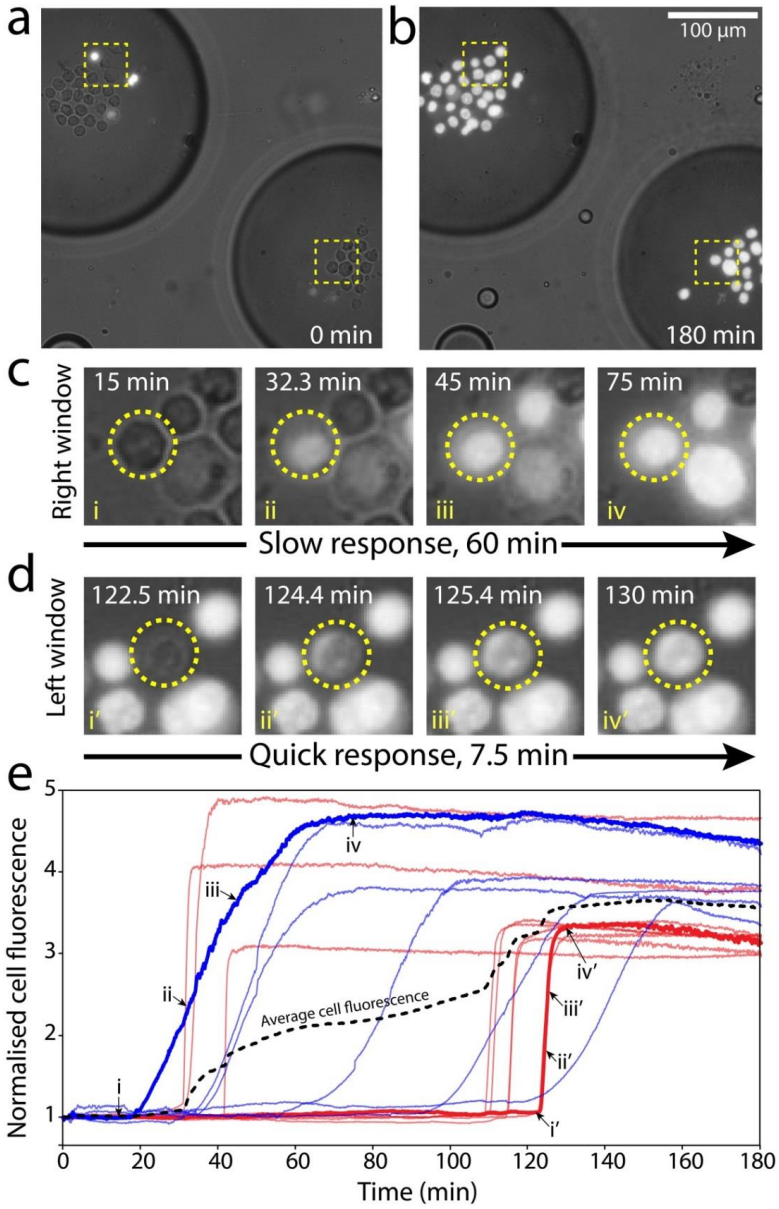

Figure 3.15: Real time, dynamic cell monitoring of encapsulated cells under H_2O_2 treatment and propidium iodide fluorescent labelling. **a-b)** 20× bright field microscopy with (Nikon G-2A filter cube) propidium iodide fluorescence at 0 min and 180 minutes. **c)** normalised intensity of H_2O_2 treated cells sampled at 5 second intervals over 180 minutes, with *slow* responding cells represented by blue and *fast* responding cells represented in red. **d)** snapshot images showing the death of a *Slow* responding cell shown over a 60-minute period, **i-iv e)** *fast* response of a circled cell undergoing *cell death* shown over a 7.5 minute period, **i-iv**.

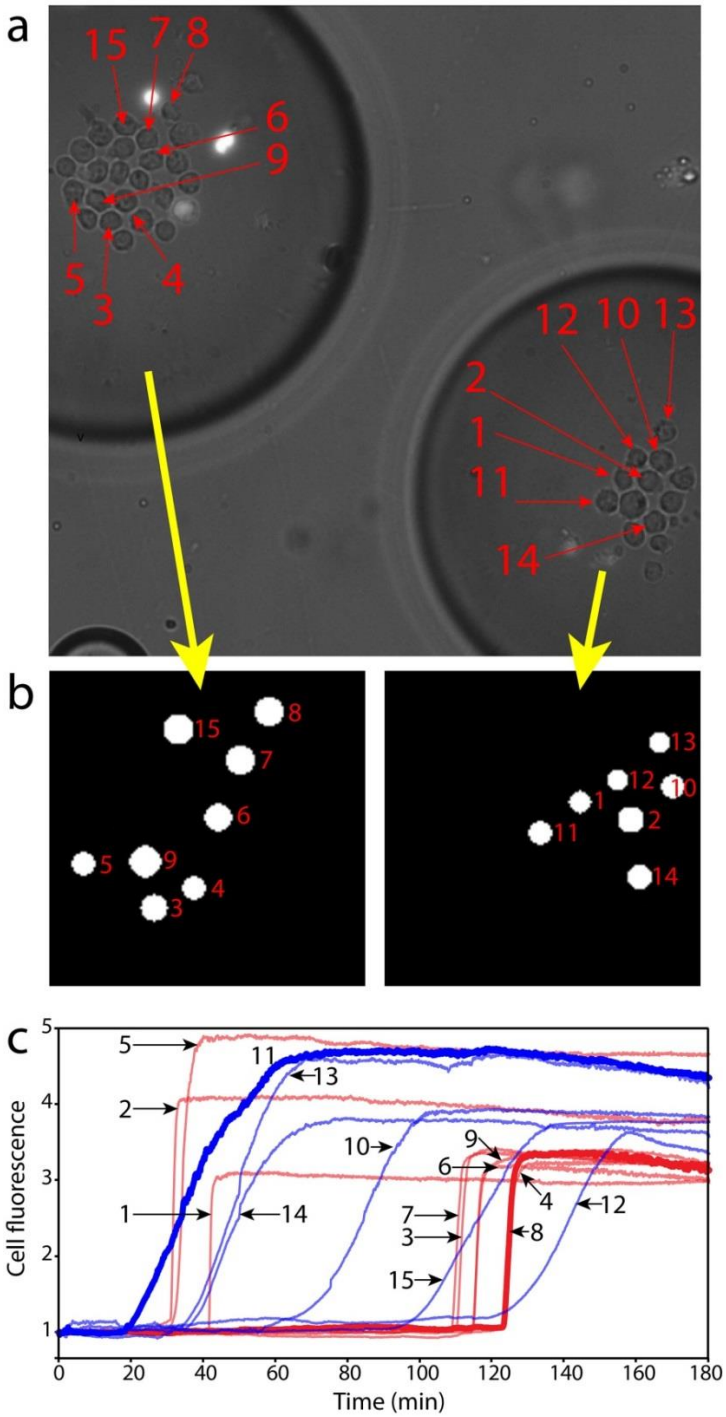

Figure 3.16: Selected cells used for analysing the dynamic response of cells treated with H_2O_2. **a)** Shows a frame of experimental data highlighting each tracked cell. **b)** ROI pattern used in NIS Elements software to obtain the fluorescent intensity curves shown in **c).**

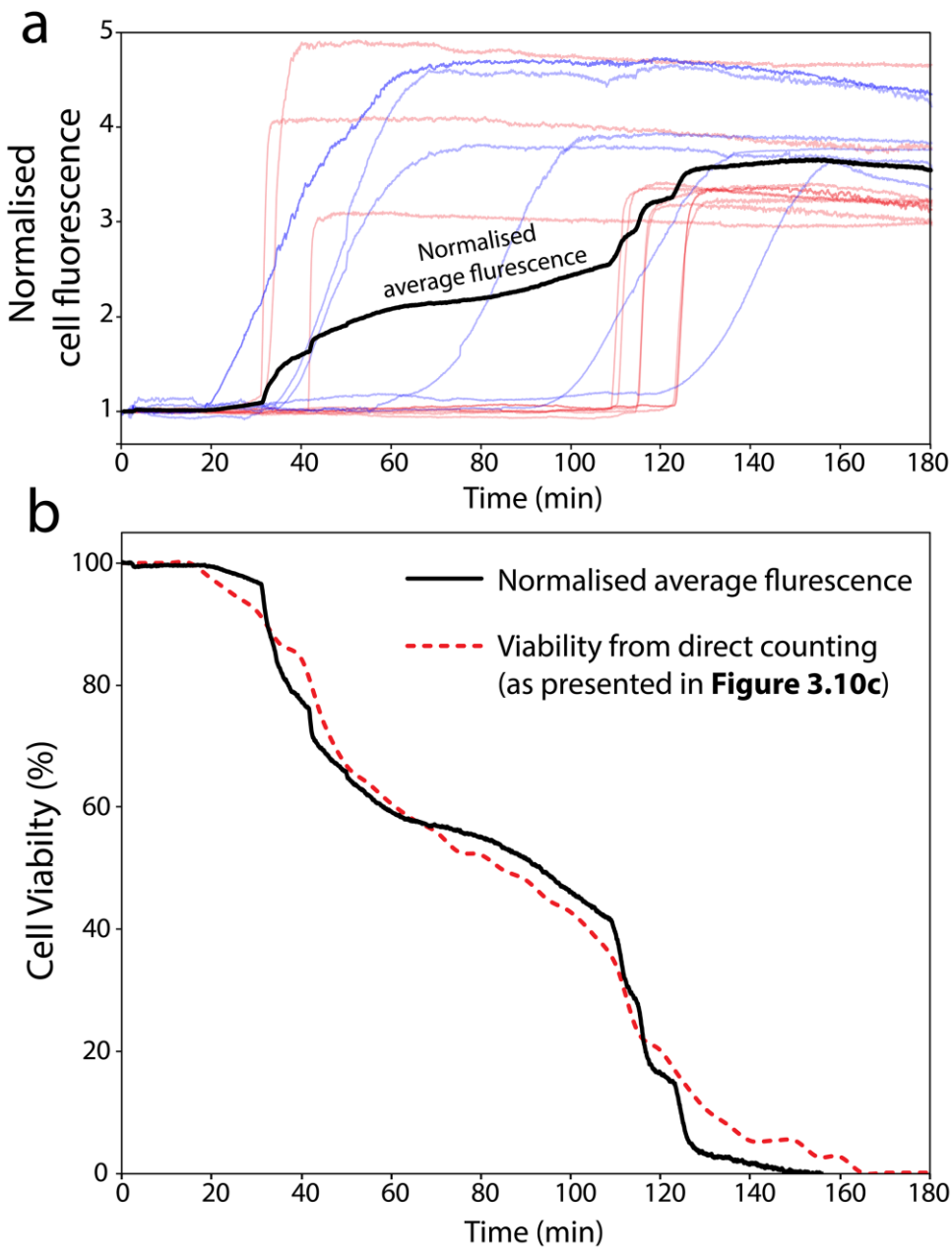

Figure 3.17: Comparing cell viability curves. **a)** The normalised fluorescent response of 14 individual cells following treatment with 20 mM H_2O_2 encapsulated inside two droplets with the average curve shown in black. **b)** Comparing cell viability curves obtained by average normalised fluorescence from **a)** versus conventional viability curves presented in **Figure 3.10c**.

3.5 Summary

In summary, a simple method for generating micro-scale droplets of aqueous solutions in oil was demonstrated, using a highly porous PDMS sponge. Upon squeezing hundreds of droplets are generated inside a cell culture well with ~90% of droplets ranging from 10 to 200 µm in diameter. Sieving of droplets using conventional cell strainers allows for removal of large droplets, increasing the homogeneity of droplet dimensions in a simple and controlled manner. This method was used for encapsulation of THP-1 human monocytic cells inside the droplets. The number of encapsulated cells is proportional to the volume of droplets, enabling us to generate isolated cell clusters with varying number of cells close to each other. The droplets are chemically isolated and mechanically stable, enabling us to monitor the viability of multiple cell clusters following treatment with hydrogen peroxide in a parallel manner.

Compared to existing microfluidic droplet generation systems, this sponge based droplet generation system is a self-sufficient, stand-alone device [56] which can be operated without any supportive equipment (pumps, tubes and valves) or microfluidic skills. The self-sufficiency and simplicity of this method facilitate the widespread use of droplet-based cellular and molecular assays in biological laboratories. In particular, the isolation of droplets enables studying the response of multiple encapsulated cells to various chemical compounds, drugs and nanomaterials [57-59]. The limited number of encapsulated cells facilitates studying the interaction of different cell types, for instance studying the response of immune cells to pathogens [60]. The limited volume of droplets facilitates the capturing and detection of target biomarkers secreted from encapsulated cells

[15, 19, 28], which might be of great interest for various biological and clinical applications [61].

The throughput of this sponge based droplet generation system is relatively low, as it only produces hundreds of droplets in each squeeze as compared to thousands of droplets generated by fully automated microfluidic droplet generation systems. This limitation can be addressed by reloading and re-squeezing the same sponge or squeezing multiple sponges in the same well. Especially, loading of sponges with different cell types or chemical stimuli facilitates multiplexed experiments in a quick and simple manner. Also, this method of droplet generation lacks controllability for producing uniformly sized droplets, and consequently homogeneously sized cell clusters. This limitation can be partially addressed by filtering the droplets through mesh filters, as demonstrated in extended experiments.

Future work involves investigating methods to improve the uniformity of the porous PDMS structure. This includes increasing the stability of water droplets injected into the uncured PDMS chamber as well as reducing the curing period of the PDMS. Future work also involves studying the viability and proliferation of encapsulated cells over extended periods (>20 hours). The sponge based droplet generation system can also be integrated other miniaturised systems to facilitate the patterning, driving, merging and sorting of droplets, enabling more complex cellular assays [62, 63].

.

3.6 References

[1] S. L. Anna, N. Bontoux, and H. A. Stone, "Formation of dispersions using “flow focusing” in microchannels," *Applied Physics Letters,* vol. 82, no. 3, pp. 364-366, 2003.

[2] P. Garstecki, M. J. Fuerstman, H. A. Stone, and G. M. Whitesides, "Formation of droplets and bubbles in a microfluidic T-junction-scaling and mechanism of break-up," *Lab on a Chip,* 10.1039/B510841A vol. 6, no. 3, pp. 437-446, 2006.

[3] L. Shang, Y. Cheng, and Y. Zhao, "Emerging Droplet Microfluidics," *Chemical Reviews,* vol. 117, no. 12, pp. 7964-8040, 2017/06/28 2017.

[4] S. L. Anna, "Droplets and Bubbles in Microfluidic Devices," *Annual Review of Fluid Mechanics,* vol. 48, no. 1, pp. 285-309, 2016.

[5] A. Huebner, S. Sharma, M. Srisa-Art, F. Hollfelder, J. B. Edel, and A. J. Demello, "Microdroplets: a sea of applications?," (in eng), *Lab on a Chip,* vol. 8, no. 8, pp. 1244-54, Aug 2008.

[6] S.-Y. Teh, R. Lin, L.-H. Hung, and A. P. Lee, "Droplet microfluidics," *Lab on a Chip,* 10.1039/B715524G vol. 8, no. 2, pp. 198-220, 2008.

[7] R. M. Maceiczyk, D. Hess, F. W. Y. Chiu, S. Stavrakis, and A. J. deMello, "Differential detection photothermal spectroscopy: towards ultra-fast and sensitive label-free detection in picoliter & femtoliter droplets," *Lab on a Chip,* 10.1039/C7LC00946A vol. 10.1039/C7LC00946A, 2017.

[8] A. S. Abdul Keyon, R. M. Guijt, C. J. Bolch, and M. C. Breadmore, "Droplet Microfluidics for Postcolumn Reactions in Capillary Electrophoresis," *Analytical Chemistry,* vol. 86, no. 23, pp. 11811-11818, 2014/12/02 2014.

[9] J. H. Kim, T. Y. Jeon, T. M. Choi, T. S. Shim, S. H. Kim, and S. M. Yang, "Droplet microfluidics for producing functional microparticles," (in eng), *Langmuir,* vol. 30, no. 6, pp. 1473-88, Feb 18 2014.

[10] H. Song, J. D. Tice, and R. F. Ismagilov, "A Microfluidic System for Controlling Reaction Networks in Time," *Angewandte Chemie International Edition,* vol. 42, no. 7, pp. 768-772, 2003.

[11] Y. Zhan, J. Wang, N. Bao, and C. Lu, "Electroporation of cells in microfluidic droplets," *Analytical Chemistry,* vol. 81, no. 5, pp. 2027-2031, 2009.

[12] S.-H. Kim, S.-J. Jeon, and S.-M. Yang, "Optofluidic Encapsulation of Crystalline Colloidal Arrays into Spherical Membrane," *Journal of the American Chemical Society,* vol. 130, no. 18, pp. 6040-6046, 2008/05/01 2008.

[13] R. Ramji *et al.,* "Single cell kinase signaling assay using pinched flow coupled droplet microfluidics," *Biomicrofluidics,* vol. 8, no. 3, p. 034104, 2014.

[14] K. J. Park *et al.*, "Micropillar arrays enabling single microbial cell encapsulation in hydrogels," *Lab on a Chip,* vol. 14, no. 11, pp. 1873-1879, 2014.

[15] T. Konry, M. Dominguez-Villar, C. Baecher-Allan, D. A. Hafler, and M. L. Yarmush, "Droplet-based microfluidic platforms for single T cell secretion analysis of IL-10 cytokine," *Biosensors and Bioelectronics,* vol. 26, no. 5, pp. 2707-2710, 2011.

[16] J. Pan *et al.*, "Quantitative tracking of the growth of individual algal cells in microdroplet compartments," *Integrative Biology,* 10.1039/C1IB00033K vol. 3, no. 10, pp. 1043-1051, 2011.

[17] R. H. Cole *et al.*, "Printed droplet microfluidics for on demand dispensing of picoliter droplets and cells," *Proceedings of the National Academy of Sciences,* p. 201704020, 2017.

[18] E. Brouzes *et al.*, "Droplet microfluidic technology for single-cell high-throughput screening," *Proceedings of the National Academy of Sciences,* vol. 106, no. 34, pp. 14195-14200, 2009.

[19] L. Mazutis, J. Gilbert, W. L. Ung, D. A. Weitz, A. D. Griffiths, and J. A. Heyman, "Single-cell analysis and sorting using droplet-based microfluidics," *Nature Protocols,* vol. 8, no. 5, p. 870, 2013.

[20] S. R. Doonan and R. C. Bailey, "K-Channel: A Multifunctional Architecture for Dynamically Reconfigurable Sample Processing in Droplet Microfluidics," *Analytical Chemistry,* vol. 89, no. 7, pp. 4091-4099, 2017/04/04 2017.

[21] J.-C. Baret *et al.*, "Fluorescence-activated droplet sorting (FADS): efficient microfluidic cell sorting based on enzymatic activity," *Lab on a Chip,* 10.1039/B902504A vol. 9, no. 13, pp. 1850-1858, 2009.

[22] P. Zhu and L. Wang, "Passive and active droplet generation with microfluidics: a review," *Lab on a Chip,* 10.1039/C6LC01018K vol. 17, no. 1, pp. 34-75, 2017.

[23] B. L. Wang *et al.*, "Microfluidic high-throughput culturing of single cells for selection based on extracellular metabolite production or consumption," *Nature Biotechnology,* vol. 32, no. 5, pp. 473-478, 2014.

[24] P. Y. Colin *et al.*, "Ultrahigh-throughput discovery of promiscuous enzymes by picodroplet functional metagenomics," *Nature Communications,* vol. 6, p. 10008, Dec 07 2015.

[25] M. T. Chung, D. Nunez, D. Cai, and K. Kurabayashi, "Deterministic droplet-based co-encapsulation and pairing of microparticles via active sorting and downstream merging," *Lab on a Chip,* 10.1039/C7LC00745K vol. 10.1039/C7LC00745K, 2017.

[26] K. Ahn, J. Agresti, H. Chong, M. Marquez, and D. A. Weitz, "Electrocoalescence of drops synchronized by size-dependent flow in microfluidic channels," *Applied Physics Letters,* vol. 88, no. 26, p. 264105, 2006.

[27] A. R. Abate, T. Hung, P. Mary, J. J. Agresti, and D. A. Weitz, "High-throughput injection with microfluidics using picoinjectors," *Proceedings of the National Academy of Sciences,* vol. 107, no. 45, pp. 19163-19166, November 9, 2010 2010.

[28] V. Chokkalingam *et al.*, "Probing cellular heterogeneity in cytokine-secreting immune cells using droplet-based microfluidics," *Lab on a chip,* vol. 13, no. 24, pp. 4740-4744, 2013.

[29] R. Zilionis *et al.*, "Single-cell barcoding and sequencing using droplet microfluidics," *Nature Protocols,* vol. 12, no. 1, pp. 44-73, 2017.

[30] M. Hosokawa, Y. Nishikawa, M. Kogawa, and H. Takeyama, "Massively parallel whole genome amplification for single-cell sequencing using droplet microfluidics," *Scientific Reports,* vol. 7, p. 5199, 2017.

[31] H. Zhang *et al.*, "Piezoresistive Sensor with High Elasticity Based on 3D Hybrid Network of Sponge@CNTs@Ag NPs," *ACS Applied Materials & Interfaces,* vol. 8, no. 34, pp. 22374-22381, 2016/08/31 2016.

[32] Y.-h. Wu *et al.*, "Channel Crack-Designed Gold@PU Sponge for Highly Elastic Piezoresistive Sensor with Excellent Detectability," *ACS Applied Materials & Interfaces,* vol. 9, no. 23, pp. 20098-20105, 2017/06/14 2017.

[33] Y. Li *et al.*, "Cellulose Sponge Supported Palladium Nanoparticles as Recyclable Cross-Coupling Catalysts," *ACS Applied Materials & Interfaces,* vol. 9, no. 20, pp. 17155-17162, 2017/05/24 2017.

[34] Y. Lu *et al.*, "Elastic, Conductive, Polymeric Hydrogels and Sponges," *Scientific Reports,* Article vol. 4, p. 5792, 07/23/online 2014.

[35] X.-c. Chen *et al.*, "Self-Healing Spongy Coating for Drug "Cocktail" Delivery," *ACS Applied Materials & Interfaces,* vol. 8, no. 7, pp. 4309-4313, 2016/02/24 2016.

[36] M. Khosravi and S. Azizian, "Synthesis of a Novel Highly Oleophilic and Highly Hydrophobic Sponge for Rapid Oil Spill Cleanup," *ACS Applied Materials & Interfaces,* vol. 7, no. 45, pp. 25326-25333, 2015/11/18 2015.

[37] K. J. Cha and D. S. Kim, "A portable pressure pump for microfluidic lab-on-a-chip systems using a porous polydimethylsiloxane (PDMS) sponge," (in eng), *Biomedical Microdevices,* vol. 13, no. 5, pp. 877-83, Oct 2011.

[38] S. Hong *et al.*, "Magnetoactive sponges for dynamic control of microfluidic flow patterns in microphysiological systems," *Lab on a Chip,* 10.1039/C3LC51076J vol. 14, no. 3, pp. 514-521, 2014.

[39] S.-J. Choi *et al.*, "A Polydimethylsiloxane (PDMS) Sponge for the Selective Absorption of Oil from Water," *ACS Applied Materials & Interfaces,* vol. 3, no. 12, pp. 4552-4556, 2011/12/28 2011.

[40] M. Costantini *et al.*, "Highly ordered and tunable polyHIPEs by using microfluidics," *Journal of Materials Chemistry B,* 10.1039/C3TB21227K vol. 2, no. 16, pp. 2290-2300, 2014.

[41] M. Costantini *et al.*, "Microfluidic Foaming: A Powerful Tool for Tailoring the Morphological and Permeability Properties of Sponge-like Biopolymeric Scaffolds," *ACS Applied Materials & Interfaces,* vol. 7, no. 42, pp. 23660-23671, 2015/10/28 2015.

[42] P. Thurgood, S. Baratchi, C. Szydzik, A. Mitchell, and K. Khoshmanesh, "Porous PDMS structures for the storage and release of aqueous solutions into fluidic environments," *Lab on a Chip,* vol. 17, pp. 2517-2527, 2017.

[43] S. Padmanabhan, T. Misteli, and D. L. DeVoe, "Controlled droplet discretization and manipulation using membrane displacement traps," *Lab on a Chip,* 10.1039/C7LC00910K vol. 10.1039/C7LC00910K, 2017.

[44] F. S. (Editor), *Bailey's industrial oil & fat products*, 6th edition ed. New York: Wiley-Intersience, 2005.

[45] E. F. Ribeiro, T. C. Polachini, G. R. Carvalho, J. T. Romero, and R. A. F. Cabral, "Thermophysical properties of different olive oils: Evaluating density and rheology through a fluid dynamic approach," *European Journal of Lipid Science and Technology,* vol. 119, no. 7, pp. 1600316-n/a, 2017, Art. no. 1600316.

[46] N. Okahashi, T. Sumitomo, M. Nakata, A. Sakurai, H. Kuwata, and S. Kawabata, "Hydrogen peroxide contributes to the epithelial cell death induced by the oral mitis group of streptococci," (in eng), *PLoS One,* vol. 9, no. 1, p. e88136, 2014.

[47] S. Guzman-Beltran *et al.*, "Nordihydroguaiaretic Acid Attenuates the Oxidative Stress-Induced Decrease of CD33 Expression in Human Monocytes," *Oxidative Medicine and Cellular Longevity,* vol. 2013, p. 14, 2013, Art. no. 375893.

[48] R. N. Germain, E. A. Robey, and M. D. Cahalan, "A Decade of Imaging Cellular Motility and Interaction Dynamics in the Immune System," *Science,* vol. 336, no. 6089, pp. 1676-1681, 2012.

[49] S. Baratchi *et al.*, "Examination of the role of transient receptor potential vanilloid type 4 in endothelial responses to shear forces," *Biomicrofluidics,* vol. 8, no. 4, p. 044117, 2014.

[50] D. Di Carlo, N. Aghdam, and L. P. Lee, "Single-Cell Enzyme Concentrations, Kinetics, and Inhibition Analysis Using High-Density Hydrodynamic Cell Isolation Arrays," *Analytical Chemistry,* vol. 78, no. 14, pp. 4925-4930, 2006/07/01 2006.

[51] K. Khoshmanesh *et al.*, "Dynamic analysis of drug-induced cytotoxicity using chip-based dielectrophoretic cell immobilization technology," *Analytical Chemistry,* vol. 83, no. 6, pp. 2133-2144, 2011.

[52] O. Osman *et al.*, "Microfluidic immunomagnetic cell separation using integrated permanent micromagnets," (in eng), *Biomicrofluidics,* vol. 7, no. 5, p. 54115, 2013.

[53] P. Jordan *et al.*, "Creating permanent 3D arrangements of isolated cells using holographic optical tweezers," *Lab on a Chip,* vol. 5, no. 11, pp. 1224-1228, 2005.

[54] R. Soffe *et al.*, "Analysing calcium signalling of cells under high shear flows using discontinuous dielectrophoresis," *Scientific reports,* vol. 5, p. 11973, 2015.

[55] S. Grootjans *et al.*, "A real-time fluorometric method for the simultaneous detection of cell death type and rate," *Nature Protocols,* vol. 11, no. 8, pp. 1444-1454, 2016.

[56] M. Boyd-Moss, S. Baratchi, M. Di Venere, and K. Khoshmanesh, "Self-contained microfluidic systems: a review," *Lab on a Chip,* vol. 16, no. 17, pp. 3177-3192, 2016.

[57] S. Behzadi *et al.*, "Cellular uptake of nanoparticles: journey inside the cell," *Chemical Society Reviews,* 10.1039/C6CS00636A vol. 46, no. 14, pp. 4218-4244, 2017.

[58] C. T. Riche, E. J. Roberts, M. Gupta, R. L. Brutchey, and N. Malmstadt, "Flow invariant droplet formation for stable parallel microreactors," *Nature Communications,* Article vol. 7, p. 10780, 02/23/online 2016.

[59] Y. Lei *et al.*, "An on-chip model for investigating the interaction between neurons and cancer cells," (in eng), *Integr Biol (Camb),* vol. 8, no. 3, pp. 359-67, Mar 14 2016.

[60] L. P. Erwig and N. A. Gow, "Interactions of fungal pathogens with phagocytes," (in eng), *Nat Rev Microbiol,* vol. 14, no. 3, pp. 163-76, Mar 2016.

[61] P. C. Gach, K. Iwai, P. W. Kim, N. J. Hillson, and A. K. Singh, "Droplet microfluidics for synthetic biology," *Lab on a Chip,* 10.1039/C7LC00576H vol. 10.1039/C7LC00576H, 2017.

[62] K. J. Bachus, L. Mats, H. W. Choi, G. T. T. Gibson, and R. D. Oleschuk, "Fabrication of Patterned Superhydrophobic/Hydrophilic Substrates by Laser Micromachining for Small Volume Deposition and Droplet-Based Fluorescence," *ACS Applied Materials & Interfaces,* vol. 9, no. 8, pp. 7629-7636, 2017/03/01 2017.

[63] S. C. Shih *et al.*, "A Versatile Microfluidic Device for Automating Synthetic Biology," (in eng), *ACS Synth Biol,* vol. 4, no. 10, pp. 1151-64, Oct 16 2015.

CHAPTER 4: Conclusions and Future Work

4.1 Concluding Remarks

The author demonstrated the utility of highly porous PDMS sponges for the storage and release of solutions into the surrounding liquid environments as well as generation of micro-scale droplets for encapsulation of cells in a self-sufficient manner, as presented in **Chapters 2** and **3**. The contributions of this research are summarised in this chapter.

4.2 Research Contributions

My research contributions can be summarised as below:

Research Contribution 1: I fabricated a highly porous PDMS sponge using a T-junction microfluidic droplet generation system. SEM characterisation revealed that the PDMS sponge consisted of large pores, which were only interconnected by small holes. The porosity and elasticity of PDMS sponge along enabled the quick loading of the sponge with aqueous solutions upon manual compression. The large pores acted as miniaturised reservoirs to store liquids, whereas the interconnecting holes acted as miniaturised diffusion barriers that limited the passive release of stored liquids into surrounding fluidic environments. This was demonstrated through a series of experiments, releasing stored aqueous solutions into straight channels (**Figures 2.5** to **2.8**). Varying the average size of interconnecting holes from 19.1 to 29.6 μm enabled me to change the passive release rate of aqueous solutions into a straight channel by a factor of 2.4 (**Figures 2.13** to **2.18**). This addresses my *Research Question 1*.

Research Contribution 2: I demonstrated the utility of fabricated porous PDMS sponge for the passive release of stored chemicals into circular shape Petri dishes, which are commonly used for cell-based assays (**Figures 2.19** to **2.20**). This feature was utilised for investigating the intracellular calcium signalling of human umbilical vein endothelial cells upon stimulation with ionomycin, which was stored and passively released from the sponge. The response of cells varied in a dose-dependent manner. For example, a maximum fold increase of 4.2 ± 0.4 was obtained in response to 2 μg/ml of stored ionomycin (**Figures 2.21** to **2.22**). This addresses my *Research Question 2*.

Research Contribution 3: I demonstrated the active release of stored aqueous solutions into surrounding fluidic environments. This was demonstrated by cyclic release of stored solutions into a microfluidic structure (**Figure 2.23**) Using a screw mechanism enabled the controlled and repeatable release cycles using a simple setup. This addresses my *Research Question 3*.

Research Contribution 4: I utilised my porous PDMS sponge for generating micro-scale droplets of aqueous solutions in oil upon manual compression. The interconnecting holes located at the surface of the PDMS acted as micro-scale orifices, and facilitated the breaking (pinch off) of aqueous solutions into micro-scale droplets upon leaving the sponge (**Figure 3.2**). Hundreds of such orifices existed at the surface of the sponge, allowing for generation of hundreds of droplets in one single squeeze. The droplets followed a positively skewed normal distribution with approximately 90% of the droplets falling between 10 to 200 µm in diameter (**Figure 3.4**) This addresses my *Research Question 4*.

Research Contribution 5: The ability for generation of micro-scale droplets was further utilised for encapsulation of THP-1 monocytic leukemia cells inside the droplets. Microscopic experiments revealed that the number of encapsulated cells is proportional to the size of droplets as wells the density of cells within the cell suspension (**Figures 3.6** to **3.7**). This feature was utilised to generate a diverse range of cell clusters consisting of small, medium and large number of cells, demonstrating the ability of this method for generation of hundreds of isolated micro-droplets inside a cell culture well. These micro-droplets were chemically isolated, mechanically stable, and did not evaporate, due to the presence of oil in the well. This addresses my *Research Question 5*.

Research Contribution 6: The chemical isolation of droplets enabled me to conduct highly parallel cellular assays. This feature was used for investigating the oxidative stress of encapsulated THP-1 cells in response to hydrogen peroxide. As opposed to cells directly injected in to a well, the encapsulated cells settled almost immediately at the lowest surface of droplets, and hence could be easily monitored using fluorescent microscopy without using any secondary immobilisation technologies The encapsulated cells exhibited similar viability characteristics as off-chip experiments (**Figure 3.8**). By applying two sponges into the same well, I could position droplets containing hydrogen peroxide-stimulated and non-stimulated cells in the same field of view, and compared their responses simultaneously (**Figure 3.12**). The stability of encapsulated cells allowed me to measure the dynamic response of stimulated cells without using any cell tracking algorithms. This feature was utilised for investigating the average dynamic response time (defined as the difference between the initial and peak response times) of THP-1 cells upon stimulation with hydrogen peroxide, based on which I observed two distinct cell death patterns. For the 'slow' responding cells, the average dynamic response time was measured as 32.84 min, while for the 'fast' responding cells the average dynamic response time decreased to 3.94 min (**Figure 3.13**). This addresses my *Research Question 6*.

4.3 Recommendations for Future Work

The current research can be further extended to make a new generation of self-sufficient microfluidic systems enabled by highly porous PDMS sponges, as summarised below:

- The passive release of stored drugs into a biological system presented in **Chapter 2** could be easily expanded to allow for more complicated cellular assays implementing multiple sponges to enable consequent preparation, stimulation and washing of cells with desired buffers, reagents, chemicals and drugs.
- The active release of stored liquids into a microfluidic channel via compression with a screw mechanism presented in **Chapter 2** could be equipped with stepper motors or solenoid actuators [1] to automate the active release of liquids from the sponge, this automation could also enable more complex compression patterns. The system could also be augmented with multiple sponges in either parallel channels or inline, allowing for the release of multiple drugs/reagents/buffers in complex patterns into a biological system.
- The effect of the pore and interconnecting hole size on the resulting micro-droplets generated upon squeezing in oil could be investigated by using sponges with different characteristics.
- The cell assays presented in **Chapter 3** could be extended to various chemical compounds, drugs and nano-materials [2-4] all studied in a parallel manner.

- The limited number of encapsulated cells facilitates studying the interaction of different cell types, for instance studying the response of immune cells to pathogens [5].
- The limited volume of droplets facilitates the capturing and detection of target biomarkers secreted from encapsulated cells [6-8], which might be of great interest for studying various cellular signaling mechanisms [9] or the diagnosis of diseases [10] using fluorescent microscopy.

4.4 References

[1] S. Elizabeth Hulme, S. S. Shevkoplyas, and G. M. Whitesides, "Incorporation of prefabricated screw, pneumatic, and solenoid valves into microfluidic devices," *Lab on a Chip*, 10.1039/B809673B vol. 9, no. 1, pp. 79-86, 2009.

[2] S. Behzadi *et al.*, "Cellular uptake of nanoparticles: journey inside the cell," *Chemical Society Reviews*, 10.1039/C6CS00636A vol. 46, no. 14, pp. 4218-4244, 2017.

[3] J. Shi, P. W. Kantoff, R. Wooster, and O. C. Farokhzad, "Cancer nanomedicine: progress, challenges and opportunities," *Nat Rev Cancer*, Review vol. 17, no. 1, pp. 20-37, 01//print 2017.

[4] C. T. Riche, E. J. Roberts, M. Gupta, R. L. Brutchey, and N. Malmstadt, "Flow invariant droplet formation for stable parallel microreactors," *Nature Communications*, Article vol. 7, p. 10780, 02/23/online 2016.

[5] L. P. Erwig and N. A. Gow, "Interactions of fungal pathogens with phagocytes," (in eng), *Nat Rev Microbiol*, vol. 14, no. 3, pp. 163-76, Mar 2016.

[6] L. Mazutis, J. Gilbert, W. L. Ung, D. A. Weitz, A. D. Griffiths, and J. A. Heyman, "Single-cell analysis and sorting using droplet-based microfluidics," *Nature Protocols*, vol. 8, no. 5, p. 870, 2013.

[7] V. Chokkalingam *et al.*, "Probing cellular heterogeneity in cytokine-secreting immune cells using droplet-based microfluidics," *Lab on a chip*, vol. 13, no. 24, pp. 4740-4744, 2013.

[8] T. Konry, M. Dominguez-Villar, C. Baecher-Allan, D. A. Hafler, and M. L. Yarmush, "Droplet-based microfluidic platforms for single T cell secretion analysis of IL-10 cytokine," *Biosensors and Bioelectronics*, vol. 26, no. 5, pp. 2707-2710, 2011.

[9] S. Nahavandi *et al.*, "Microfluidic platforms for the investigation of intercellular signalling mechanisms," *Small*, vol. 10, no. 23, pp. 4810-4826, 2014.

[10] M. Gao, F. Yu, C. Lv, J. Choo, and L. Chen, "Fluorescent chemical probes for accurate tumor diagnosis and targeting therapy," *Chemical Society Reviews*, 10.1039/C6CS00908E vol. 46, no. 8, pp. 2237-2271, 2017.